

AD-A021 876

AN EXPERIMENTAL INVESTIGATION OF METHODS OF SUPPRESSING
THE UNSTEADY TORQUE EXERTED ON THE UPPER TURNING
MIRROR OF AN AIRCRAFT MOUNTED COELOSTAT TURRET

Richard M. Mullane

Air Force Institute of Technology
Wright-Patterson Air Force Base, Ohio

June 1975

DISTRIBUTED BY:

NTIS

National Technical Information Service
U. S. DEPARTMENT OF COMMERCE

PII Redacted

AN EXPERIMENTAL INVESTIGATION OF
METHODS OF SUPPRESSING
THE UNSTEADY TORQUE EXERTED ON
THE UPPER TURNING MIRROR OF
AN AIRCRAFT MOUNTED COELOSTAT TURRET

✓
THESIS

GAE/AE/75J-6

Richard M. Mullane
Captain USAF

D D C
MAR 15 1976
R
C

Approved for public release; distribution unlimited.

SEARCHED	INDEXED
SERIALIZED	FILED
MAR 15 1976	
FBI - MEMPHIS	
White Section	<input checked="" type="checkbox"/>
Ref Section	<input type="checkbox"/>
REGISTRATION AVAILABILITY CODES	
AVAIL. AND SPECIAL	
A	

Unclassified

SECURITY CLASSIFICATION OF THIS PAGE (When Data Entered)

REPORT DOCUMENTATION PAGE		READ INSTRUCTIONS BEFORE COMPLETING FORM
1. REPORT NUMBER GAE/AE/75J-6	2. GOVT ACCESSION NO.	3. RECIPIENT'S CATALOG NUMBER
4. TITLE (and Subtitle) An Experimental Investigation of Methods of Suppressing the Unsteady Torque Exerted on the Upper Turning Mirror of an Aircraft Mounted Coelostat Turret		5. TYPE OF REPORT & PERIOD COVERED AFIT Thesis
		6. PERFORMING ORG. REPORT NUMBER
7. AUTHOR(s) Mullane, Richard M. Capt, USAF		8. CONTRACT OR GRANT NUMBER(s)
9. PERFORMING ORGANIZATION NAME AND ADDRESS Air Force Institute of Technology (AU) Wright-Patterson AFB, Ohio 45433		10. PROGRAM ELEMENT, PROJECT, TASK AREA & WORK UNIT NUMBERS
11. CONTROLLING OFFICE NAME AND ADDRESS		12. REPORT DATE June 1975
		13. NUMBER OF PAGES 130
14. MONITORING AGENCY NAME & ADDRESS (if different from Controlling Office) Air Force Institute of Technology (AU) Wright-Patterson AFB, Ohio 45433		15. SECURITY CLASS. (of this report)
		15a. DECLASSIFICATION/DOWNGRADING SCHEDULE
16. DISTRIBUTION STATEMENT (of this Report) Approved for public release; distribution unlimited.		
17. DISTRIBUTION STATEMENT (of the abstract entered in Block 20, if different from Report)		
18. SUPPLEMENTARY NOTES Approved for public release, IAW AFR/190-17 Jerry C. Hix Capt. USAF Director of Information		
19. KEY WORDS (Continue on reverse side if necessary and identify by block number) Coelostat Turret Turret Unsteady Torque		
20. ABSTRACT (Continue on reverse side if necessary and identify by block number) Various methods of reducing the unsteady torque exerted on the upper turning mirror (UTM) of a coelostat turret were experimentally evaluated. The effect of an aft fairing and the turret aperture on the pressure distribution across the turret was also measured. Areas of flow separation were determined from oil flow patterns. A coelostat model with a turret diameter of five inches and capable of rotating 120° in azimuth		

(Block 20 continued:

was wall mounted in a transonic wind tunnel. Data was collected for Mach numbers of .7, .85, and .95. Passive methods, consisting of external fairings and active methods, consisting of blowing and suction, were employed to reduce UTM torque. The passive methods were totally ineffective in this regard. Mass flow injection at the rear of the bottom light pipe and aperture lip were found to lower base line torque values by approximately 50% and 67% respectively. Static pressures recorded on the turret revealed that the aft fairing had little effect on the pressure distribution. The aperture was noted to produce a higher local C_p in the downstream direction. Oil flow patterns showed that the point of flow separation from the turret was velocity dependent, being near the 90° meridians for velocities above Mach = .85 but further aft for Mach = .7.

GAE/AE/75J-6

**AN EXPERIMENTAL INVESTIGATION OF METHODS OF SUPPRESSING
THE UNSTEADY TORQUE EXERTED ON THE UPPER TURNING MIRROR
OF AN AIRCRAFT MOUNTED COELOSTAT TURRET**

THESIS

**Presented to the Faculty of the School of Engineering
of the Air Force Institute of Technology
Air University
in Partial Fulfillment of the
Requirements for the Degree of
Master of Science**

by

Richard M. Mullane, B.S.

Captain USAF

Graduate Aerospace and Mechanical Engineering

June 1975

Approved for public release; distribution unlimited

ici

Preface

The utilization of optical pointing and tracking devices in various areas of aircraft operations is of continuing interest to the USAF and NASA. A unique aerodynamic problem that has been identified with such airborne optical systems is the unsteady torque exerted on the mirror surfaces that are exposed to high velocity airflow. The investigation I conducted was one of the first aimed at finding various methods of reducing this torque on large, second generation pointing and tracking devices. The success I achieved in this endeavor was in two forms. First, I did find some configurations that reduced unwanted torques and second, I found that other suggested configurations were totally ineffective as torque reducers. Hopefully, both results will be of assistance to future researchers.

I would like to extend my sincerest thanks to Dr. Harold Wright of the Air Force Institute of Technology for his invaluable assistance in helping me throughout this investigation. I also acknowledge my frequent reliance upon the counsel of Dr. James Van Kuren and Capt William Conner of the Flight Dynamics Laboratory. Additionally, I would like to make special note of the professionalism of Mr. Wolfe and Mr. Brohas of the AFIT machine shop who prepared my model.

Lastly, I submit that the patience, love, and understanding of my wife were key ingredients in the completion of this work.

Richard M. Mullane

Table of Contents

	Page
Preface.	ii
List of Figures.	v
List of Tables	viii
List of Symbols.	ix
Abstract	x
I. Introduction.	1
Background.	1
Objective	3
Scope	3
Supplemental Data Collection.	5
II. Theory.	6
Upper Turning Mirror Unsteady Torque.	7
Non-dimensionalizing Terms.	8
III. Description of Apparatus.	10
Model	10
Model Configurations.	13
Wind Tunnel	13
Pressure Transducers.	13
RMS Meters.	16
Tape Recorder	16
Flow Meter.	16
IV. Experimental Procedures	18
Wind Tunnel Calibration	18
Test Phases	18
Phase I - Turret Steady Pressures	20
Phase II - Upper Turning Mirror Unsteady Pressures.	20
Phase III - Oil Flow Visualization.	23

Table of Contents

	Page
V. Results.	24
Upper Turning Mirror Unsteady Torque.	24
Turret Pressure Distribution.	33
Oil Flow Visualization.	36
VI. Conclusions and Recommendations.	44
Conclusions	44
Recommendations	47
Bibliography.	48
Appendix A: Model Configurations	49
Appendix B: Boundary Layer Data.	62
Appendix C: Upper Turning Mirror Unsteady Pressures and Torques.	63
Appendix D: Turret Static Pressure Distribu- tion	98
Appendix E: Oil Flow Visualization Drawings. .	109
Vita.	114

List of Figures

Figure	Page
1 Coelostat Nomenclature.	2
2 Definition of Roll and Azimuth Angles for a Coelostat Turret.	4
3 Upper Turning Mirror of Coelostat with Pressure Transducers.	7
4 Flow Diagram Illustrating Procedure by which Root-Mean-Square Torque is obtained from Transducer Voltage Signal.	9
5 Location of Static Pressure Taps Placed in Turret	11
6 Arrangement of Wall-Mounted Model in Wind Tunnel.	12
7 Data Collection Flow Diagram.	19
8 Non-dimensionalized RMS Torque about the Elevation Axis of the Upper Turning Mirror Resulting from Various Passive Model Modifications Compared to Base Line (Model 2) Elevation Torque at Mach = .7 .	25
9 Non-dimensionalized RMS Torque about the Azimuth Axis of the Upper Turning Mirror Resulting from Various Passive Model Modifications Compared to Base Line (Model 2) Azimuth Torque at Mach = .7 . .	26
10 Non-dimensionalized RMS Torque about the Elevation Axis of the Upper Turning Mirror Resulting from Various Active Model Modifications Compared to Base Line (Model 2) Elevation Torque at Mach = .7 .	27
11 Non-dimensionalized RMS Torque about the Azimuth Axis of the Upper Turning Mirror Resulting from Various Active Model Modifications Compared to Base Line (Model 2) Azimuth Torque at Mach = .7 . .	28

List of Figures

Figure		Page
12	Diversion of Approaching Flow by Mass Injection.	29
13	Comparison of Upper Turning Mirror Torques for Models 2 and 12 for $\theta = 0^\circ$ and Mach = .7	30
14	Comparison of Upper Turning Mirror Torques for Models 2 and 16 for $\theta = 0^\circ$ and Mach = .7	30
15	Comparison of Local Turret Flow C_p with and without the Aft Fairing Installed with Free Stream Mach = .7.	34
16	Comparison of Local Turret Flow Mach Number with and without the Aft Fairing Installed with Free Stream Mach = .7.	35
17	Comparison of Local Turret Flow C_p Measured 70° Downstream of Aperture to Local Turret Flow C_p Measured without an Upstream Aperture for Model 1, Free Stream Mach = .7	37
18	Comparison of Local Turret Flow C_p Measured 70° Downstream of Aperture to Local Turret Flow C_p Measured without an Upstream Aperture for Model 1, Free Stream Mach = .85.	38
19	Comparison of Local Turret Flow C_p Measured 70° Downstream of Aperture to Local Turret Flow C_p Measured without an Upstream Aperture for Model 1, Free Stream Mach = .95.	39
20	Position of the Pressure Tap Meridian as θ is Varied.	40
21	Oil Visualization of Flow Over Model 2 with $\theta = 0^\circ$ and Mach = .7	42
22-33	Model Configurations.	50-61

List of Figures

Figure		Page
34	Measured Boundary Layer Compared to Theoretical $1/7$ Power Law Velocity Profile.	62
35-66	Pressure Variations on the Upper Turning Mirror Surface as Function of Cavity Orientation and Model Configuration for Various Mach Numbers	64-95
67	Non-dimensionalized Root-Mean-Square Torque about the Model 2 Upper Turning Mirror Azimuth Axis as a Function of the Orientation of the Turret Aperture for Various Values of the Free Stream Mach Number.	96
68	Non-dimensionalized Root-Mean-Square Torque about the Model 2 Upper Turning Mirror Elevation Axis as a Function of the Orientation of the Turret Aperture for Various Values of the Free Stream Mach Number.	97
69-73	Comparison of Local Turret Flow Mach Number with and without the Aft Fairing Installed for Various Free Stream Mach Numbers	99-103
74-78	Comparison of Local Turret Flow C_p with and without the Aft Fairing Installed for Various Free Stream Mach Numbers . .	104-108
79-82	Oil Visualization of Flow Over Model 2 for Various θ and Various Mach Numbers .	110-113

List of Tables

Table		Page
I	Passive Model Configurations.	14
II	Active Model Configurations	15
III	Upper Turning Mirror Elevation Torque Compared for Similar Models	32

List of Symbols

C_p	Coefficient of pressure
D	Diameter of turret aperture
LTM	Lower turning mirror
\dot{m}	Mass flow rate
\bar{m}	Non-dimensionalized mass flow rate ($\dot{m}/\rho\pi\frac{D^2}{4}U_\infty$)
θ	Azimuth angle of turret aperture
$P(t)$	Unsteady Pressure
P_{rms}	Root-mean-square of unsteady pressure
PSD	Power spectral density
ρ	Density of air
q, Q	Dynamic pressure
t	Time
T	Period of signal sample
TD	Turret diameter
$T_q(t)$	Unsteady torque
T_{rms}	Root-mean-square of unsteady torque
\bar{T}_{rms}	Non-dimensionalized root-mean-square of unsteady torque ($T_{rms}/\sqrt{\rho q D^3}$)
u	Local velocity of flow
U_∞	Free stream velocity
UTM	Upper turning mirror
V	Voltage
VDC	Volts, direct current

Abstract

Various methods of reducing the unsteady torque exerted on the upper turning mirror (UTM) of a coelostat turret were experimentally evaluated. The effect of an aft fairing and the turret aperture on the pressure distribution across the turret was also measured. Areas of flow separation were determined from oil flow patterns. A coelostat model with a turret diameter of five inches and capable of rotating 120° in azimuth was wall mounted in a transonic wind tunnel. Data was collected for Mach numbers of .7, .85, and .95. Passive methods, consisting of external fairings and active methods, consisting of blowing and suction, were employed to reduce UTM torque. The passive methods were totally ineffective in this regard. Mass flow injection at the rear of the bottom light pipe and aperture lip were found to lower base line torque values by approximately 50% and 67% respectively. Static pressures recorded on the turret revealed that the aft fairing had little effect on the pressure distribution. The aperture was noted to produce a higher local C_p in the downstream direction. Oil flow patterns showed that the point of flow separation from the turret was velocity dependent, being near the 90° meridians for velocities above Mach = .85 but further aft for Mach = .7.

AN EXPERIMENTAL INVESTIGATION OF METHODS OF SUPPRESSING
THE UNSTEADY TORQUE EXERTED ON THE UPPER TURNING MIRROR
OF AN AIRCRAFT MOUNTED COELOSTAT TURRET

I. Introduction

Background

In recent years the United States Air Force (USAF) has identified numerous missions for aircraft mounted optical radiation devices (Ref 1:52). For example, airborne lasers have been earmarked for roles as reconnaissance sensors, communication devices, and target illuminators for guided munitions. In many of these applications it is desirable to house the optical radiator in a traversable, fuselage-mounted turret which contains a viewing port. With this arrangement, the narrow light beam of the device can be aimed at an object independently of the aircraft heading and/or attitude. In some laser applications however, a stringent requirement for an unimpeded optical light path, demands that the turret viewing port contain no protective window. Previous researchers have found that high velocity flow over such windowless turret configurations produces pressure fluctuations within the open cavity of the turret (Refs 2:1, 3:17). These unsteady pressures, in some cases amplified

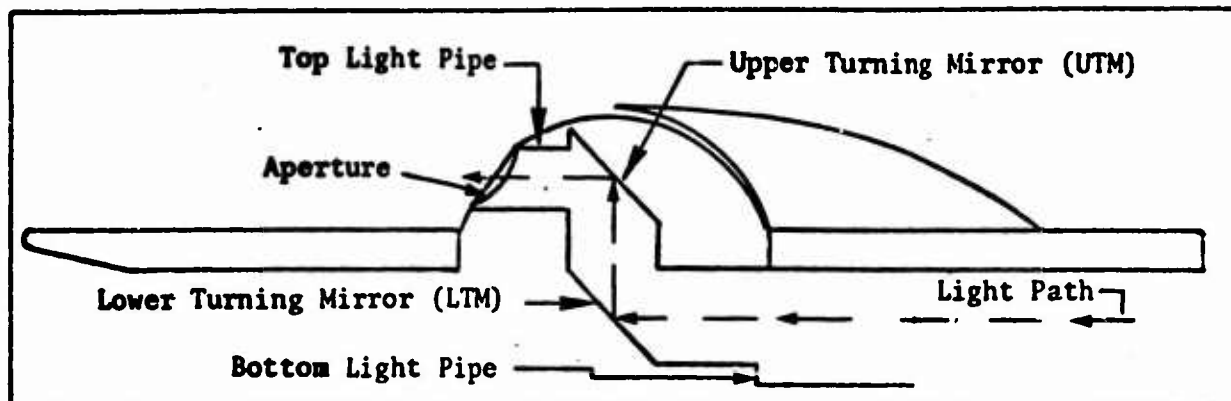


Fig. 1. Coelostat Nomenclature

by the process of acoustic resonance, act upon non-rigid mirror surfaces to produce vibrations that degrade the performance of the device.

Large, second generation airborne lasers will be particularly vulnerable to flow induced mirror vibrations. Therefore, the USAF and NASA have jointly conducted two wind tunnel tests in a search for a windowless turret design that will minimize the vibration problem for these larger devices. The first study, involving an evaluation of four basic designs, highlighted the coelostat turret configuration as the most promising (Ref 4:4).

The second wind tunnel test, hereafter referred to as the Ames II test, was a detailed evaluation of the unsteady pressures being exerted on the mirror train in a coelostat turret (Fig. 1.). Additionally, the response of the pressure amplitude and frequency to changes in the internal cavity geometry were measured. Results

from this most recent test have indicated that the unsteady torque around the elevation axis of the movable upper turning mirror (UTM) is the primary contributor to vibration (Fig. 3.). This torque, although reduced in magnitude by some design modifications, remained at such high levels at forward aperture azimuth angles as to make it questionable if the device was usable at these angles (Ref 4:30). (See Fig. 2. for definition of coelostat roll and azimuth angles.) Obviously, such a viewing restriction severely limits the mission capability of a particular aircraft/laser combination.

Objective

The major objective of the research project described herein is to find a modification to the best Ames II coelostat design that will reduce the torque on the UTM at forward azimuth angles. It should be emphasized at this point that the actual level of torque that would be acceptable in a second generation airborne laser/turret arrangement is still an unknown. This limiting value will be a function of the size of the mirrors and the capability of the mirror stabilization and positioning system, both of which are not yet precisely defined. However, any torque reduction that can be achieved now will undoubtedly enhance the airborne mission capability of future, large scale lasers.

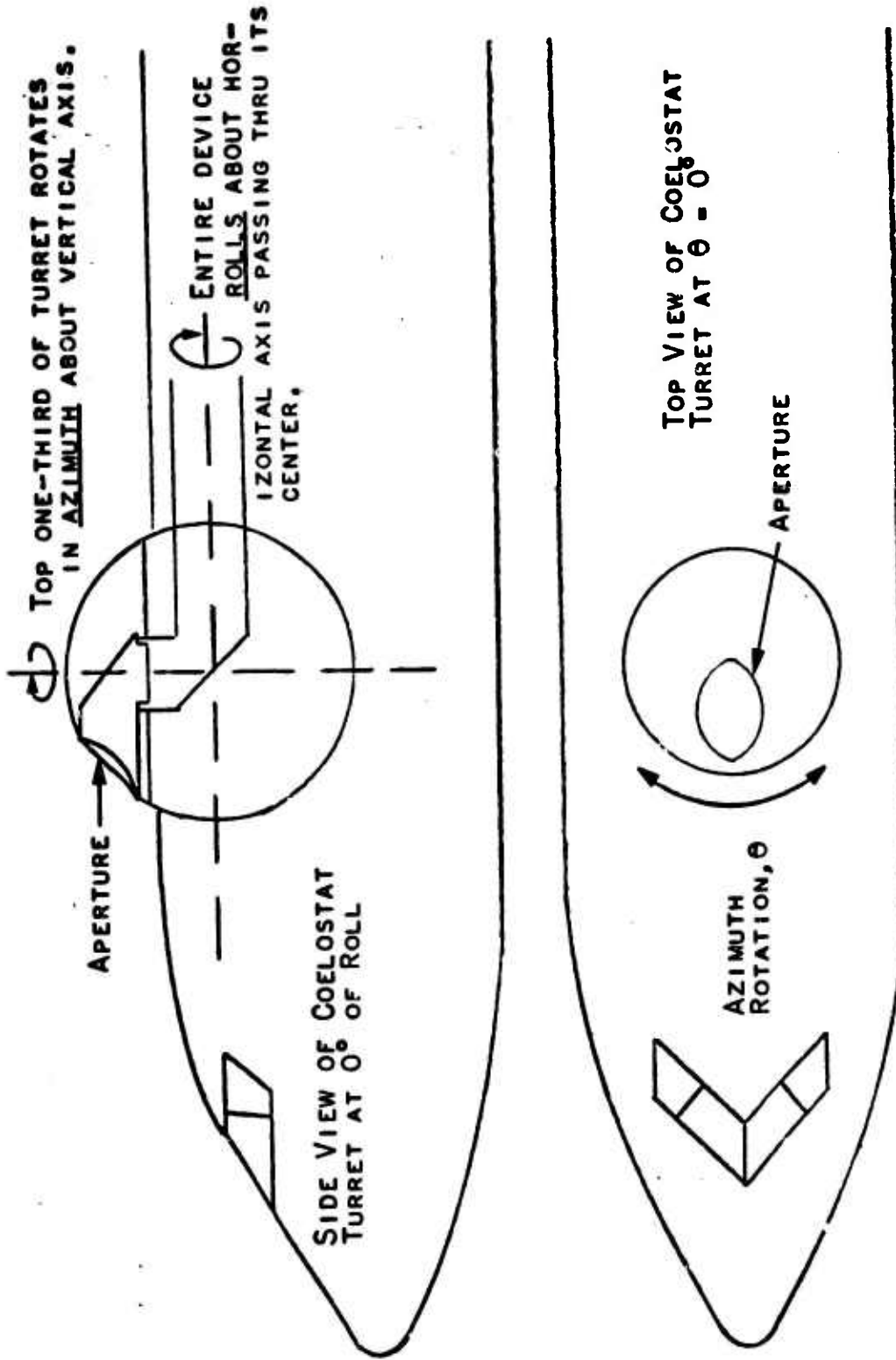


FIG. 2. DEFINITION OF ROLL AND AZIMUTH ANGLES FOR A COELOSTAT TURRET

Scope

The Ames II test indicated that the unsteady pressure response of the open cavity of a coelostat was primarily a function of the azimuth angle of the open port, defined as θ , and only weakly dependent upon the roll angle. Additionally, a zero degree roll angle was found to produce the most adverse unsteady pressure upon the UTM (Ref 4:30, 42). For these reasons this investigation utilized a model fixed at zero degrees of roll and capable of traversing 120° in azimuth.

The other test variables that define the scope of this investigation include the free stream Mach number and the model configurations. Mach numbers of .7, .85, and .95 were selected to determine the speed dependence of the cavity unsteady pressures. Model variations that were selected for the experiment are discussed in Chapter III.

Supplemental Data Collection

Although the sole objective of this test was to suppress UTM torque, the experiment also provided an excellent opportunity to survey some properties of the flow across the turret. Toward the exploitation of this opportunity, pressure taps were added to the model and data was collected on the local pressure distribution and velocity of flow over the external surface of

the coelostat. Also, through oil visualization techniques, the attached/separated pattern of this flow was recorded. The results of this data collection effort are given in Appendices D and E and discussed in Chapter V. Conclusions drawn from the data are given in Chapter VI.

II. Theory

Past wind tunnel testing has shown there are several aerodynamic processes responsible for the unsteady pressures that occur within a cavity open to free stream airflow. Rossiter (Ref 5) and Dunham (Ref 6) reported that vortex shedding off the upstream edge of an open cavity was one such process. Van Kuren concluded that unstable shock waves formed in the vicinity of a blunt protruding turret being propelled at transonic speeds were an additional source of cavity pressure fluctuations (Ref 2:2). Belik (Ref 7) noted the formation of a strong vortex at the forward base of a circular cylinder mounted to a flat plate. Van Kuren surmises such a vortex also contributes to unsteady pressures within the open cavity of a coelostat turret (Ref 4:30).

The net result of any or all such processes is to produce a time varying pressure field across surfaces within the open cavity. If such a surface is a movable mirror, the resultant unsteady force acts through a moment arm about the axis of movement to produce unsteady torques. Obviously mirror vibration will result if its positioning system is incapable of withstanding such varying torque.

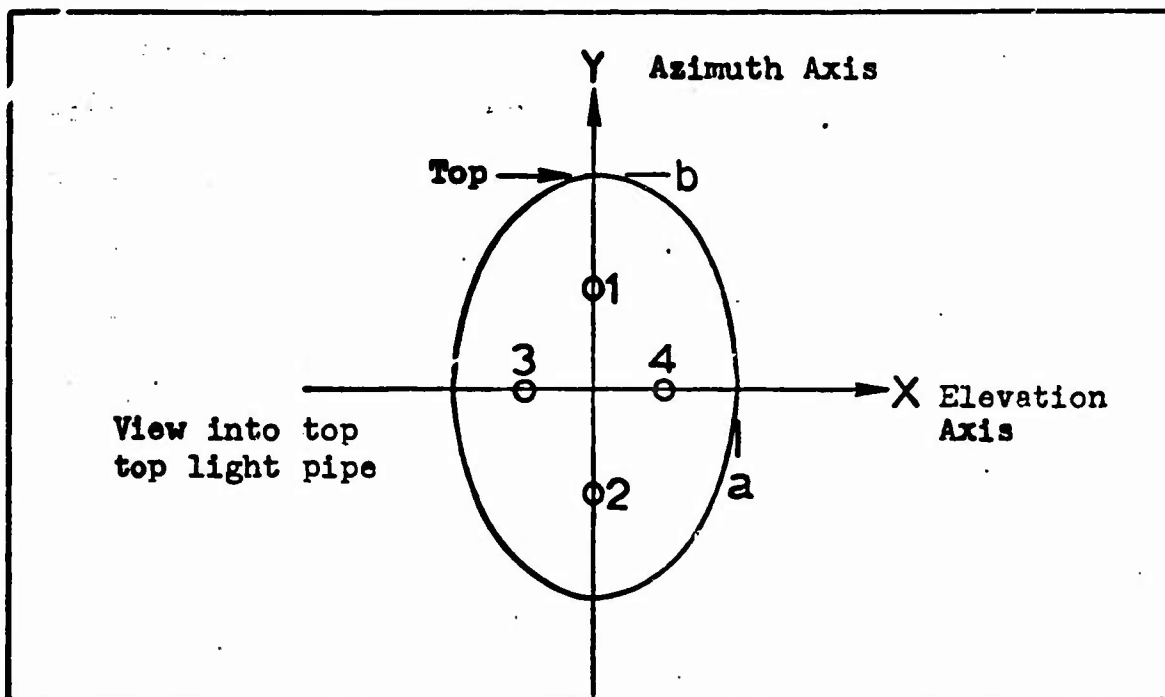
UTM Unsteady Torque

Fig. 3. UTM of Coelostat with Pressure Transducers

If the UTM of a coelostat is instrumented with four pressure transducers as shown in Fig. 3. and if it is assumed the pressures recorded by these transducers act over one half of the mirror surface, then the torque about the elevation axis (X-axis) is

$$T_{qx}(t) = P_1(t) \iint_{A/2} y dA + P_2(t) \iint_{A/2} (-y) dA \quad (1)$$

where

$$\iint_{A/2} y dA = \frac{2ab^2}{3} \quad (2)$$

Similarly, the torque about the azimuth axis (Y-axis) is

$$T_{ay}(t) = P_4(t) \iiint_{A/2} x dA + P_3(t) \iiint_{A/2} (-x) dA \quad (3)$$

where

$$\iiint_{A/2} x dA = \frac{2ba^2}{3} \quad (4)$$

For comparative analysis the root-mean-square torque given by

$$T_{rms} = \sqrt{\frac{1}{T} \int_0^T T_q^2(t) dt} \quad (5)$$

is a more meaningful figure.

Figure 4 gives a pictorial display of how the elevation T_{rms} would be determined from the output of pressure transducers 1 and 2 in Fig. 3.

Non-dimensionalizing Terms

To facilitate future comparative analysis, the data given in this report has been non-dimensionalized. Root-mean-square pressures, P_{rms} , have been made dimensionless through division by the free stream dynamic pressure, q . Root-mean-square torques, T_{rms} , have similarly been non-dimensionalized by the factor $(\pi/4)qD^3$, where D is the diameter of the turret aperture. Mass flow injection rates, \dot{m} , have also been made dimensionless through division by a factor equal to the mass flow rate of free stream flow through an area the size of the turret aperture, $\rho \pi D^2 U_\infty / 4$. In this text a bar above a symbol will be used to denote non-dimensionalized terms.

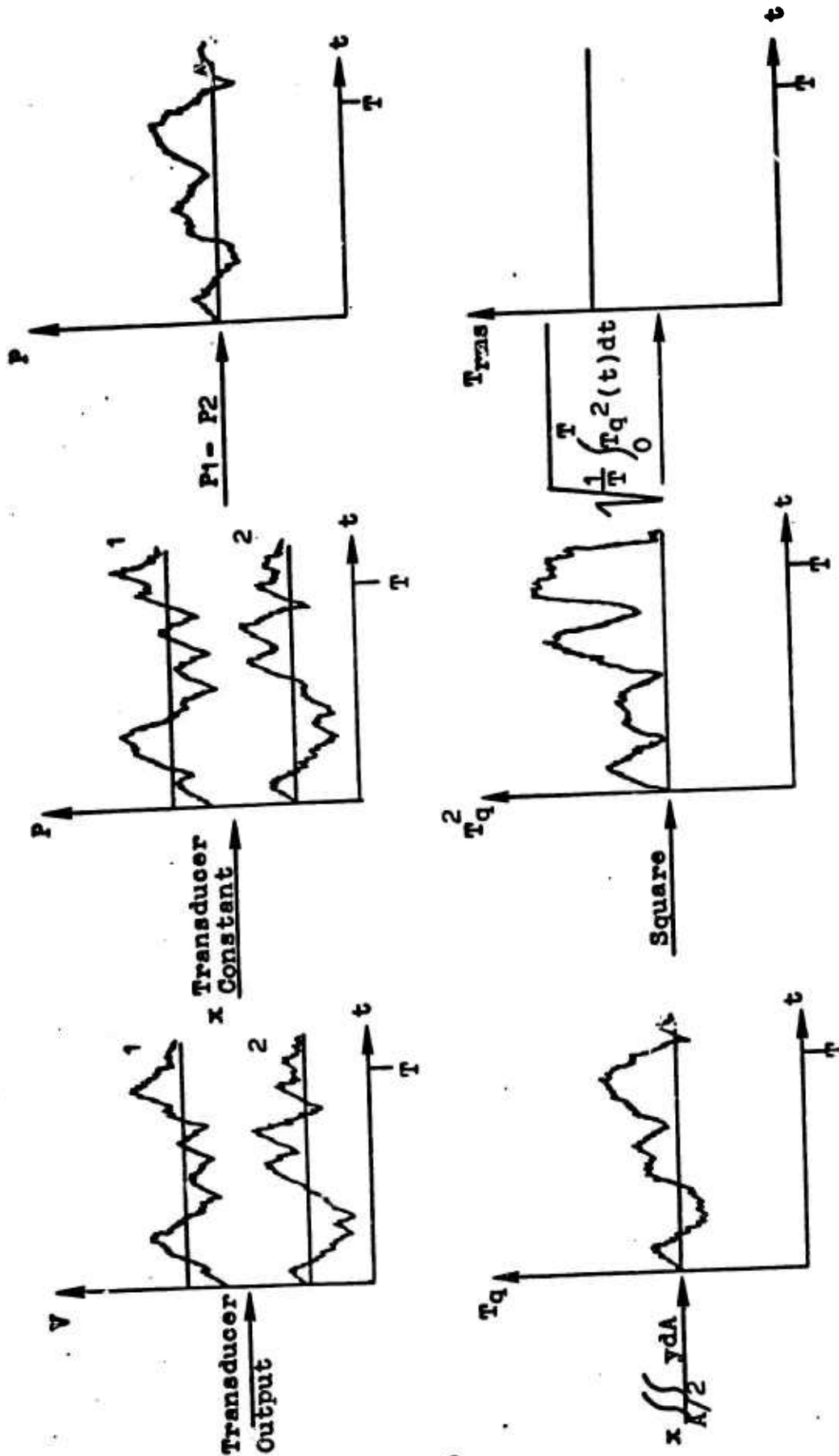


FIG. 4. Flow diagram illustrating procedure by which T_{rms} is obtained from transducer voltage signal.

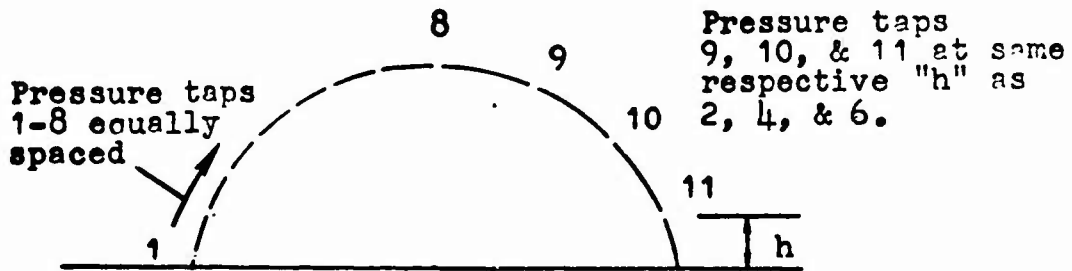
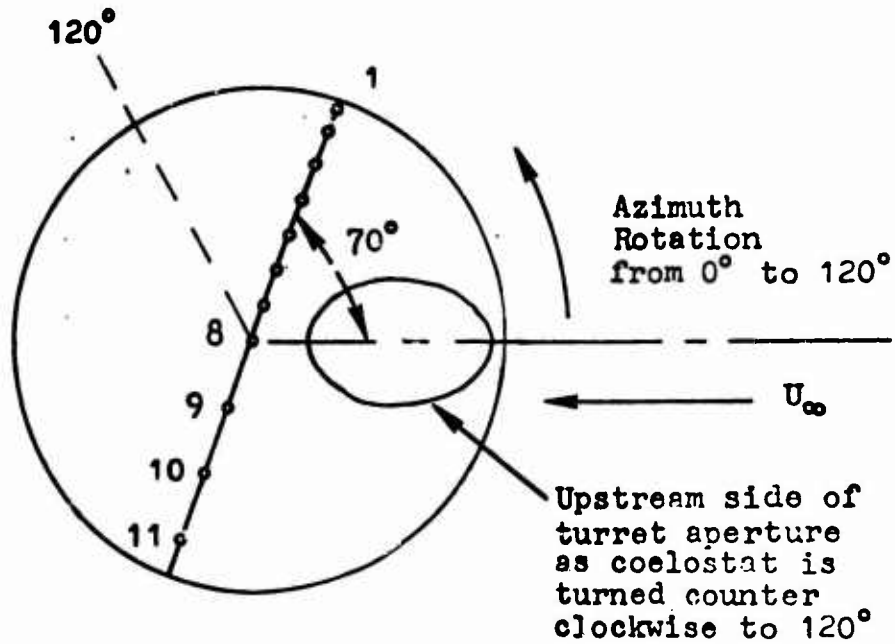
III. Description of Apparatus

Model

The coelostat model utilized in this test duplicated, in one-sixth scale, the major internal and external features of the model utilized in the Ames II test (Ref 4:7). The device was fixed at zero degrees of roll and could be remotely positioned at azimuth angles from zero degrees (forward) to 120° aft (Fig. 2). A 27 VDC motor was employed to turn the coelostat thru these angles. Attached to the azimuth gear drive of the model was a 10 turn rotary potentiometer, the output of which defined the open port position, θ . Four Kulite high frequency response pressure transducers were mounted on a fixed plane surface that simulated the UTM. The pattern of installation was as depicted in Fig 3. The physical dimensions of the model prevented the emplacement of more than four transducers on this surface. Additionally, 11 static pressure taps were positioned on top of the model as seen in Fig. 5.

The test model was built into a plate, which, when mounted in the wind tunnel, projected $1\frac{1}{2}$ inches away from the inside wall of the tunnel and into the plenum (Fig. 6). This arrangement was adopted so as to allow a thin boundary layer to form and impinge upon the model.

Top View of Turret



Side View of Pressure Tap Meridian

Fig. 5. Location of static pressure taps placed in turret. The 70° meridian was the closest the taps could be positioned to the aperture because of space limitations on the inside of the turret.

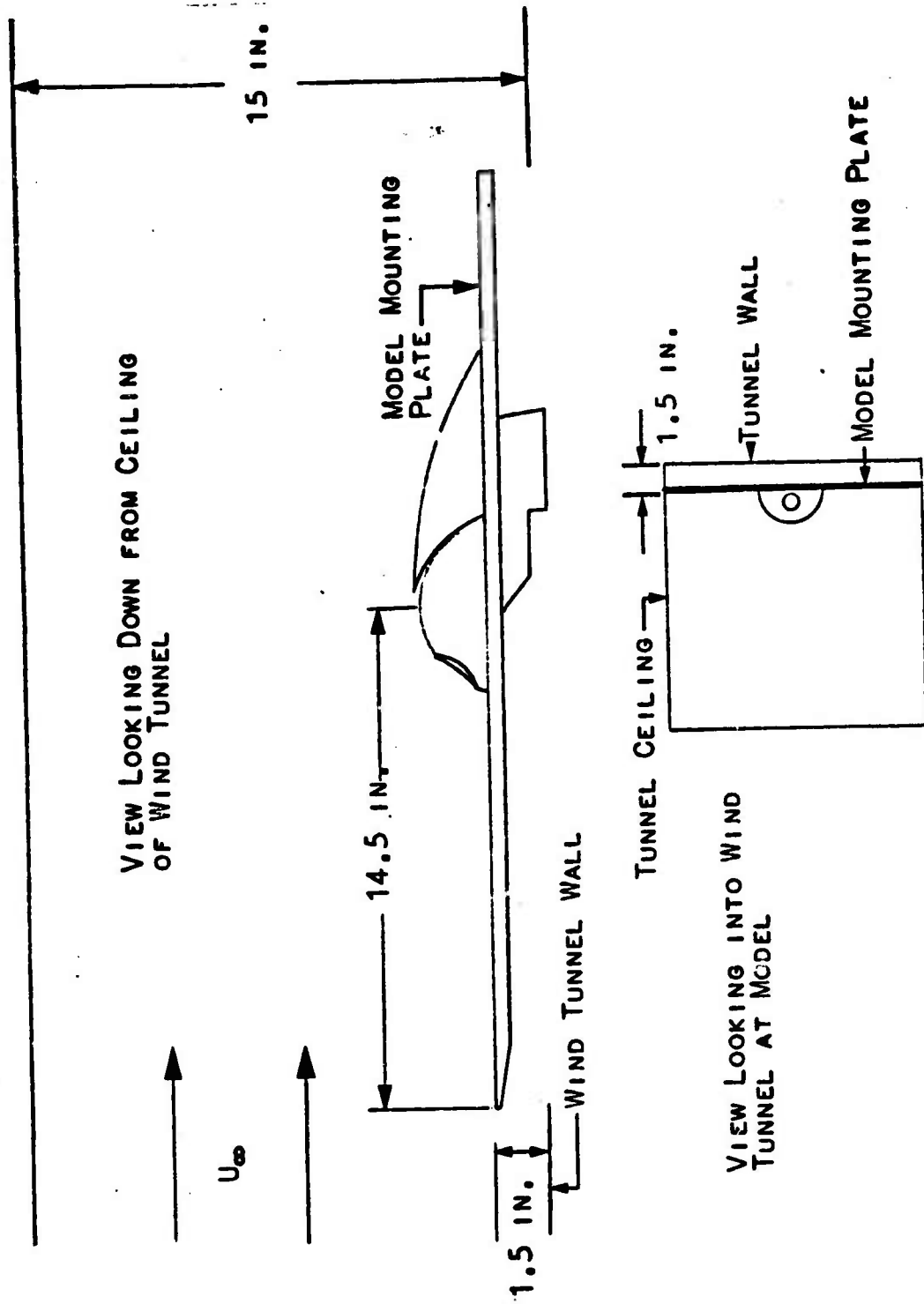


FIG. 6. ARRANGEMENT OF WALL-MOUNTED MODEL IN WIND TUNNEL

Model Configurations

Model configurations are depicted in Appendix A. The rationale behind the design of each model change is discussed in the figures. It should be noted that all model variations were empirically designed to eliminate the sources of cavity pressure fluctuations that were identified in Chapter II. Tables I and II give a reference summary of model modifications. These tables divide the model configurations into two functional categories, passive and active. This is done to distinguish between modifications that are complete in themselves such as fairings and fences and those that employ accessories to operate such as blowing and suction modifications. Models 4, 7, and 13, near duplicates of other listed configurations, were deleted from the report in the interest of brevity.

Wind Tunnel

The USAF Flight Dynamics Laboratory Trisonic Wind Tunnel configured with a 15 inch X 15 inch slotted transonic test section was utilized in this investigation. Complete details on this facility can be found in Ref 9.

Pressure Transducers

Kulite model XCGL-14-093-25 high frequency response, variable reference pressure transducers were installed in

Table I

Passive Model Configurations















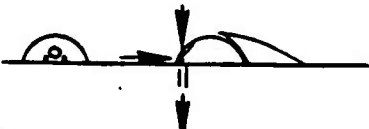

<u>Model No.</u>	<u>Description</u>	
1	Coelostat turret without aft fairing.	
2	Base line, turret with aft fairing.	
3	Configuration 2 with bottom light pipe truncated.	
5	Configuration 2 with forward porous fence 8 in. from turret center.	
6	Configuration 2 with forward porous fence 5 in. from turret center.	
8	Configuration 2 with forward conical fairing.	
9	Configuration 2 with .33 in. aperture lip fence.	
10	Configuration 2 with bottom light pipe relief.	
11	Configuration 2 with large forward splitter plate.	
14	Configuration 2 with non-porous top light pipe.	

Table II

Active Model Configurations

<u>Model No.</u>	<u>Description</u>	
12	Configuration 2 with mass flow injection at rear of bottom light pipe.	
15	Configuration 2 with blowing through bottom perimeter holes and first 2 rows of holes in top light pipe.	
16	Configuration 15 except bottom perimeter holes closed.	
17	Configuration 2 with blowing through first row of holes in top light pipe.	
18	Configuration 17 except with suction applied and bottom perimeter holes open.	
19	Configuration 17 with blowing also through all perimeter holes except bottom, upstream hole.	

the model to collect unsteady pressure data. These instruments are self-compensating for temperature and are responsive to frequency inputs up to 20 KHz.

RMS Meters

The output signals of the pressure transducers were routed through Hewlett-Packard model 3400A rms volt meters. These instruments utilized a two second integration time to obtain a root-mean-square voltage. By multiplying this voltage by the transducer constant, pressure/volt, the root-mean-square of the unsteady pressure, P_{rms} , was obtained.

Tape Recorder

Unsteady pressure data was recorded by an Ampex model CP 100, 14 channel, FM, tape recorder. This device has a maximum frequency response of 10 KHz and a maximum input voltage limit of 1.4 volts/channel. Input signals to the recorder were monitored on a Fourier Analyzer and oscilloscope to insure they were within frequency and voltage limits.

Flow Meter

In those model variations employing mass flow injection, a standard, flange tapped, orifice plate flow meter was used to determine \dot{m} values. This device consisted of a .25 inch diameter, square edged orifice

GAE/AE/75J-6

mounted in a 2 inch inside diameter pipe. Pressure and temperature data from the flow meter instrumentation was input to a Hewlett-Packard model 9810A calculator which computed flow rates.

IV. Experimental Procedures

Figure 7 depicts the flow diagram of the on-line and post test data collection procedures that were utilized in this experiment.

Wind Tunnel Calibration

Prior to the recording of any test data, the optimum wind tunnel diffuser flap and side wall porosity settings were first determined. This was accomplished by manipulating these settings until static pressures measured on the forward and aft portions of the model plate were equal to the free stream static pressure.

Test Phases

Three types of test data were recorded during three different phases of the experiment. First, measurements of the static pressures across the top of the coelostat were made. Also during this phase the thickness of the boundary layer approaching the model was measured by a three probe rake. Next, unsteady pressure data was collected from the transducers located within the model. The final phase of the test was the oil flow visualization experiment in which the flow patterns across various model configurations were photographically recorded.

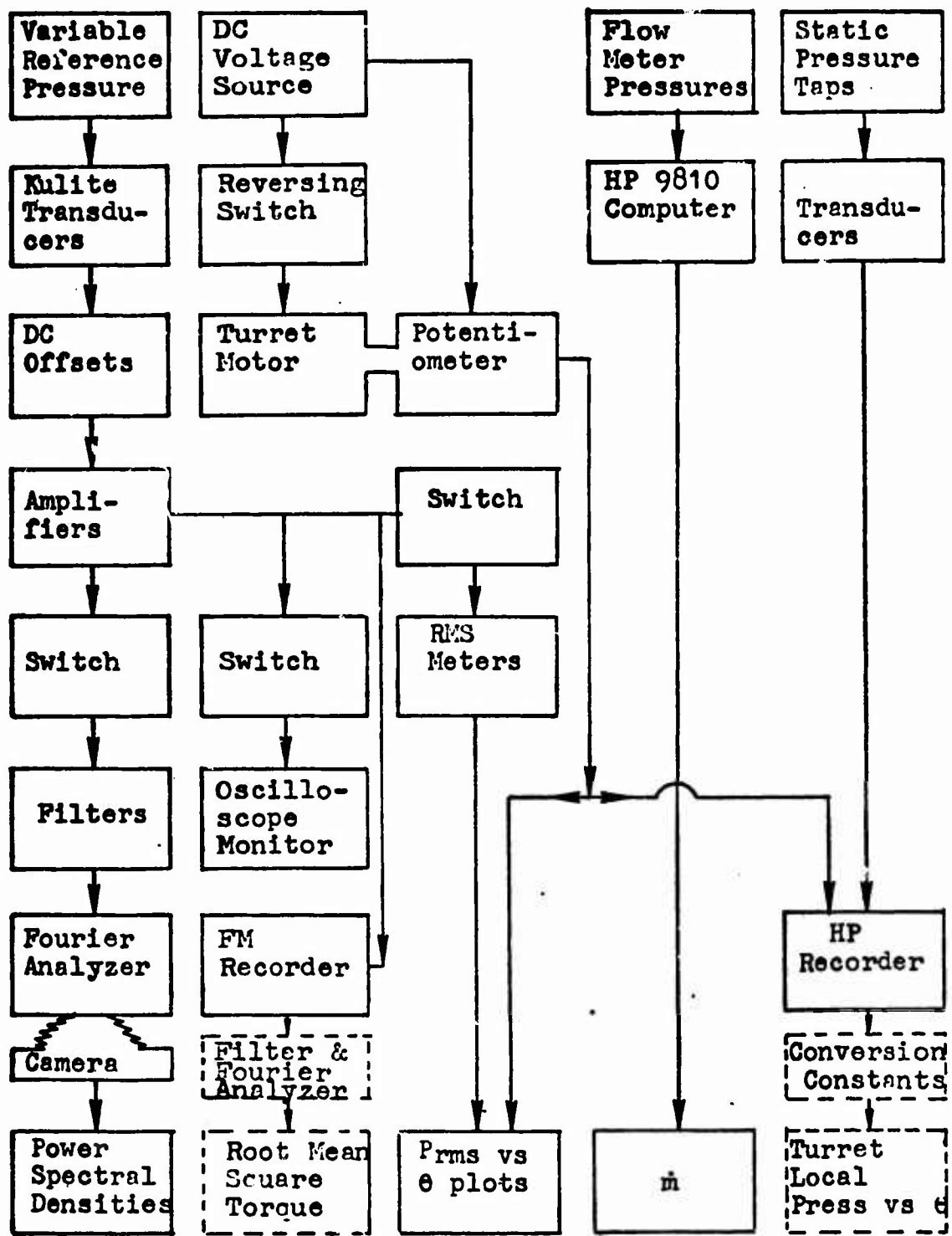


Fig. 7. Data collection flow diagram. Solid boxes enclose those procedures that were accomplished during the test. Dashed boxes indicate post test analysis procedures.

Phase I - Turret Steady Pressures

The outputs of the 11 static pressure taps across the top of the model were recorded as the coelostat was rotated in azimuth from 0 to 120 degrees. This data was collected for free stream Mach numbers of .7, .85, and .95, with and without the aft fairing installed.

A three probe rake, installed $8\frac{1}{2}$ in. aft of the leading edge of the model mounting plate and $3\frac{1}{2}$ in. forward of the turret was utilized to determine the thickness of the boundary layer approaching the model. An analysis of this data can be found in Appendix B.

Phase II - UTM Unsteady Pressures

Though the primary purpose of this phase of the experiment was to determine and minimize the torque being exerted about the elevation and azimuth axes of the UTM, limitations on test instrumentation prohibited the on-line measurement of these values. However, analysis of the Ames II torque data indicated that the root-mean-square of the unsteady pressure signals, P_{rms} , were a reliable indication of the relative torque magnitude. This data showed that a reduction in the P_{rms} signals invariably resulted in a reduction in torque. Since wind tunnel instrumentation did allow real time recording of transducer P_{rms} signals, phase II of the experiment was aimed at the on-line analysis of these values, while post test data eval-

uation was made to determine torque magnitudes. A description of the procedures utilized in this test phase is given in the following paragraphs.

The output of transducers 8 and 10, those about the elevation axis of the UTM, were routed through RMS meters, then to a two pen, analog, X-Y plotter. The output of the model potentiometer was also input to this plotter. After a model configuration and Mach number was established, the coelostat would be rotated from 0 to 120 degrees and a plot of P_{rms} vs azimuth angle would be generated for these transducers. At this point the output of transducers 9 and 11, those about the azimuth axis of the UTM, would be switched to the plotter and a trace of their P_{rms} values would be made as the coelostat was turned back to 0 degrees. Analysis of these plots were then made to determine those azimuth angles at which P_{rms} values were highest and/or differed significantly from base line values. The coelostat would then be positioned at these angles and a one minute tape recording of the output of all pressure transducers would be made.

It should be noted at this point that these procedures were first utilized while model 2, i.e., the base line model configuration was installed in the wind tunnel. Plots of the outputs of transducers 8 thru 12 vs azimuth angle were obtained for this model at Mach numbers of .7, .85 and

.95. In subsequent model configurations plots of transducer outputs were made at higher Mach numbers only if an improvement in P_{rms} values were noted at Mach=.7. This procedure was strictly a time conserving measure to allow data to be collected on a greater number of model variations at a minimum of one Mach number. Also, to validate the repeatability of the experimental procedures, transducer output plots for the base line model configuration were accomplished at the completion of this phase of the test. Comparison of these plots with the original Model 2 plots indicated there was no change in values.

While data tape recordings were being made, the power spectral densities (PSD) of the output of the transducers were observed and photographically recorded.

Following the completion of the experiment the tape recorded unsteady pressure data was utilized to determine UTM torque values. Transducer signals were routed through filters which were set to pass data of the range 80 to 10000 Hz. The lower limit of 80 Hz was selected to eliminate low magnitude 60 Hz noise signals that were superimposed on the data signal. The filtered information was then input to a computer that multiplied each signal by a constant which represented the conversion from voltage to torque. The difference of the signals, representing the net UTM torque, was then computed and displayed.

Phase III - Oil Flow Visualization

The procedure utilized in this phase of the experiment was standard for wind tunnel oil flow visualization. Prior to its installation a mixture of STP oil treatment, oleic acid and titanium dioxide would be painted onto the model. After a delay of approximately 10 minutes at a particular Mach number, this oil would be arranged into the pattern of air flow across the model. A Polaroid camera would then photographically record these patterns.

V. Results

In this chapter the results of the three primary areas of investigation, i.e., UTM unsteady torque, turret static pressure distribution and oil flow visualization, will be addressed separately.

UTM Unsteady Torque

Figures 8 thru 11 portray the UTM torque for forward θ as a function of model configuration. As is apparent from these displays, a significant reduction in torque magnitude can be achieved through the use of some active model modifications. Specifically, mass flow injection at the rear of the bottom light pipe (Model 12) can reduce azimuth and elevation torque by approximately 50% of base line values. Also, mass flow injection at the forward lip of the turret aperture (Model 16) can lower torque to 33% of base line values for $\theta = 0^\circ$. Other blowing and suction modifications reduced torque by lesser amounts.

The passive model modifications consisting of various external fairings were almost totally ineffective. Indeed, in most cases these fairings were noted to amplify rather than dampen UTM torques.

The physical processes that are responsible for these results can not be exactly determined from the

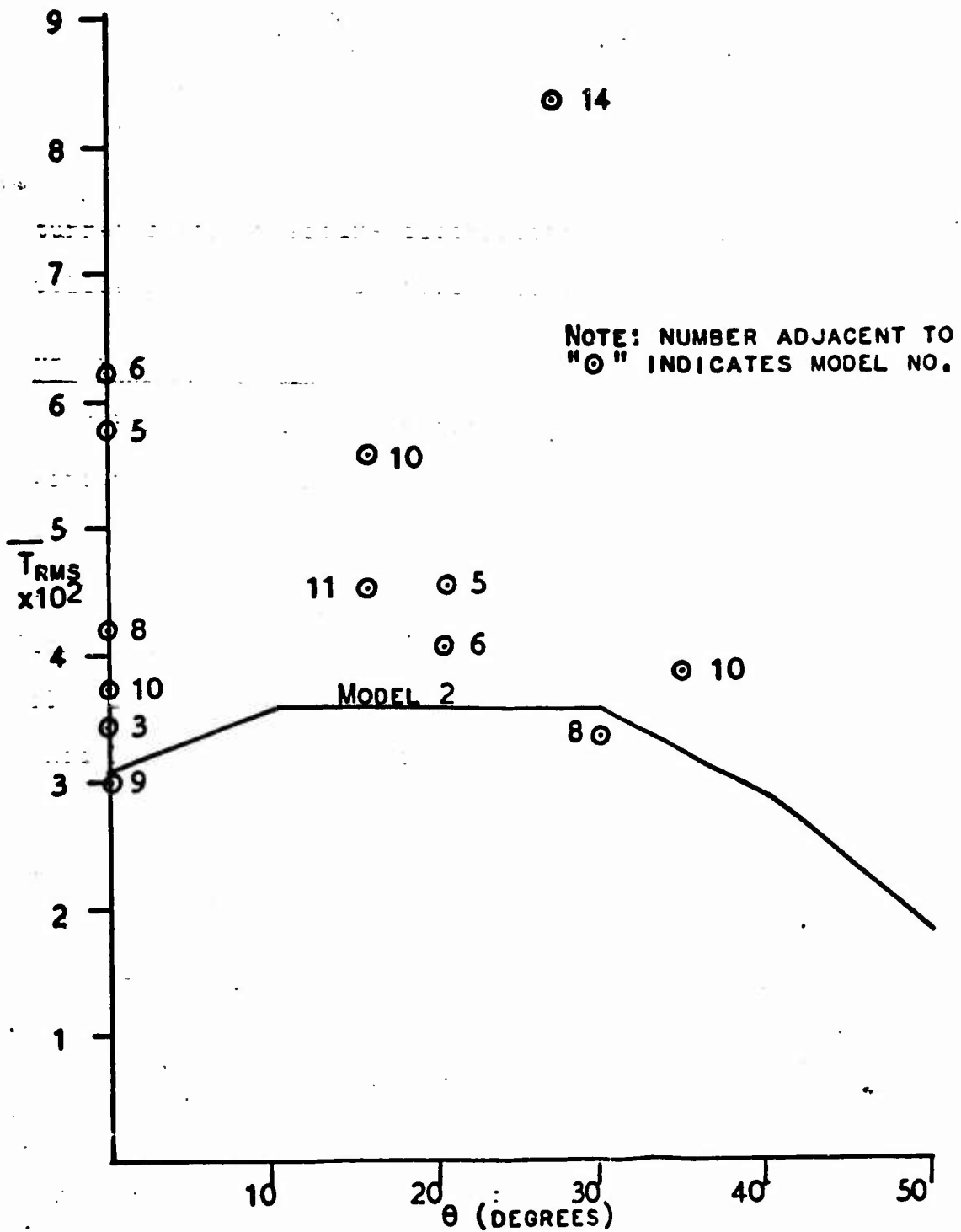


Fig. 8. NON-DIMENSIONALIZED RMS TORQUE ABOUT THE ELEVATION AXIS OF THE UTM RESULTING FROM VARIOUS PASSIVE MODEL MODIFICATIONS COMPARED TO BASE LINE (MODEL 2) ELEVATION TORQUE AT MACH = .7

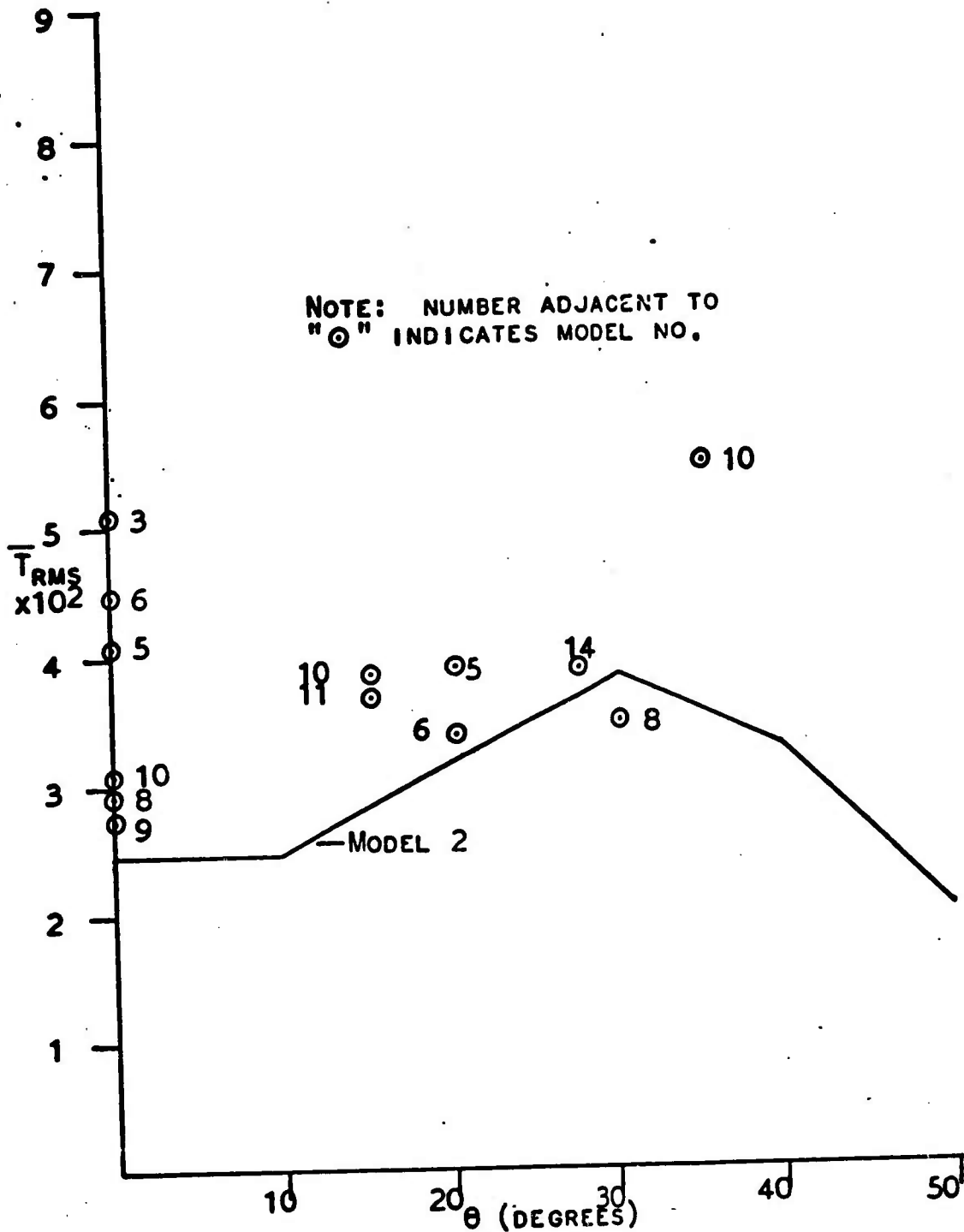


Fig. 9. NON-DIMENSIONALIZED RMS TORQUE ABOUT THE AZIMUTH AXIS OF THE UTM RESULTING FROM VARIOUS PASSIVE MODEL MODIFICATIONS COMPARED TO BASE LINE (MODEL 2) AZIMUTH TORQUE AT MACH = .7

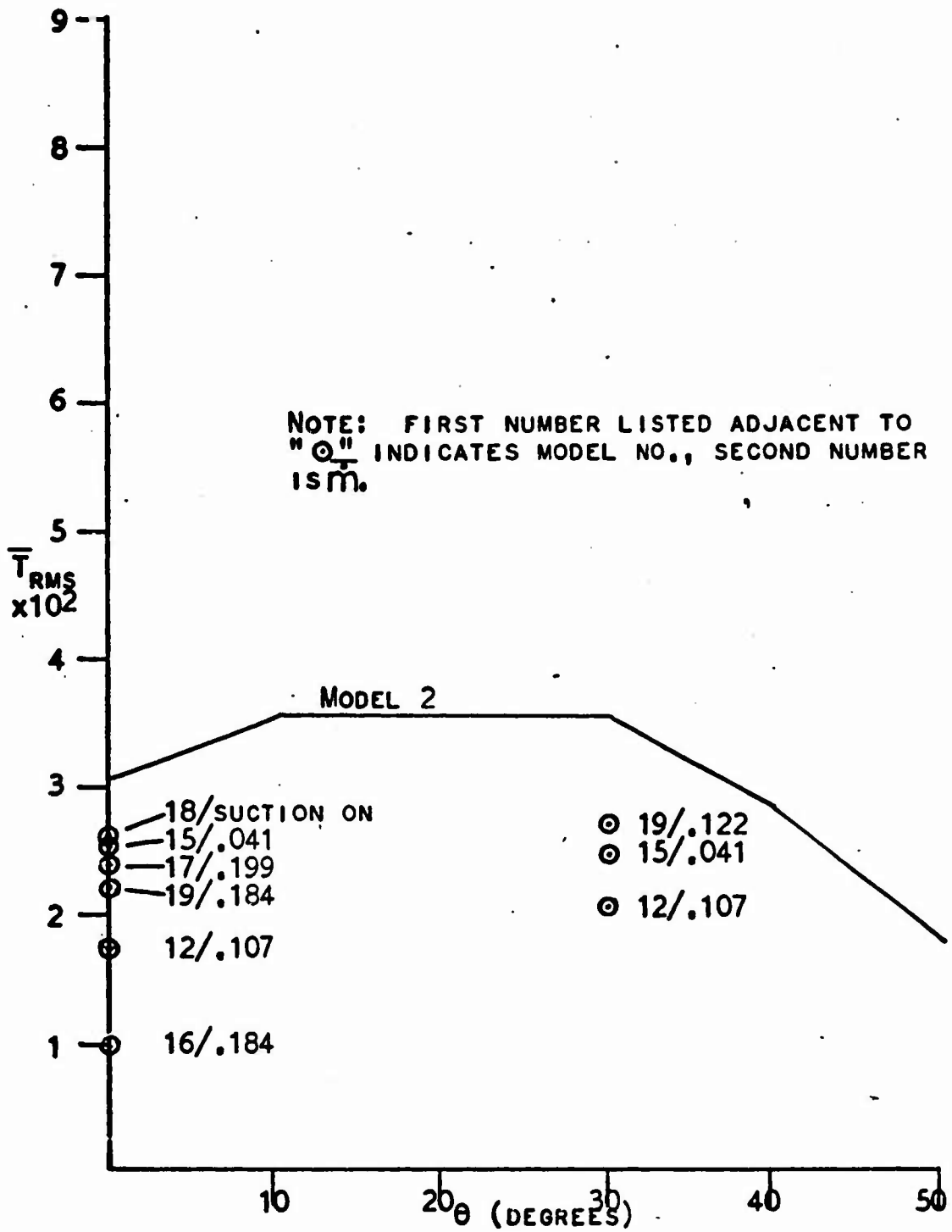


FIG. 10. NON-DIMENSIONALIZED RMS TORQUE ABOUT THE ELEVATION AXIS OF THE UTM RESULTING FROM VARIOUS ACTIVE MODEL MODIFICATIONS COMPARED TO BASE LINE (MODEL 2) ELEVATION TORQUE AT MACH = .7

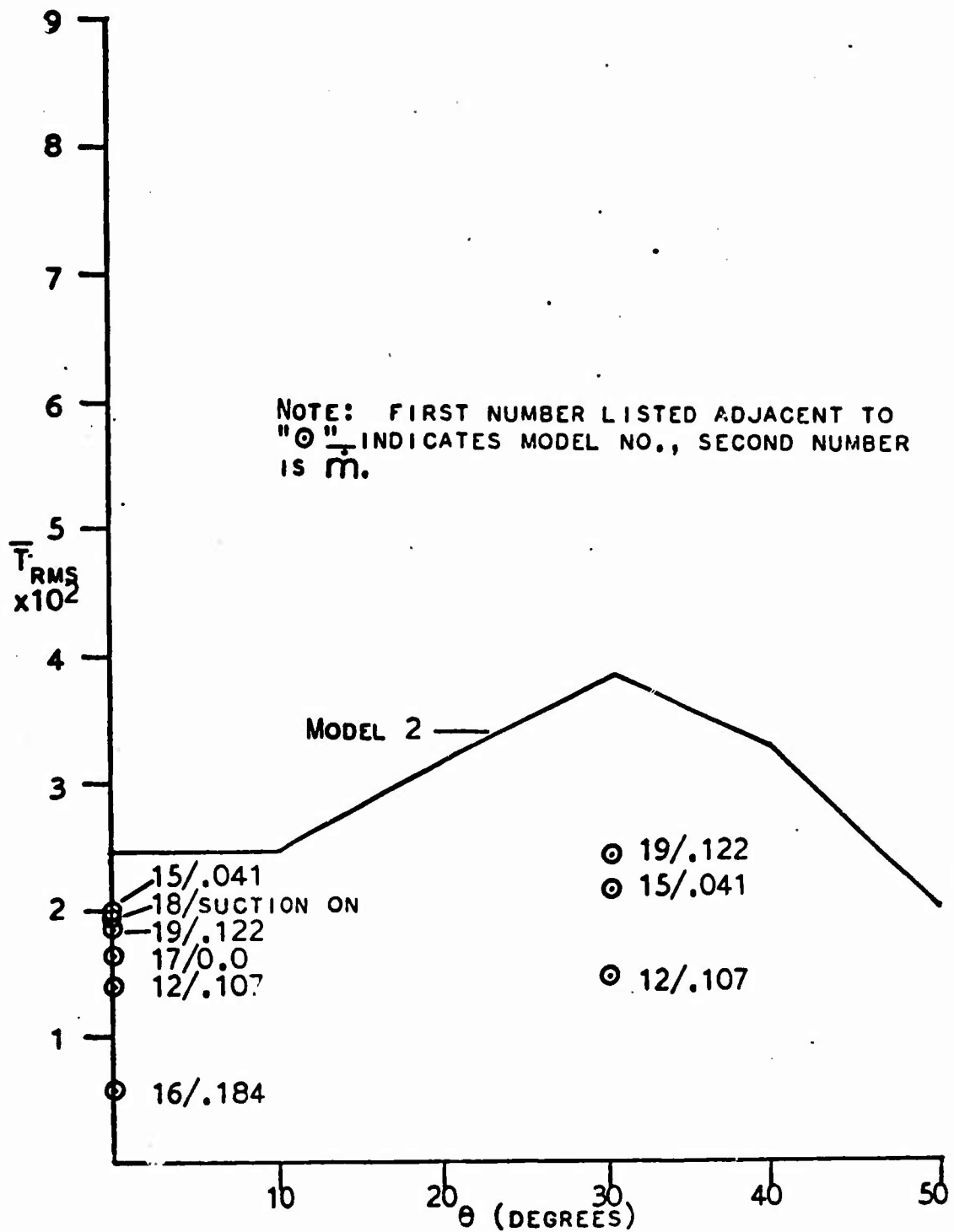


FIG. 11. NON-DIMENSIONALIZED RMS TORQUE ABOUT THE AZIMUTH AXIS OF THE UTM RESULTING FROM VARIOUS ACTIVE MODEL MODIFICATIONS COMPARED TO BASE LINE (MODEL 2) AZIMUTH TORQUE AT MACH = .7

data collected. It would appear, however, that the pronounced success of Models 12 and 16 is due to the diversion of high energy air away from the turret opening (Fig 12). Model 16 was more efficient in this respect

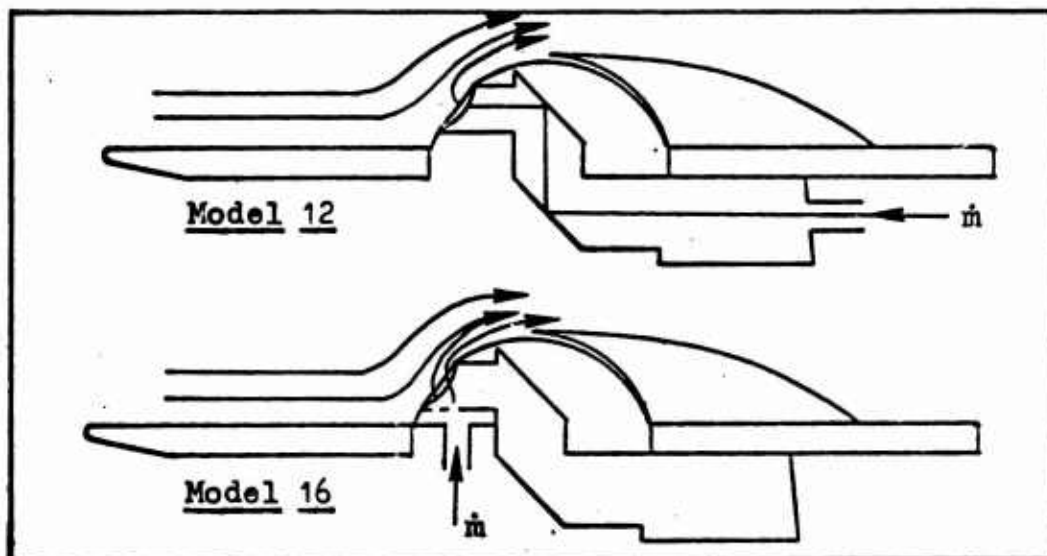


Fig. 12. Diversion of Approaching Flow by Mass Injection

since it imparted a definite upward velocity to the approaching fluid. Also, it should be noted that in Model 12 the impingement of injected air upon the UTM may, of itself, introduce some component of unsteady torque.

The variations in the Model 12 and 16 UTM torques with \bar{m} (Figs 13 & 14) suggest that limits exist on the torque damping capabilities of these models. The real time analysis of Model 12 UTM unsteady pressures showed there was little effect on these pressures (and most probably on torque also) as \bar{m} was increased above .107. Evidently, at these higher \bar{m} values, any reduction in

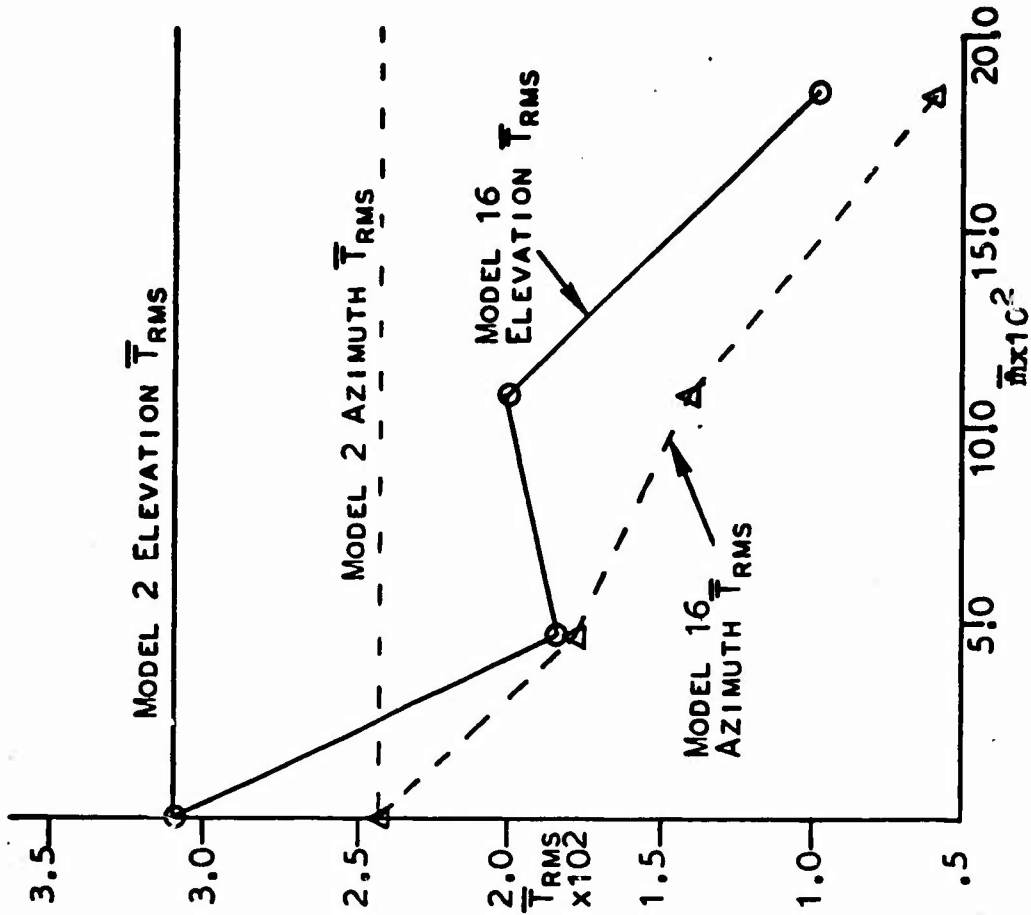


FIG. 14. COMPARISON OF UTM TORQUES FOR MODELS 2 & 16 FOR $\theta=0^\circ$ AND MACH=.7

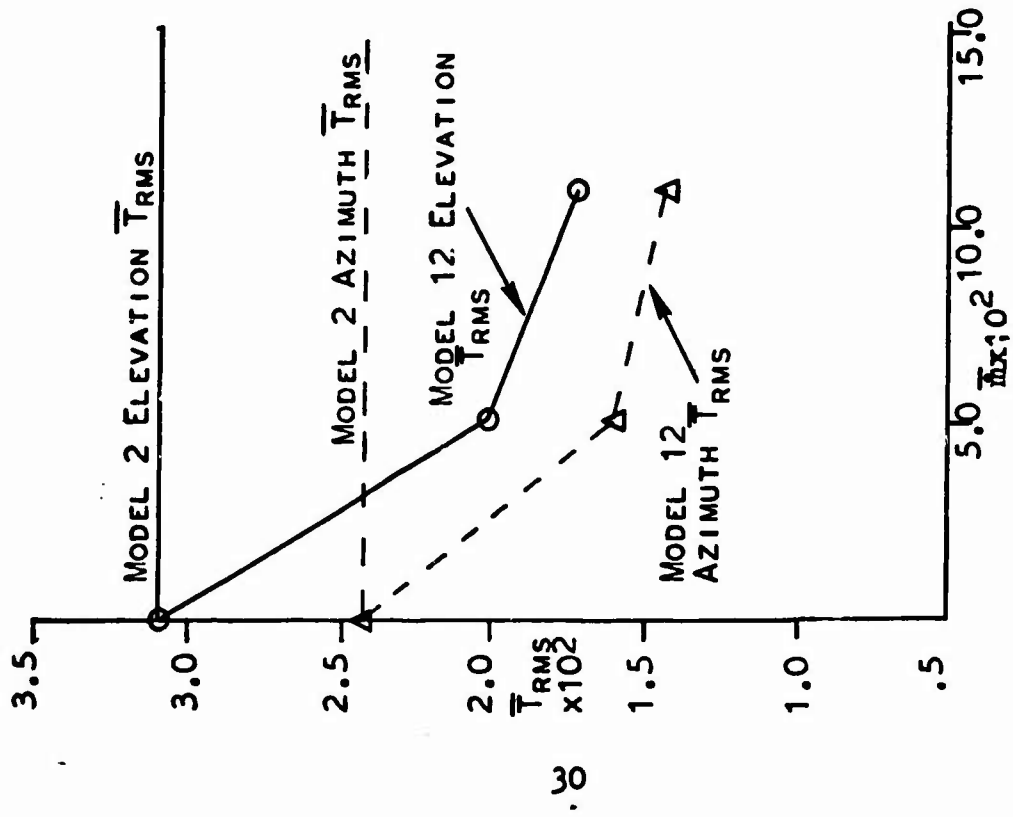


FIG. 13. COMPARISON OF UTM TORQUES FOR MODELS 2 & 12 FOR $\theta=0^\circ$ AND MACH=.7

torque achieved through the diversion of more air away from the aperture is offset by an increase in torque induced by the impact of injected flow on the UTM. In Model 16 however, reductions in torques were still being recorded at the maximum \bar{m} that could be attained with the experimental apparatus. It appears that Model 16 would be limited in its torque reducing capability by the mass flow rate that could be delivered by an aircraft engine bleed air system.

Tests of Model 3, representing a possible configuration for future coelostat turrets, revealed a significant rise in P_{rms} and azimuth torque due to the truncation of the bottom light pipe. This result is indicative of an internal geometry that is inducing a resonance condition.

The reader is referred to Appendix C for more detailed information relating to the unsteady pressures and torques on the UTM.

A concluding remark is in order concerning the accuracy of the UTM torque data presented in this report. It should be recalled that only four pressure transducers could be installed on the UTM. This necessitated that some assumption be made on the pressures being exerted on those portions of the mirror not instrumented with transducers. The assumption adopted was that each

transducer recorded the unsteady pressure across one half of the UTM. Obviously, this introduces an unknown error into the results. However, some insight into the acceptability of this assumption can be gleaned from a comparison of torque data on those model configurations common to both this test and the Ames II test (Table III). (The Ames II model was instrumented with eight UTM transducers.) First, this comparison shows that the order

Table III

UTM Elevation Torque
Compared for Similar Models

Model Numbers for Similar Configurations		Description	Maximum Elevation Torques x 10 ² (in-lbs)	
This Test	Ames II		This Test	Ames II (Scaled)
2	11	Porus top light pipe with foam	8.4	6.0
9	12	Aperture lip fence	7.2	5.1

of magnitude of the torques is comparable. Additionally, the percentage difference in torque magnitude between Models 9 and 2 and Ames II Models 12 and 11 are nearly equal at 17% and 18% respectively. Also the variation in torque with θ and Mach number for similar models was found to be coincident. These a posteriori

observations tend to justify the aforementioned assumption. Finally, it should be noted that any error induced by the assumption will be constant and as such should not jeopardize the comparative evaluation of various model configurations.

Turret Pressure Distribution

Data concerning this area of investigation can be found in Appendix D. Figures 15 and 16 are typical plots of the turret flow C_p and Mach number as a function of the local angle to U_∞ . Examination of these traces reveal that the presence of the aft fairing had only a small effect on the properties of flow across the turret. The widest deviations noted in measurements on the two models occurred as the pressure tap meridian was turned under the aft fairing. Here the C_p was higher than that measured when no fairing was installed.

The results of this portion of the experiment also indicated that the local flow velocities across the turret are significantly higher than the velocities predicted by the theory of incompressible flow about a sphere. This could be the result of the fact that the coelostat configuration is approximating a highly tapered, 37% thick airfoil. It has been established that some thinner airfoils exhibit the same phenomenon, i.e., lower coefficients of pressure and higher local flow

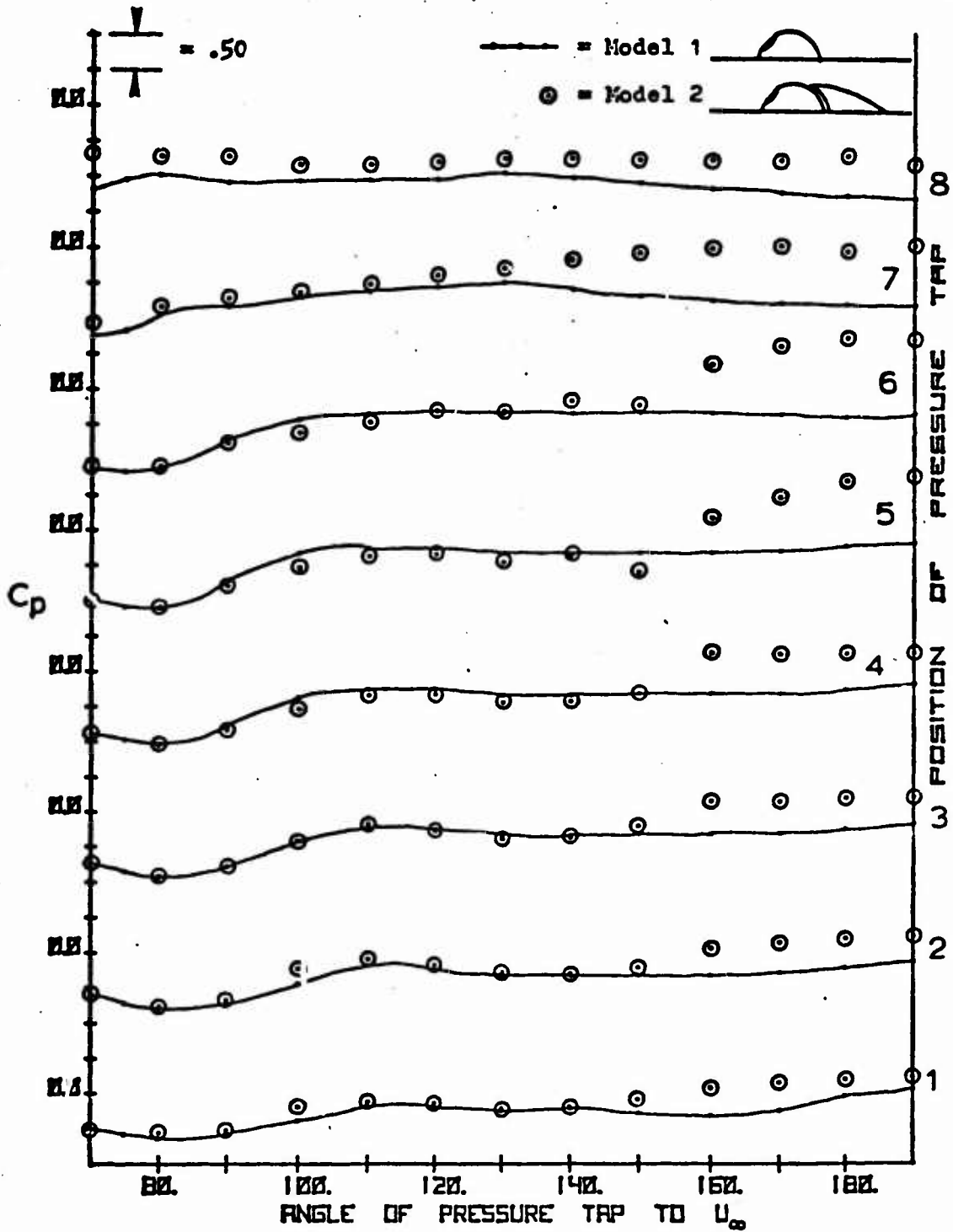


FIG. 15. COMPARISON OF LOCAL TURRET FLOW C_p WITH AND WITHOUT THE AFT FAIRING INSTALLED WITH FREE STREAM MACH = .7. SEE PAGE 11 FOR PRESSURE TAP LOCATION.

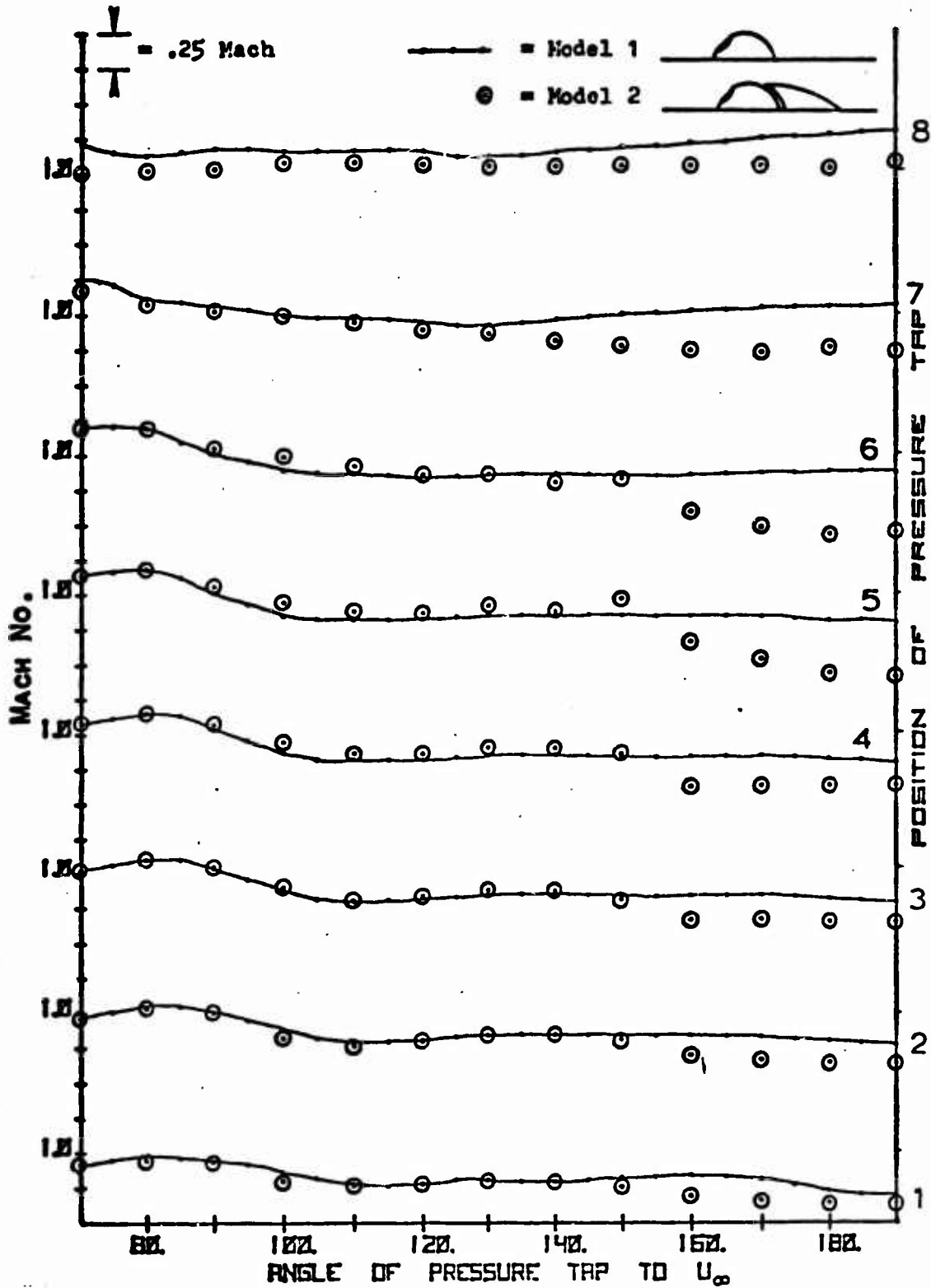


FIG. 16. COMPARISON OF LOCAL TURRET FLOW MACH WITH AND WITHOUT THE AFT FAIRING INSTALLED WITH FREE STREAM MACH = .7. SEE PAGE 11 FOR PRESSURE TAP LOCATION.

velocities at compressible speeds than those predicted by incompressible theory (Ref 10:256).

Figures 17 thru 19 depict the effect of the turret aperture on the local flow C_p . The arrangement of the pressure taps limited this comparison to angles of 70° thru 110° ($\theta = 0^\circ$ thru 40° , refer to Fig 20). It can be seen that from approximately 90° rearward there is an increase in the local C_p of flow downstream of the aperture over that which is unaffected by the opening. However, the differences that are noted from 90° to 110° tend to become less pronounced as the Mach number is increased. It is probable that this result is a function of the point at which flow separates from the turret. Figures 79 and 80 depicting oil flow patterns for Mach = .85 and .95, show that static pressure measurements made downstream of about 90° will be in an area of separated flow. Thus, any effect of the upstream aperture would probably be masked by the high levels of turbulence in this area. However at Mach = .7 the line of flow separation extends well past the 90° meridian (Fig 21) and static pressure measurements to 110° would most likely record the effects of the upstream turret aperture.

Oil Flow Visualization

Appendix E contains drawings of observed oil flow

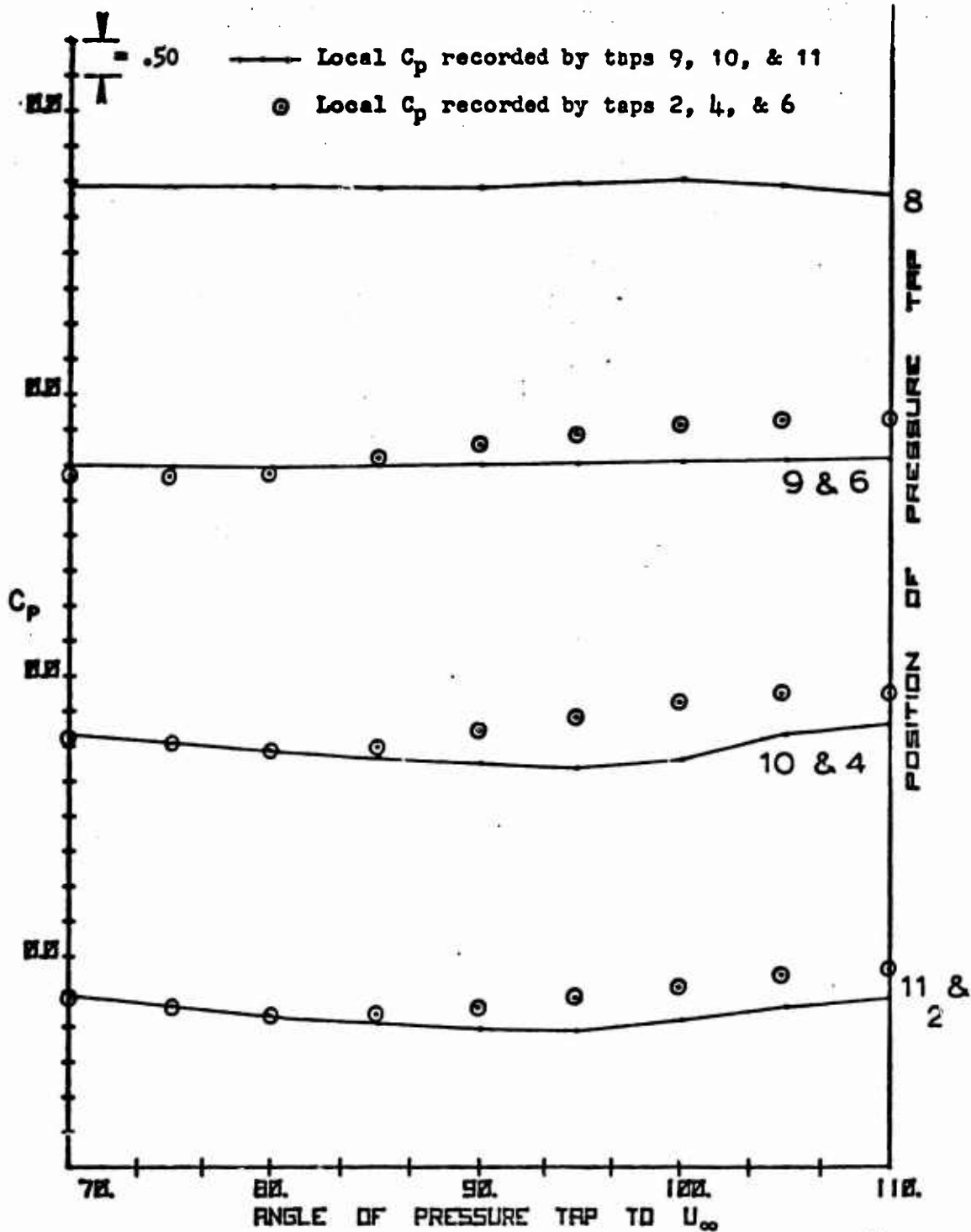


FIG. 17. COMPARISON OF LOCAL TURRET FLOW C_p MEASURED 70° DOWNSTREAM OF APERTURE (PRESSURE TAPS 2, 4, & 6) TO LOCAL TURRET FLOW C_p MEASURED WITHOUT AN UPSTREAM APERTURE (PRESSURE TAPS 9, 10, & 11) FOR MODEL 1, FREE STREAM MACH = .7. SEE PAGE 11 FOR PRESSURE TAP LOCATION.

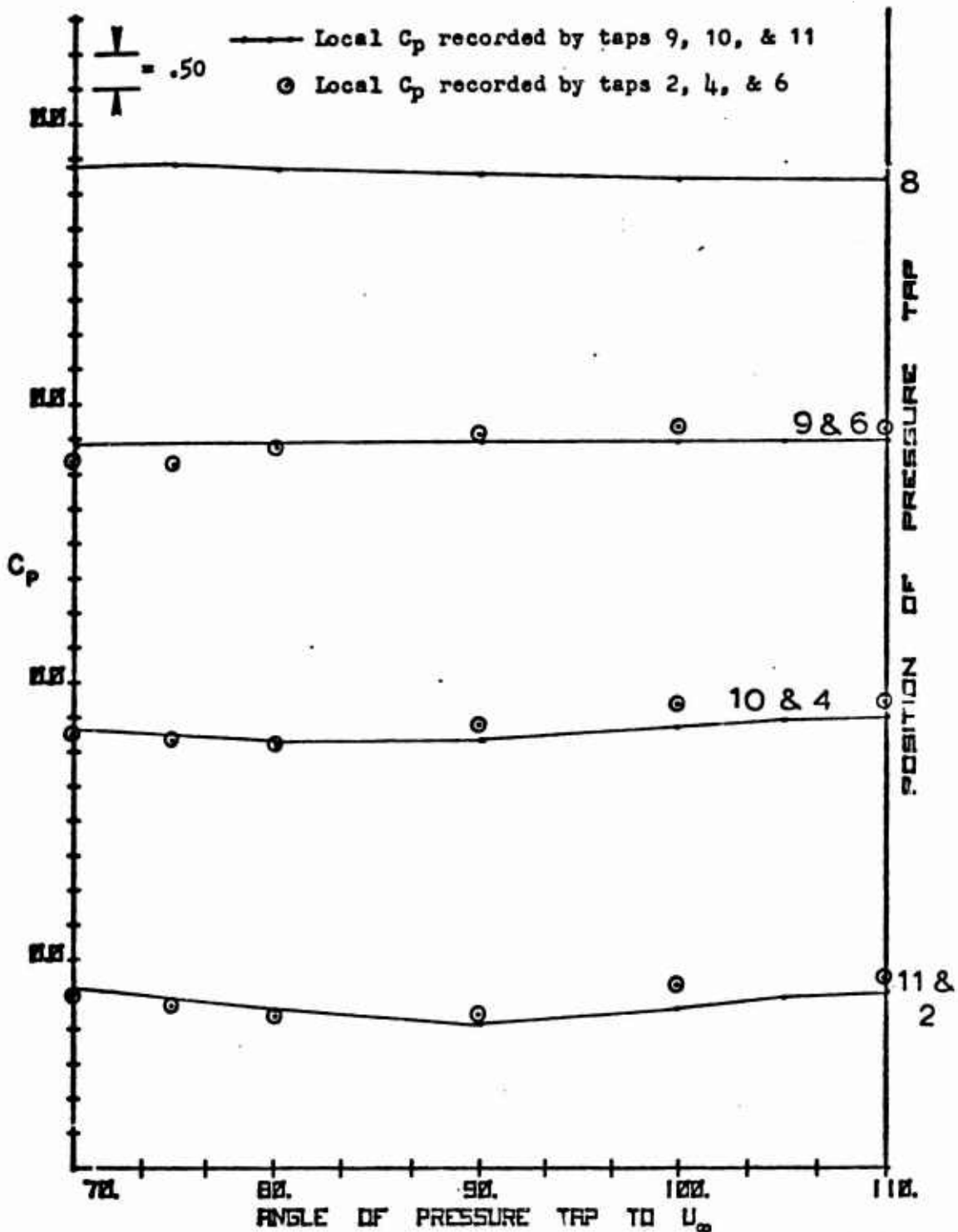


FIG. 18. COMPARISON OF LOCAL TURRET FLOW C_p MEASURED 70° DOWNSTREAM OF APERTURE (PRESSURE TAPS 2, 4, & 6) TO LOCAL TURRET FLOW C_p MEASURED WITHOUT AN UP-STREAM APERTURE (PRESSURE TAPS 9, 10, & 11) FOR MODEL 1, FREE STREAM MACH = .85. SEE PAGE 11 FOR PRESSURE TAP LOCATION.

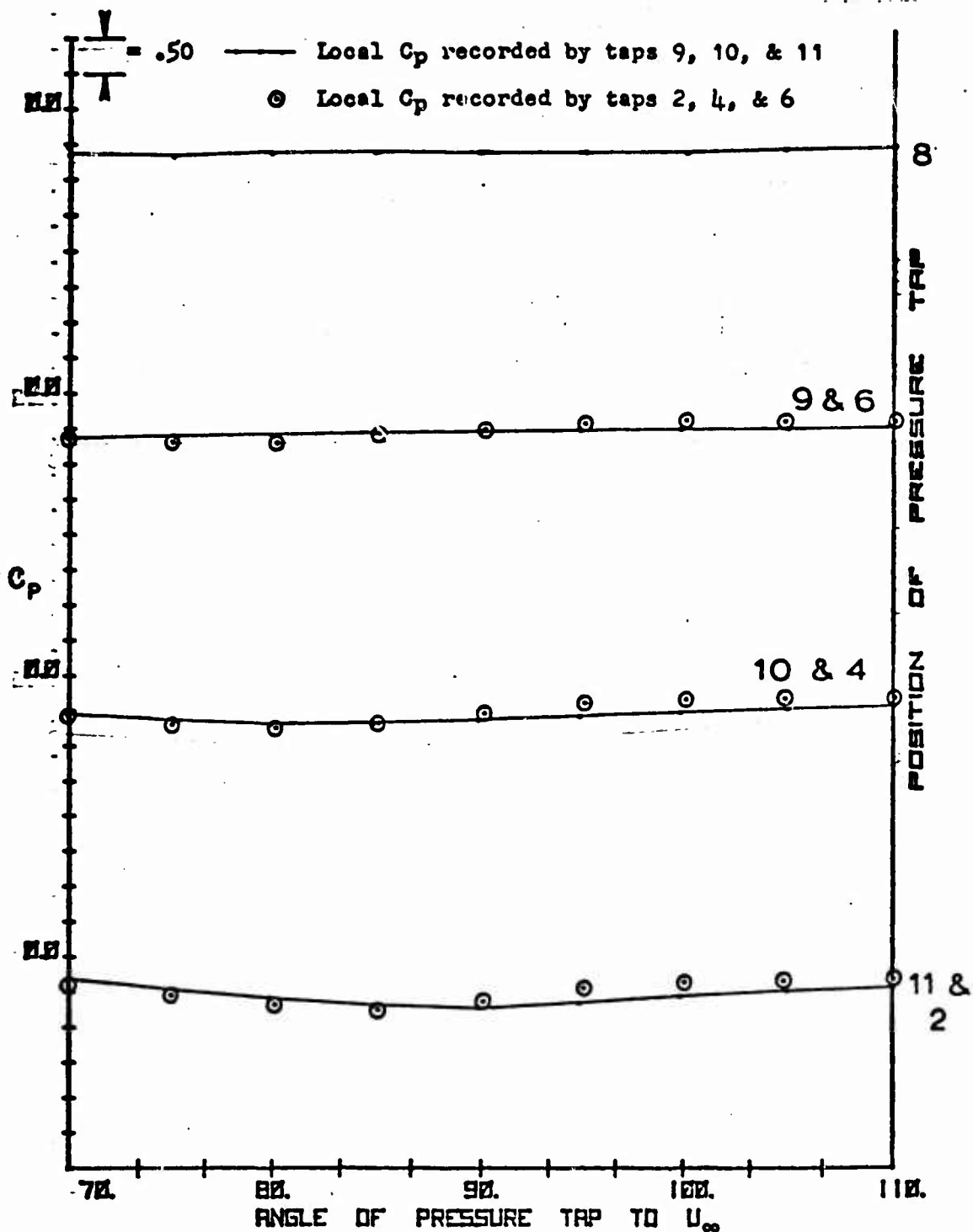
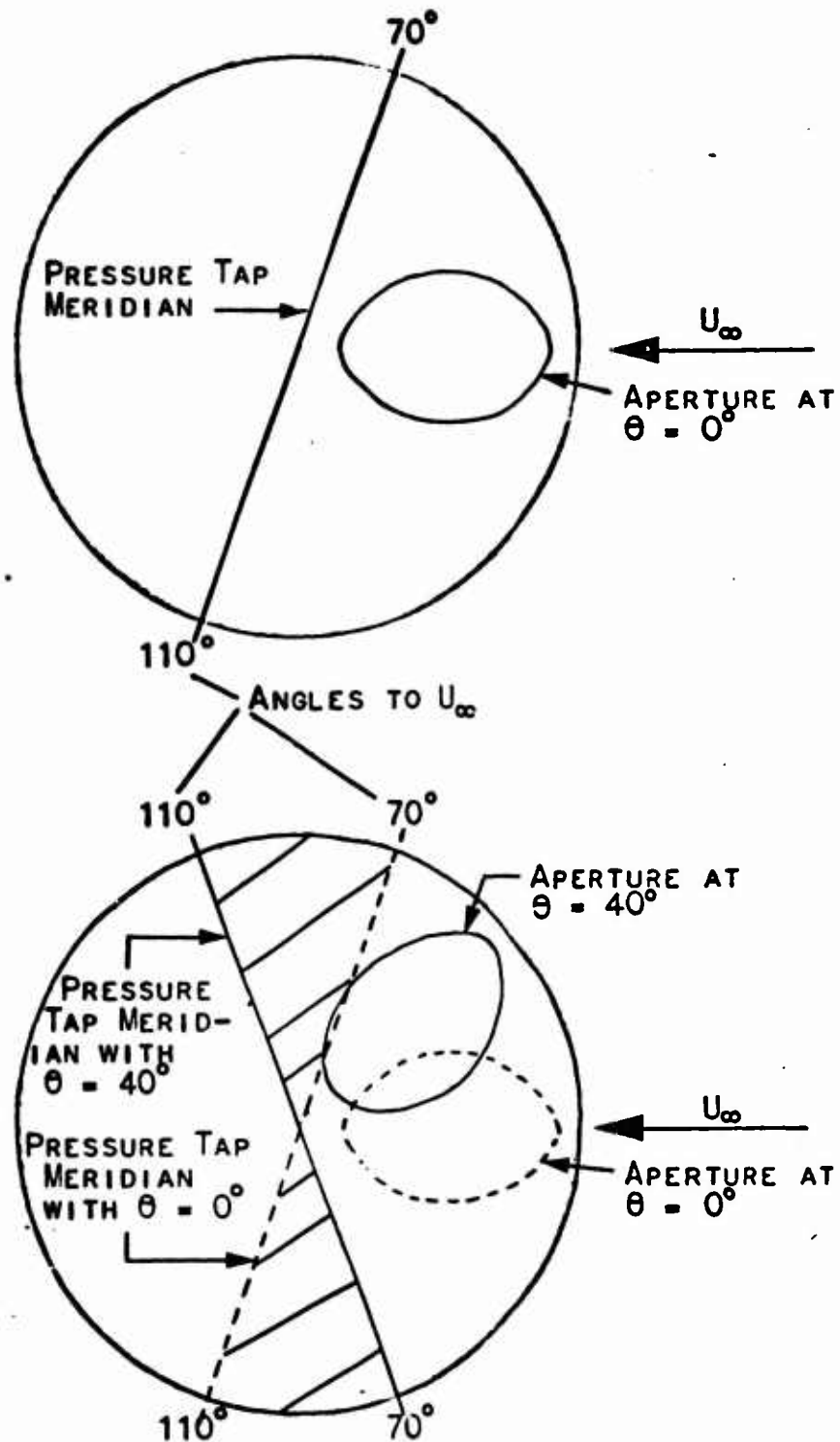


FIG. 19. COMPARISON OF LOCAL TURRET FLOW C_p MEASURED 70° DOWNSTREAM OF APERTURE (PRESSURE TAPS 2, 4, & 6) TO LOCAL TURRET FLOW C_p MEASURED WITHOUT AN UP-STREAM APERTURE (PRESSURE TAPS 9, 10, & 11) FOR MODEL 1, FREE STREAM MACH = .95. SEE PAGE 11 FOR PRESSURE TAP LOCATION.



NOTE: THE SYMMETRY, WITH RESPECT TO U_∞ , OF THE CROSS HATCHED AREA PERMITS STATIC PRESSURE MEASUREMENTS MADE ON BOTH SIDES OF THE TURRET TO BE COMPARED.

FIG. 20 POSITION OF THE PRESSURE TAP MERIDIAN AS θ IS VARIED

patterns across the coelostat turret. The photographs that were taken during this portion of the experiment were distorted because of the necessity to view through the slotted walls of the wind tunnel. For this reason they are not included in the report.

Figure 21 is typical of the flow patterns that were observed. The line of flow separation for Mach = .7 was curved and included symmetrical standing vortices near the 130° meridians. At the higher velocities however, flow separation was nearly constant along the 90° meridians. As the turret was turned, little effect was noted on the point of flow separation though the strength of the standing vortices on the top of the model were weakened. With the exception of a small area beneath the aperture, flow remained attached to the turret in the immediate vicinity of the opening. Also, it was noted that the geometric extent of the area of separated flow immediately in front of the turret increased from .2 turret diameter at Mach = .7 to .3 turret diameter at Mach = .95. This result is in close agreement with oil flow experiments performed on coelostat models at the Air Force Academy (Ref 4:46).

Though not depicted in this text, oil flow patterns were also observed at the leading and side edges of the coelostat mounting plate. These showed that

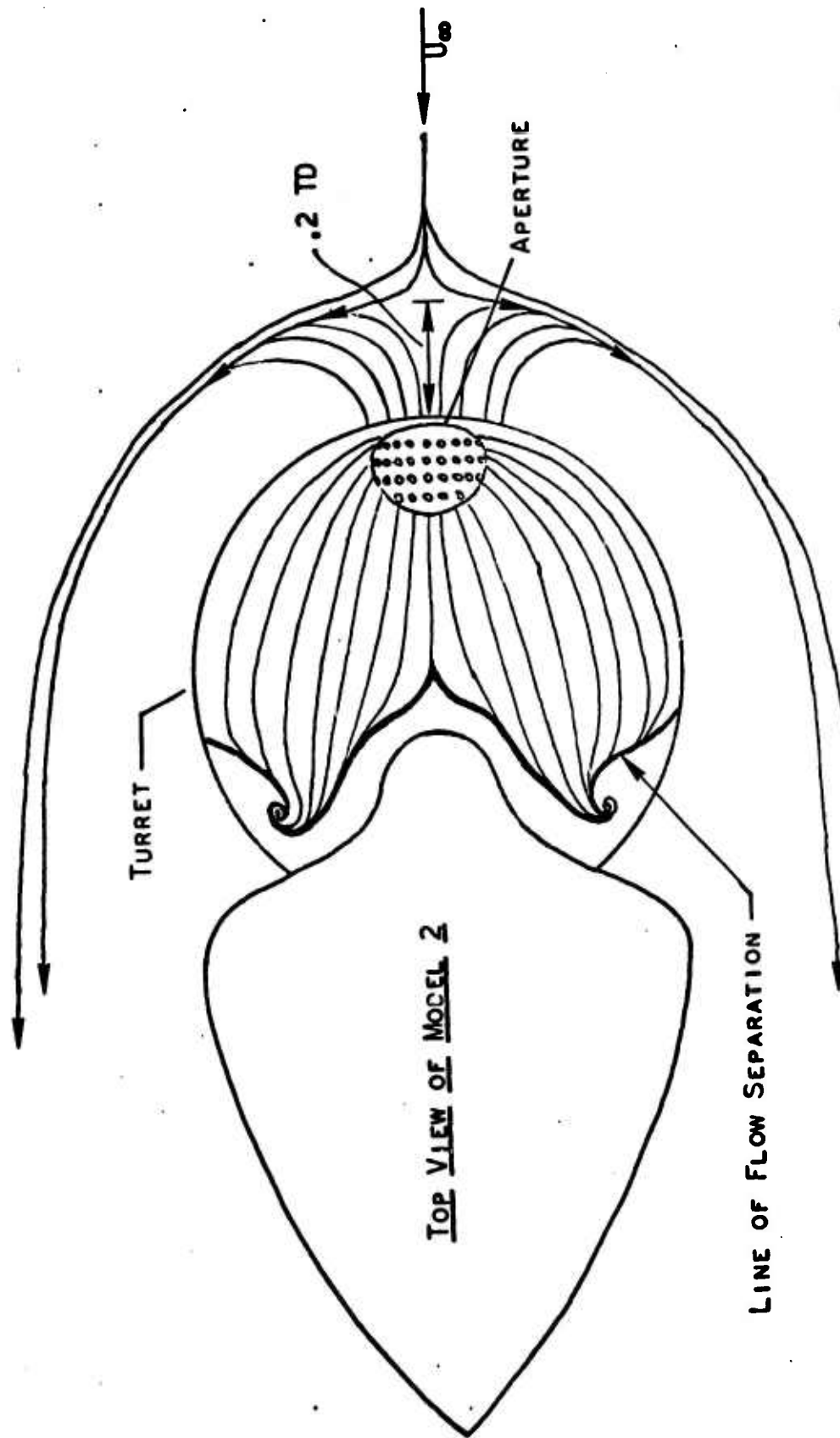


FIG. 21. OIL VISUALIZATION OF FLOW OVER MODEL 2 WITH $\theta = 0^\circ$ AND MACH = .7

GAE/AE/75J-6

the flow attached to the plate almost immediately.

Also, disturbances generated at the corners formed by the plate and the wind tunnel floor and ceiling were very localized.

VI. Conclusions and RecommendationsConclusions

In reference to the stated test objective, it can be concluded that coelostat upper turning mirror unsteady torques can be significantly reduced through the use of some blowing configurations. Limits on torque reduction would most probably be set by the maximum mass flow rate that a particular engine bleed air system could deliver. If available mass flow rates, \bar{m} , approach .2 and if a lower aperture lip blowing arrangement is adopted (configuration 16), then torque reductions of 67% of base line ($\bar{m} = 0$) could be expected. Such a reduction would almost certainly permit the coelostat turret to be employed in a wide range of USAF missions. Additionally, this low level of torque would probably reduce Air Force development costs for the mirror stabilization and positioning system.

The performances of the externally mounted fairings, which increased torque anywhere from 10% to 100%, do not entirely rule out the possibility that reductions in torque can be achieved through passive design modifications. However, it is doubtful that a non-interfering fairing could be so designed. The maximum height of such a device could only be .06 turret diameter, i.e.,

the height of the lower lip of the aperture above the aircraft fuselage. This places the fairing entirely in the region of stagnated flow and would most certainly limit its influence on the high energy air passing over it.

A very important conclusion can be drawn from the comparative analysis of model configurations that were common to both this test and the Ames II test. This comparison (Table III) showed a very similar performance between the different scale models. This is not such an expected result when viewed in light of the differences in test Reynolds number, i.e., 1.25×10^6 for this test compared to 11.25×10^6 for the Ames II test (Reynolds number based upon turret diameter). From this it can be concluded that the unsteady torque on the UTM of a coelostat turret is relatively independent of Reynolds number. This, in turn, indicates that expensive, large scale wind tunnel testing of coelostat turrets would not be necessary. Instead, small scale testing at in-house USAF wind tunnels could provide required data.

Analysis of test data also leads to the conclusion that the flow over a significant portion of the coelostat turret will be supersonic, especially at flight Mach numbers above .85. At aperture pointing

angles from approximately 60° to 110° , shock waves formed by this flow would be in the optical path and degradation of the performance of some optical devices may occur. If such was the case, lower flight Mach numbers and/or restricted aircraft headings and attitudes would eliminate the problem. Of course such limitations may not be compatible with a particular mission.

The pressure distribution across the turret indicates a substantial lifting force will be generated by the device. The effect of such a force on the stability of the carrying aircraft may be significant.

Two secondary, but still important conclusions can be drawn from this investigation. First, wall mounting models in the Flight Dynamics Laboratory trisonic wind tunnel pose no great operational difficulties. This was the first time such a testing arrangement had been attempted and it was found to present no particular problems. Model changes could be done in less time than required for internally mounted models and access to model instrumentation was facilitated.

Second, this test marked the first time unsteady pressure data was output for real time analysis as well as recorded for post test examination. Again, no difficulties were encountered which would discourage the future use of such an arrangement.

Recommendations

Since the adaptation of equipment accessories to accomplish mass flow injection in a full scale coelostat will be expensive, heavy and increase system complexity, further examination of passive torque reducing modifications should be accomplished. If it is then found that an externally mounted, non-interfering fairing cannot produce the desired results, then an examination of internal modifications should proceed. Only after this is accomplished should an active model configuration be accepted for full scale development.

It is also recommended that, since Reynolds number appears to have little effect on UTM unsteady torque, future coelostat tests be conducted on a scale model similar to that used in this test. Only after specific areas of interest are identified in these tests should the expense of large scale wind tunnel operations be incurred.

An investigation into the effect of shock wave and vortex density gradients on laser beam propagation is also recommended. It is entirely possible that the gradients associated with coelostat turret flow phenomena are sufficiently weak so as to pose no viewing angle restrictions.

GAE/AE/75J-6

Finally, the exact magnitude of the lifting force being generated by the coelostat and its effect on aircraft stability should be measured.

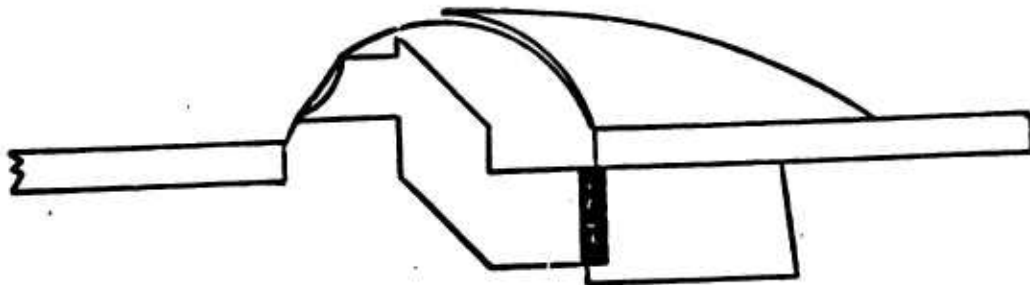
BibliographyReproduced from
best available copy.

1. "Photograph Caption" Aviation Week & Space Technology, Vol. 99: page 52 (Oct 1, 1973).
2. Van Kuren, J. T., and L. J. Otten. Acoustic Phenomena of Open Cavity Airborne Cassegrainian Telescopes. AFFDL TM-73-54. Wright-Patterson AFB, Ohio: AF Flight Dynamics Laboratory, May 1973.
3. Van Kuren, J., and W. R. Connor. Transonic Ten-Pin Tests Phase II Configuration Studies and Pressure Fluctuations. AFFDL TM-73-159FXM. Wright-Patterson AFB, Ohio: AF Flight Dynamics Laboratory, Sept 1972.
4. Van Kuren, James T. Wind Tunnel Test of a Large Pointing System. AFFDL-TM-74-186-FX. Wright-Patterson AFB, Ohio: AF Flight Dynamics Laboratory, August 1974.
5. Rossiter, J. E. Wind Tunnel Experiments on the Flow Over Rectangular Cavities at Subsonic and Transonic Speeds. TR-64037. Royal Aircraft Establishment, Oct 1964.
6. Dunham, W. H. Flow-Induced Cavity Resonance in Viscous Compressible and Incompressible Fluids. ACR 92. Washington: Office of Naval Research, 1962.
7. Belik, L. "The Secondary Flow about Circular Cylinders Mounted Normal to a Flat Plate". The Aeronautical Quarterly, Volume XXIV: p. 47-54 (Feb 1973).
8. Buell, D. A. An Experimental Investigation of the Airflow Over a Cavity with Antiresonance Devices. NASA TN-D-6205. Washington: National Aeronautics and Space Administration, March 1971.
9. White, H. L. Trisonic Gasdynamic Facility Users Manual. AFFDL TM-73-82 FXM. Wright-Patterson AFB, Ohio: AF Flight Dynamics Laboratory, June 1973.
10. Liepmann, H. W. and A. Roshko. Elements of Gasdynamics. New York: John Wiley & Sons, Inc., 1957.
11. Schlichting, H. Boundary-Layer Theory. New York: McGraw-Hill, Inc., 1968.

Appendix A

Model Configurations

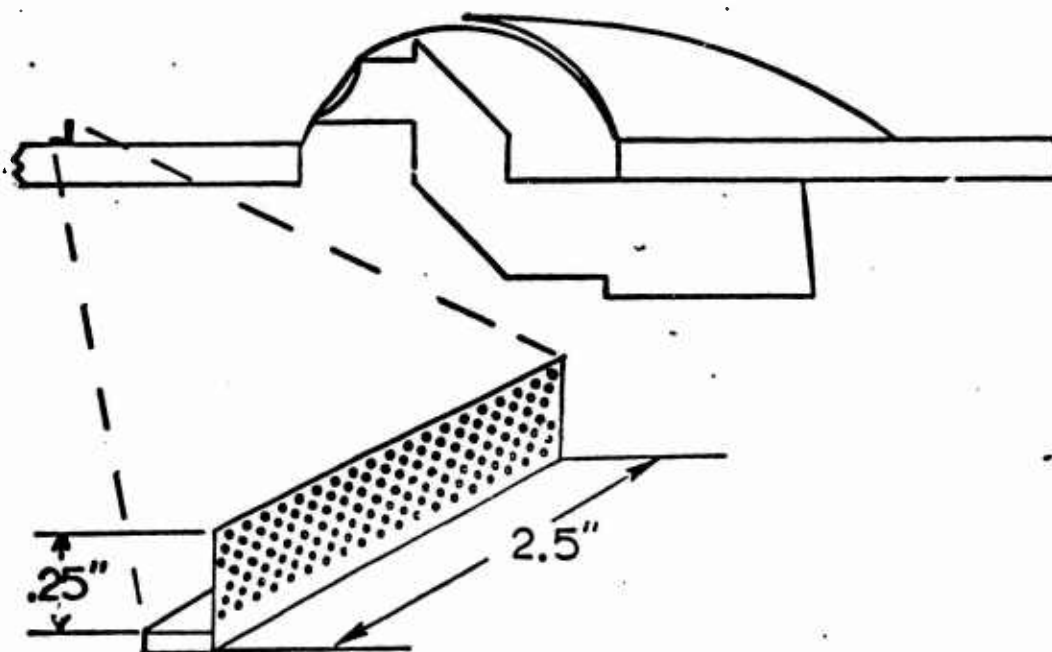
This Appendix contains Figures 22 thru 33 which illustrate and include discussion on the various model configurations utilized in the experiment. Models 4, 7, and 13, near duplicates of other listed configurations, were deleted from the report in the interest of brevity.



Configuration 3

Note: A possibility exists that improvements in future pointing and tracking equipment will eliminate the need for an extended bottom light pipe. To approximate the geometry of such a configuration, a plug was inserted into the coelostat model at the position indicated.

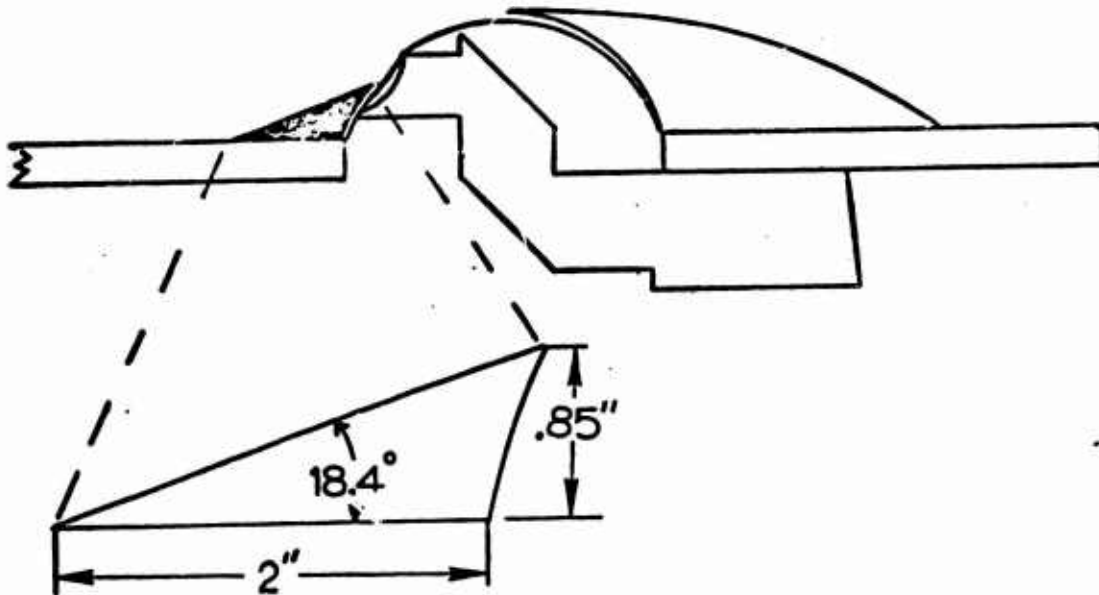
Fig. 22. Model Configuration 3



Configurations 5 & 6

Note: A fence of 31% porosity could be positioned at varying distances in front of the model. Previous wind tunnel tests have shown that such a device creates a large bubble of low energy air which extends down wind of the fence. By enveloping the coelostat with this bubble it was anticipated that less intense vortices would be generated by flow over the open cavity.

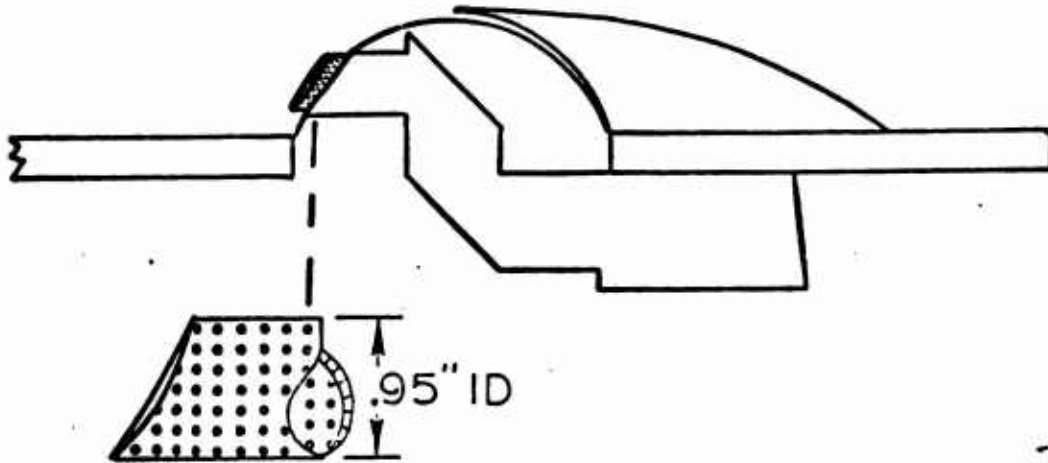
Fig. 23. Model Configurations 5 & 6



Configuration 8

Note: A cone of half angle 18.4 degrees was split and mounted at the leading edge of the coelostat as shown. This modification was an attempt to streamline the turret and thus eliminate the vortex generating forward stagnation zone observed by Belik (Ref 7).

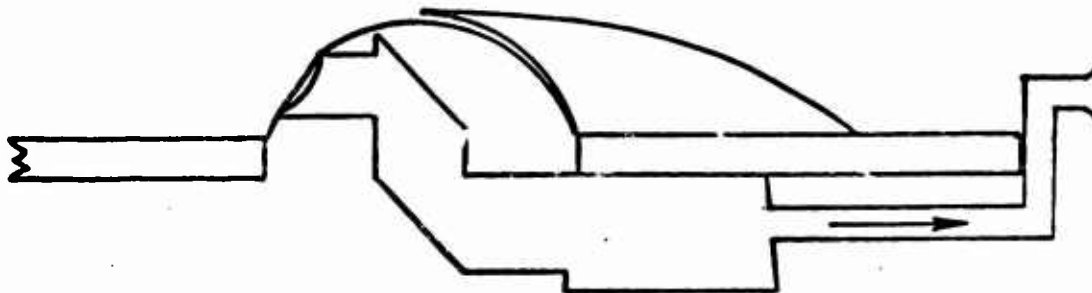
Fig. 24. Model Configuration 8



Configuration 9

Note: A thin walled, perforated tube of 31% porosity was designed for installation within the coelostat top light pipe. The leading edge of this tube could be extended from the aperture to form a wrap around cavity lip fence of .333 inch height. Buell found that such spoilers are an effective means of impeding vortex formation at the cavity lip (Ref 8:13). Also, data from the Ames II test indicated that lip fences produce a damping effect on UTM pressure fluctuations (Ref 4:42).

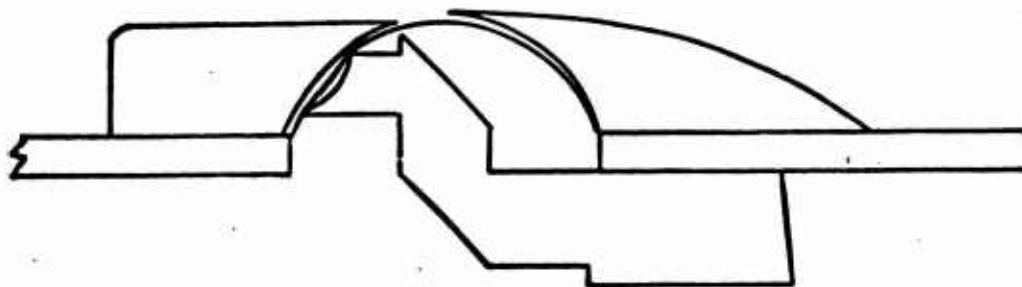
Fig. 25. Model Configuration 9



Configuration 10

Note: The rear of the bottom light pipe was vented to the low pressure area formed by a flared tube. The objective of such a configuration was to eliminate shear layer oscillations in the cavity opening by permanently "swallowing" the shear layer.

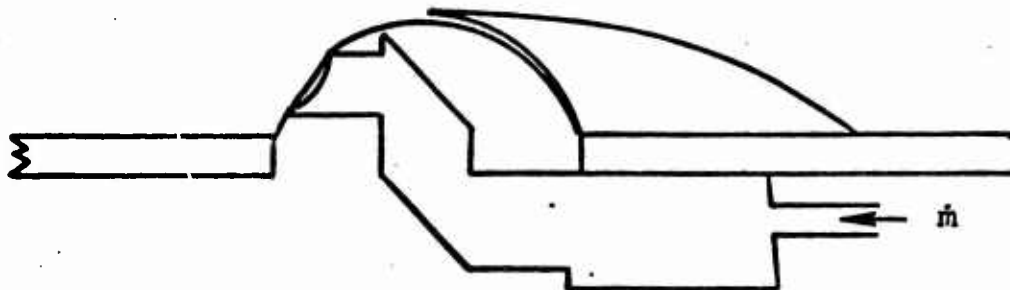
Fig. 26. Model Configuration 10



Configuration 11

Note: A thin vertical splitter could be positioned on the centerline of the coelostat mounting plate as depicted above. Previous wind tunnel tests have shown that such splitter plates stabilize turret leading edge flow which in turn reduces internal cavity pressure fluctuations (Ref 3:64).

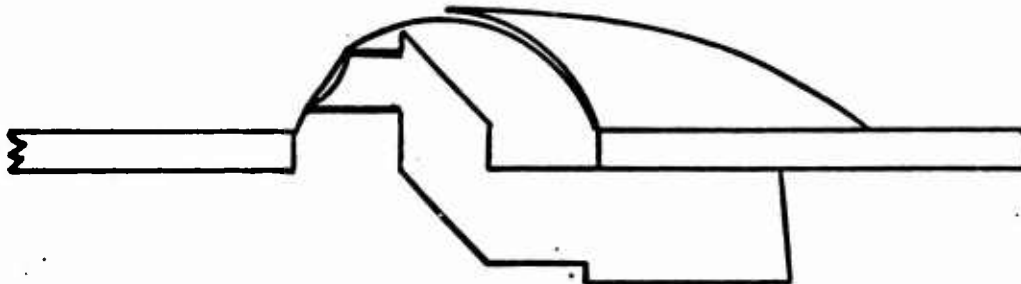
Fig. 27. Model Configuration 11



Configuration 12

Note: A flow channel was placed at the rear of the bottom light pipe through which air could be injected. The rationale behind such a design is to divert high energy air away from the turret aperture at forward facing angles of θ . Additionally such a design would tend to prevent the down wind side of the aperture shear layer from being alternately moved in and out of the top light pipe by lip vortex shedding when the turret was at side facing θ angles. A similar arrangement was successfully employed in the Ames II test. However it was desired to recertify the validity of this earlier success.

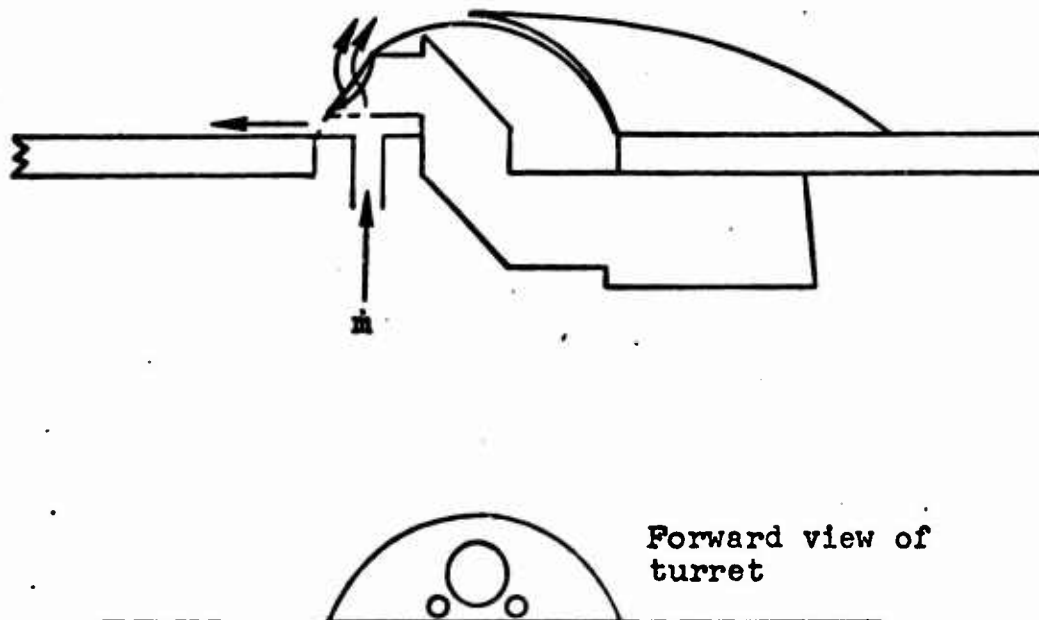
Fig. 28. Model Configuration 12



Configuration 14

Note: A thin walled tube was placed inside the top light pipe to form a non-porous surface. Such a configuration was utilized as the base line in the Ames II test. Its purpose in this investigation was to provide an additional check on the performance of the scaled model relative to the Ames model.

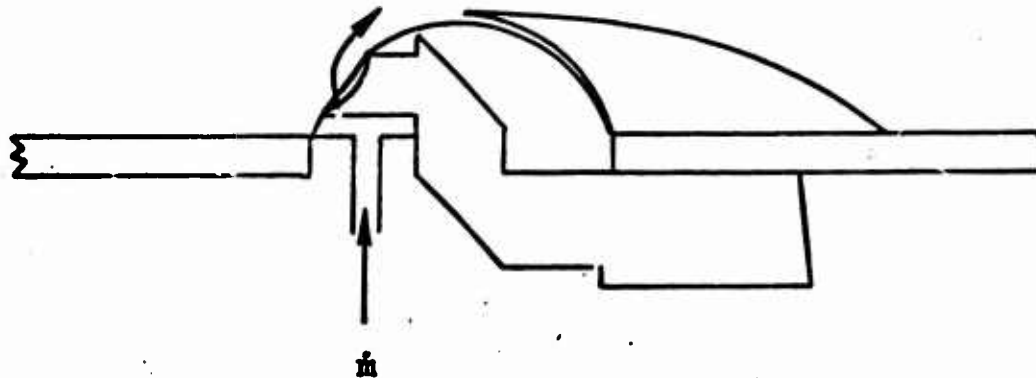
Fig. 29. Model Configuration 14



Configurations 15 & 16

Note: In configuration 15 air was injected into the base of a baffle surrounding the porous top light pipe and could exit through the first two rows of holes in the pipe and through two holes at the base of the aperture. It was hoped that such flow would divert high energy air away from the aperture and thus stabilize the pressure field on the UTM. Configuration 16 was the same as configuration 15 except the aperture perimeter holes were closed.

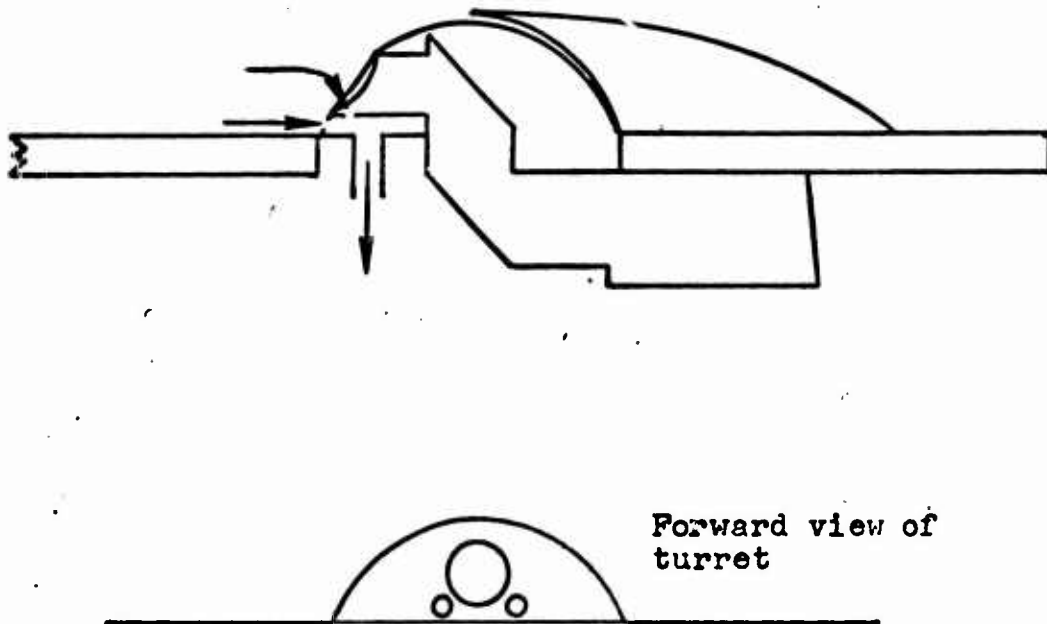
Fig. 30. Model Configurations 15 & 16



Configuration 17

Note: The model was identical to configuration 16 except that blowing was only through the first row of holes in the top light pipe. By concentrating the upward flow injection at the aperture lip it was believed a better possibility existed for diverting high energy free stream flow.

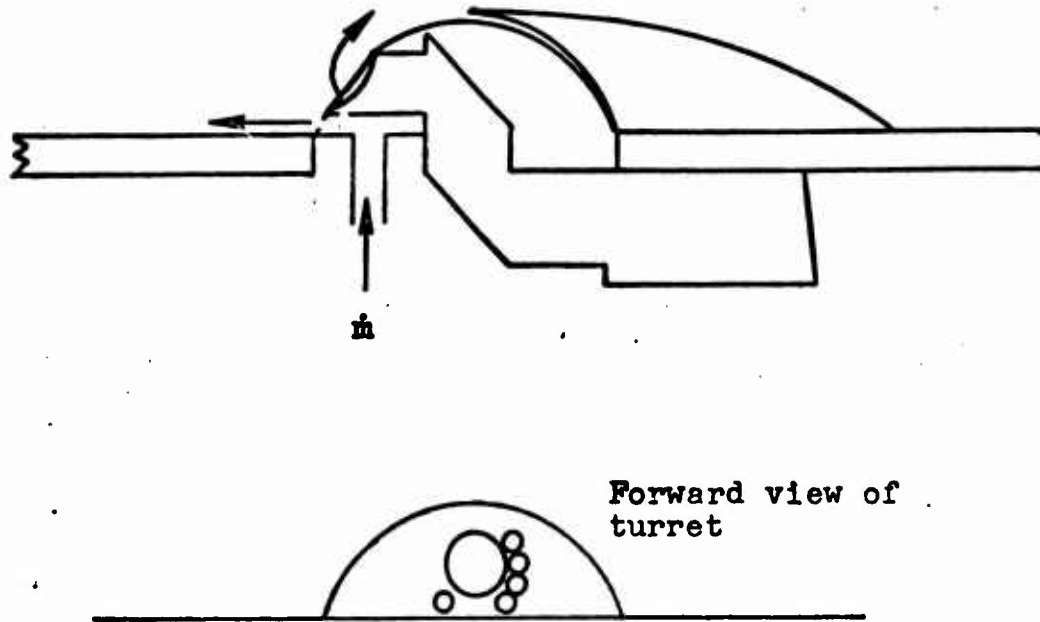
Fig. 31. Model Configuration 17



Configuration 18

Note: The two aperture perimeter holes were opened and suction was applied at the base of the baffle. It was recognized that such an arrangement would have the possibly adverse effect of entraining free stream fluid into the opening. However the additional effect of bleeding off the stagnation zone in front of the turret could, it was believed, stabilize UTM pressures.

Fig. 32. Model Configuration 18



Configuration 19

Note: Injected air could exit through five aperture perimeter holes and the first row of top light pipe holes as depicted above. Again, the objective of this arrangement was to divert the high energy free stream flow from impinging directly upon the opening.

Fig. 33. Model Configuration 19

Appendix B

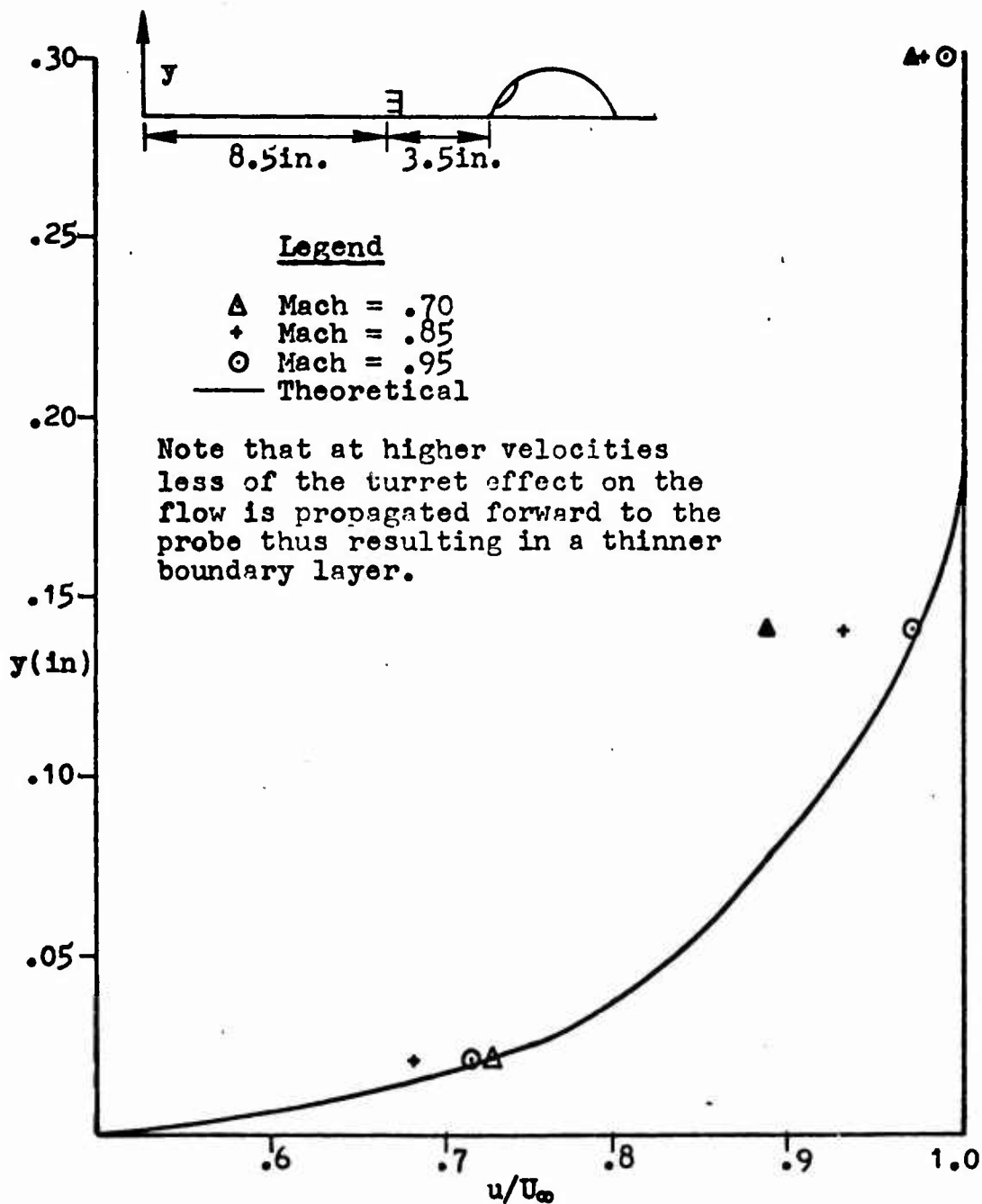
Boundary Layer Data

Fig. 34. Measured boundary layer compared to theoretical 1/7 power law velocity profile (Ref 11:598). Since the test Reynolds number was constant at $3 \times 10^6/\text{ft}$, the single theoretical line applies to all test Mach numbers.

Appendix C

UTM Unsteady Pressures and Torques

This section contains P_{rms}/q values of the four UTM pressure transducers as functions of θ for various model configurations and Mach numbers (Fig 35 thru 66). The base line (Model 2) values are superimposed on each figure as dotted lines. Generally a reduction in the P_{rms}/q value can be interpreted as a reduction in torque.

Because of the fact that each transducer had a different constant relating voltage to pressure, the vertical scale in the figures assumes two values. Also, where given, the values of \dot{m} have been non-dimensionalized (see page 8). No measurements were made on the rate of suction applied to Model 18.

Figures 67 and 68, also included in this Appendix, give plots of the Model 2 UTM azimuth and elevation torques as functions of θ and Mach number.

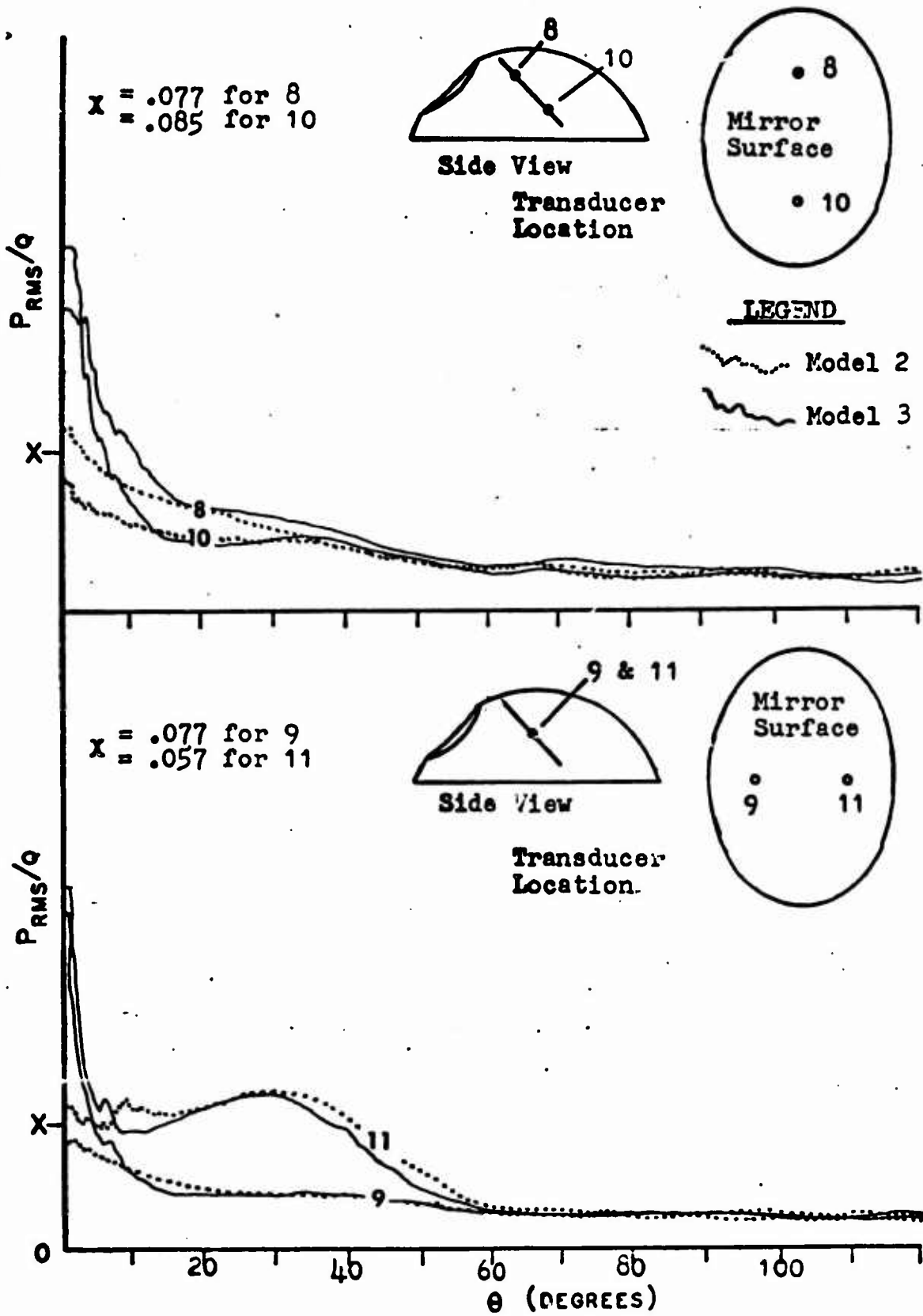


Fig. 35. PRESSURE VARIATIONS ON THE UTM SURFACE AS FUNCTION OF CAVITY ORIENTATION AND MODEL CONFIGURATION, $M=.70$

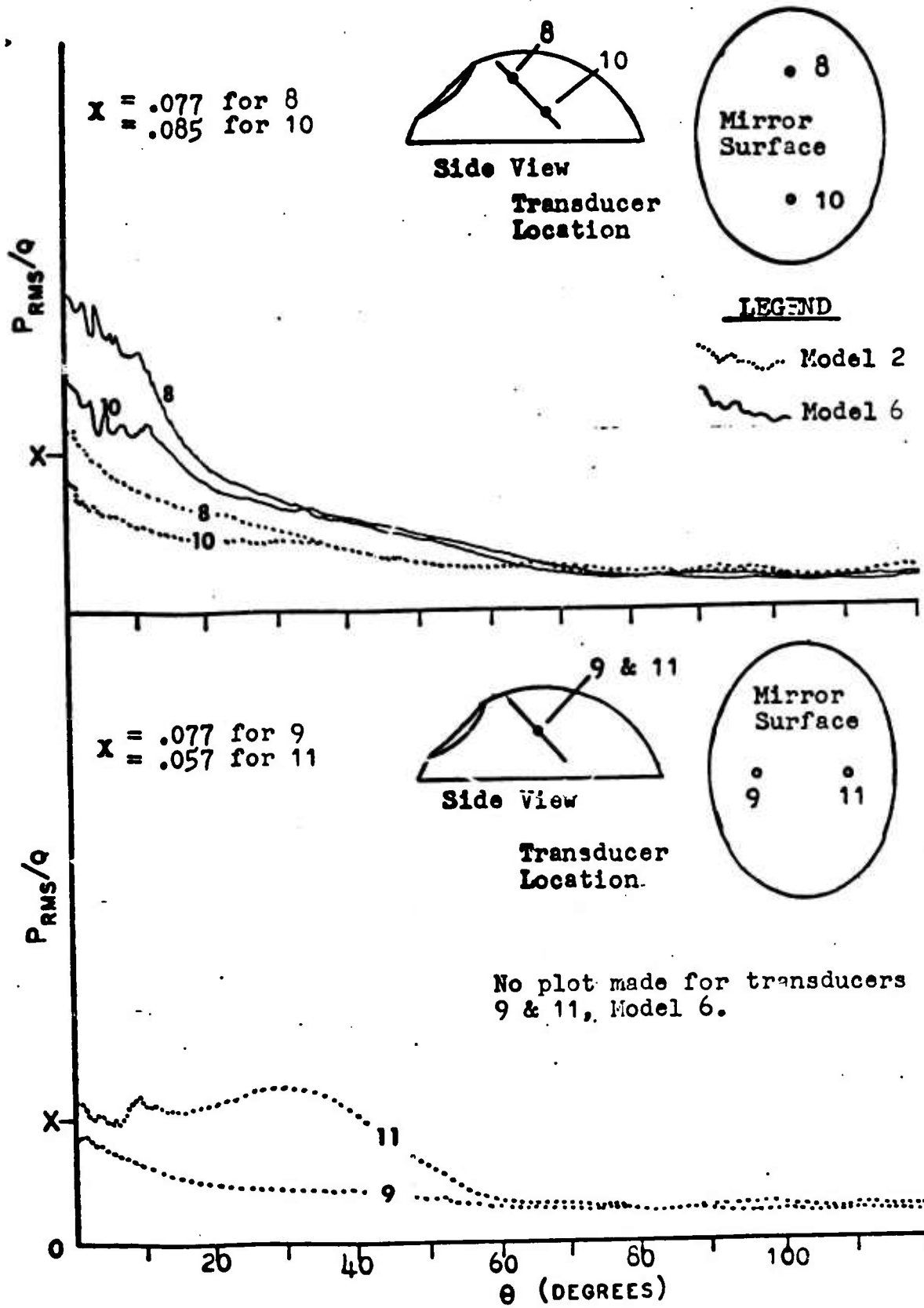


Fig. 36. PRESSURE VARIATIONS ON THE UTM SURFACE AS FUNCTION OF CAVITY ORIENTATION AND MODEL CONFIGURATION, $M = .70$

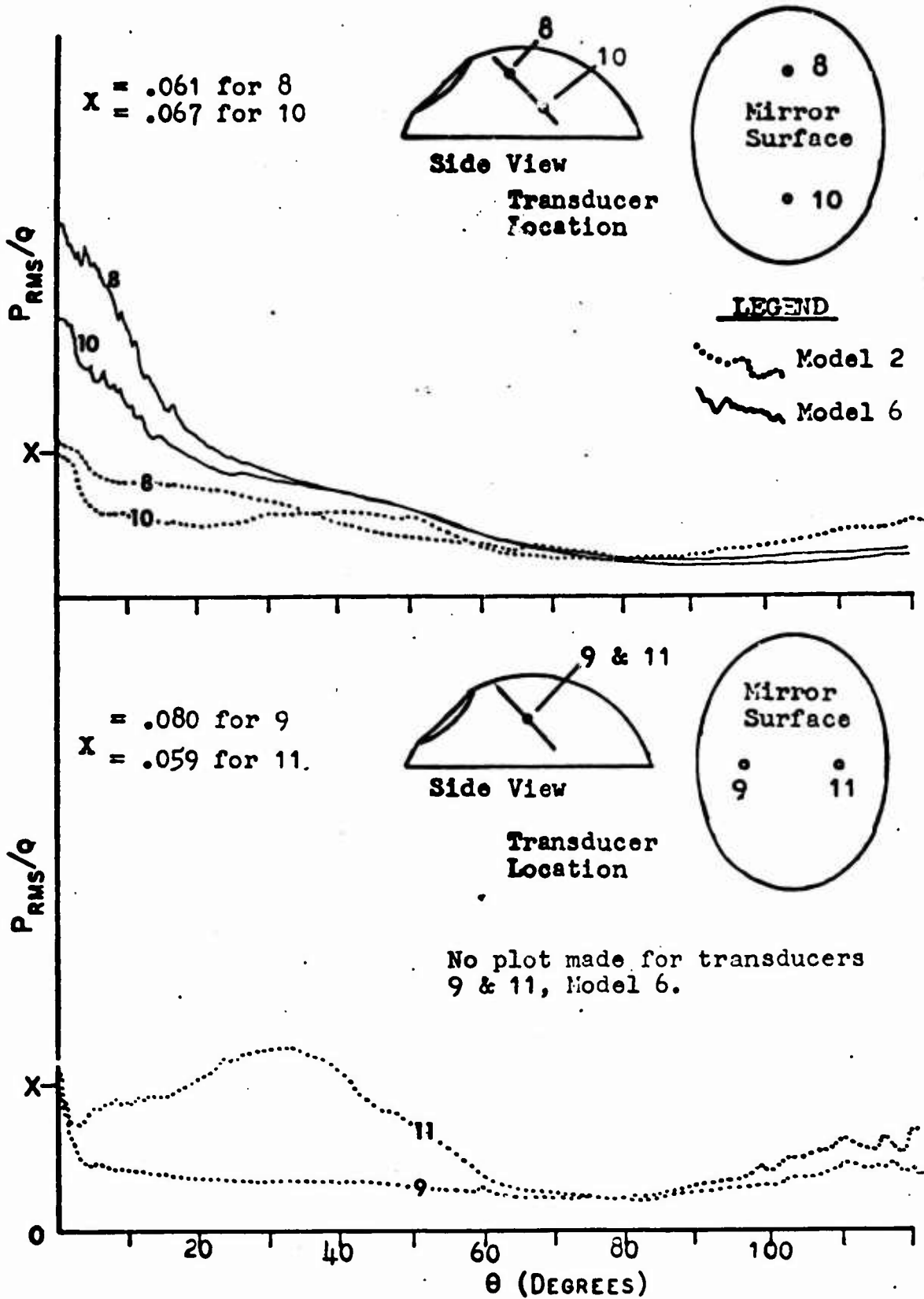


Fig. 37. PRESSURE VARIATIONS ON THE UTM SURFACE AS FUNCTION OF CAVITY ORIENTATION AND MODEL CONFIGURATION, $M_\infty = .85$

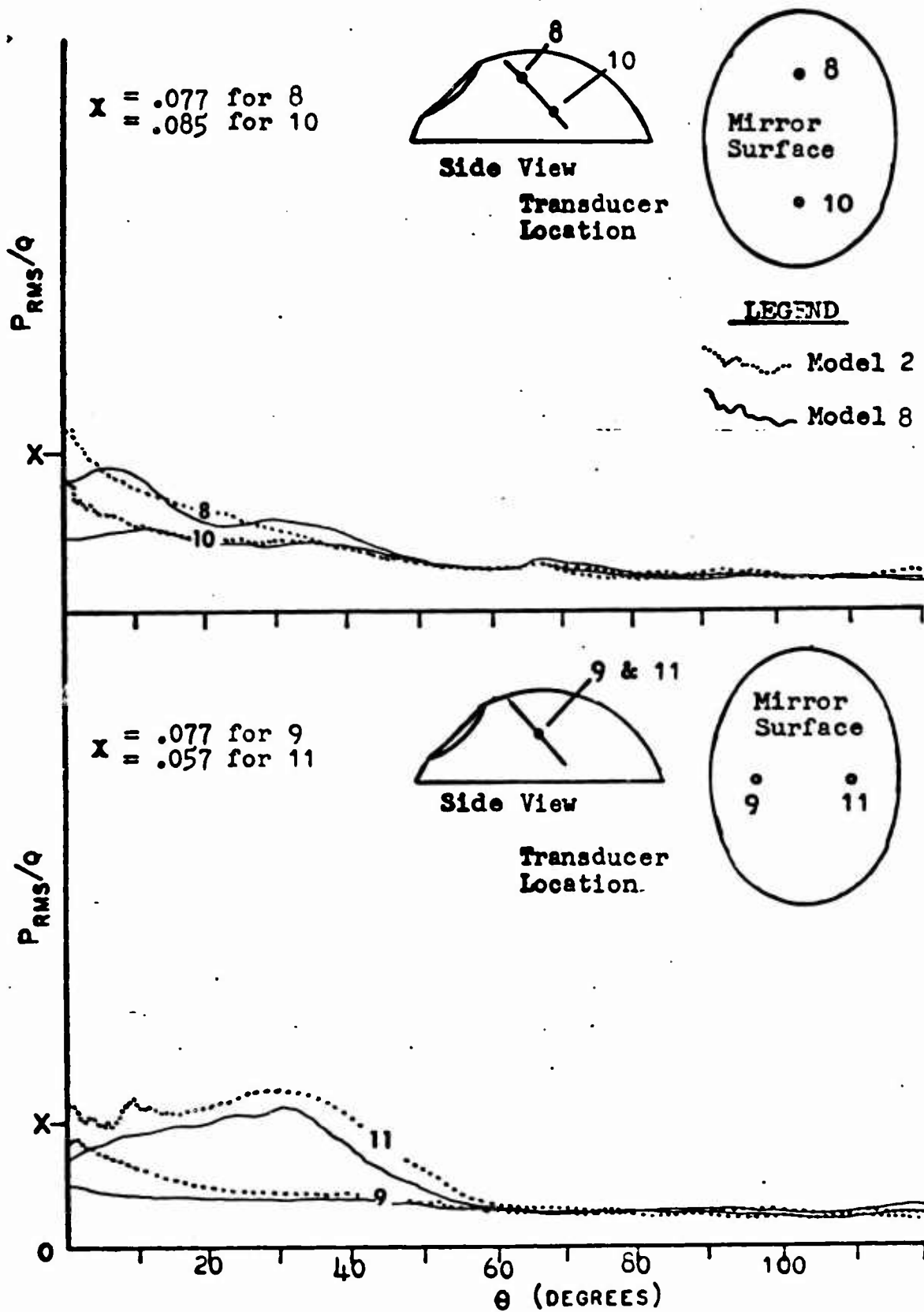


Fig. 38. PRESSURE VARIATIONS ON THE UTM SURFACE AS FUNCTION OF CAVITY ORIENTATION AND MODEL CONFIGURATION, $M = .70$

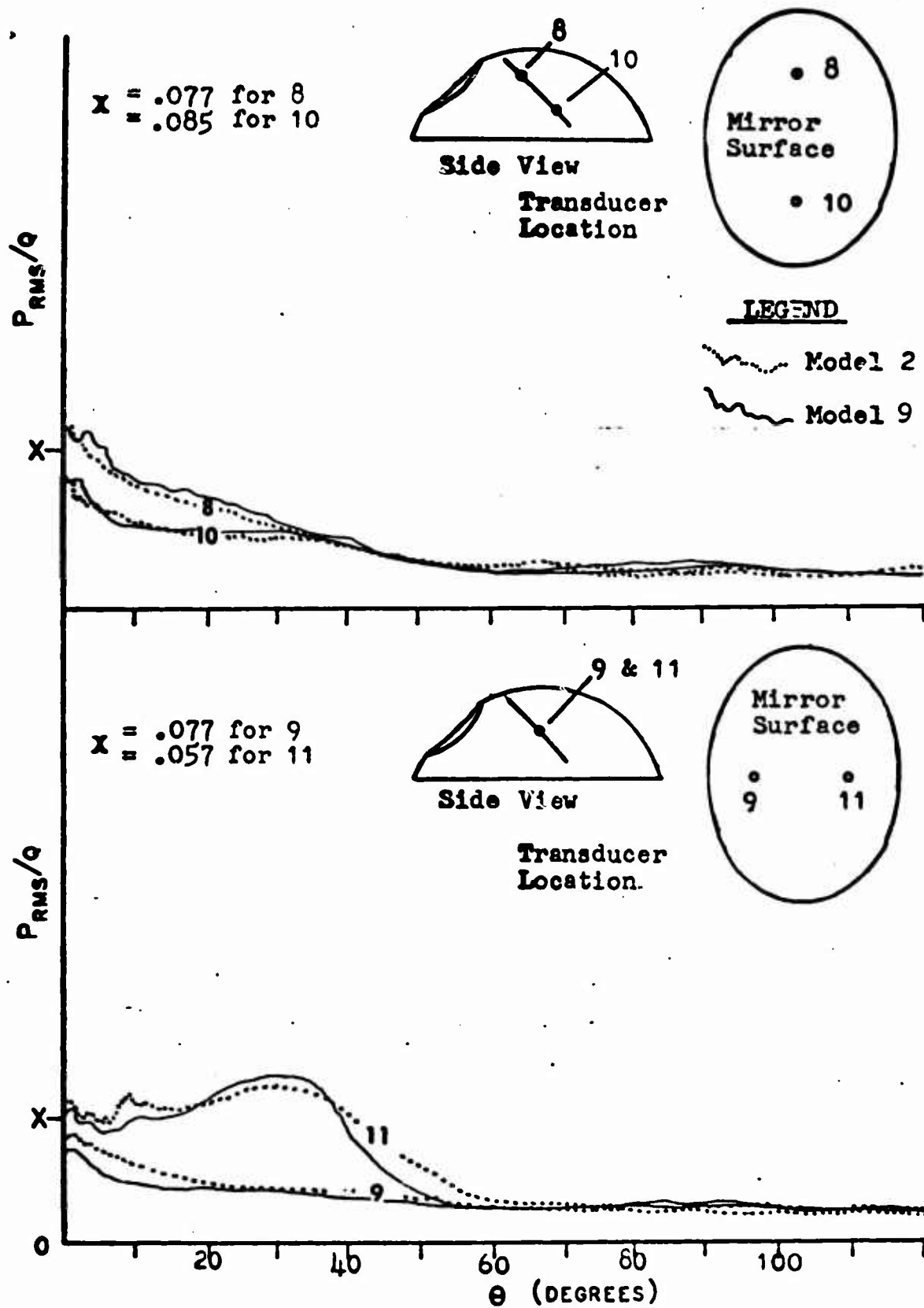


Fig. 39. PRESSURE VARIATIONS ON THE UTM SURFACE AS FUNCTION OF CAVITY ORIENTATION AND MODEL CONFIGURATION, $M = .70$

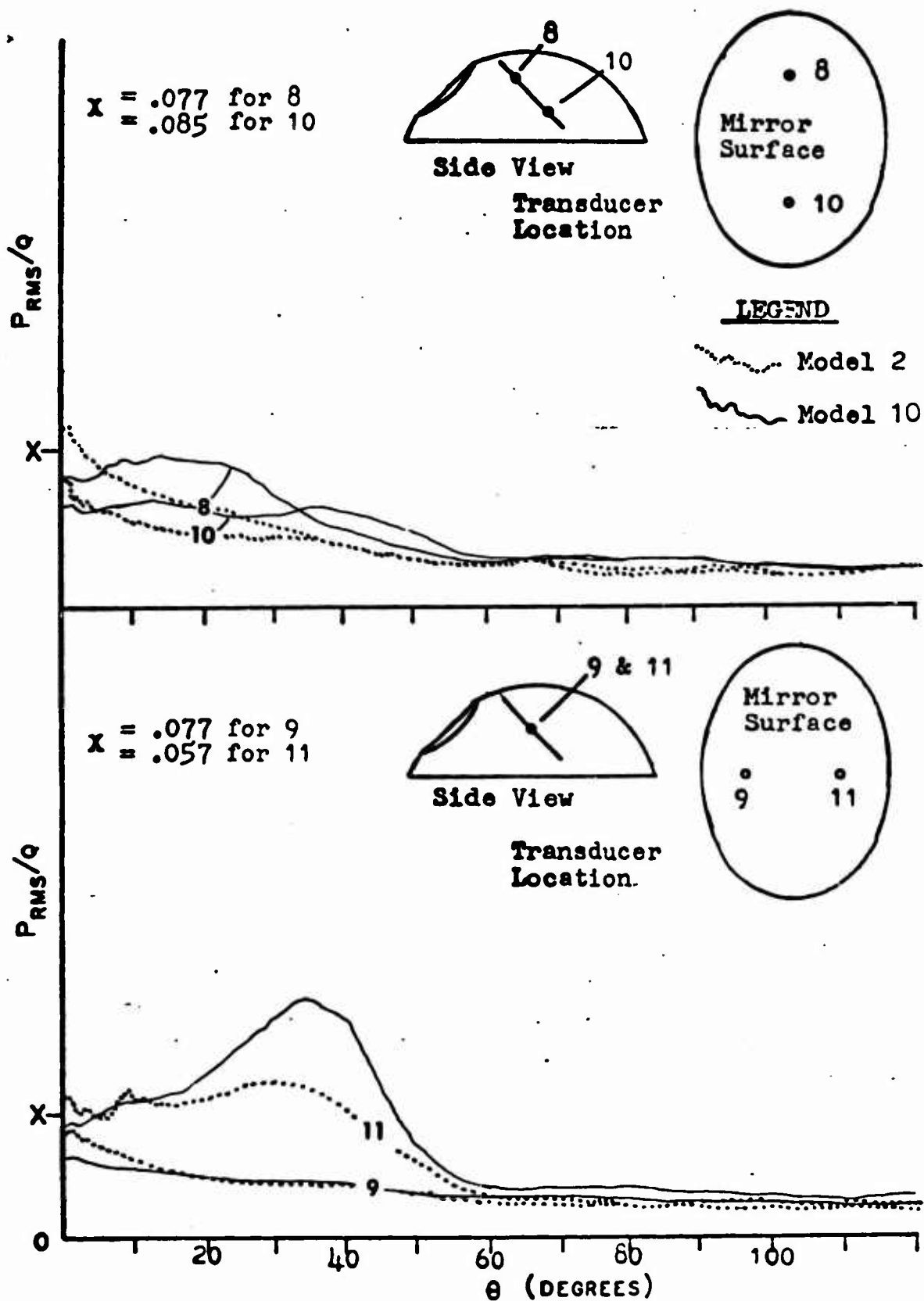


Fig. 40. PRESSURE VARIATIONS ON THE UTM SURFACE AS FUNCTION OF CAVITY ORIENTATION AND MODEL CONFIGURATION, $M = .70$

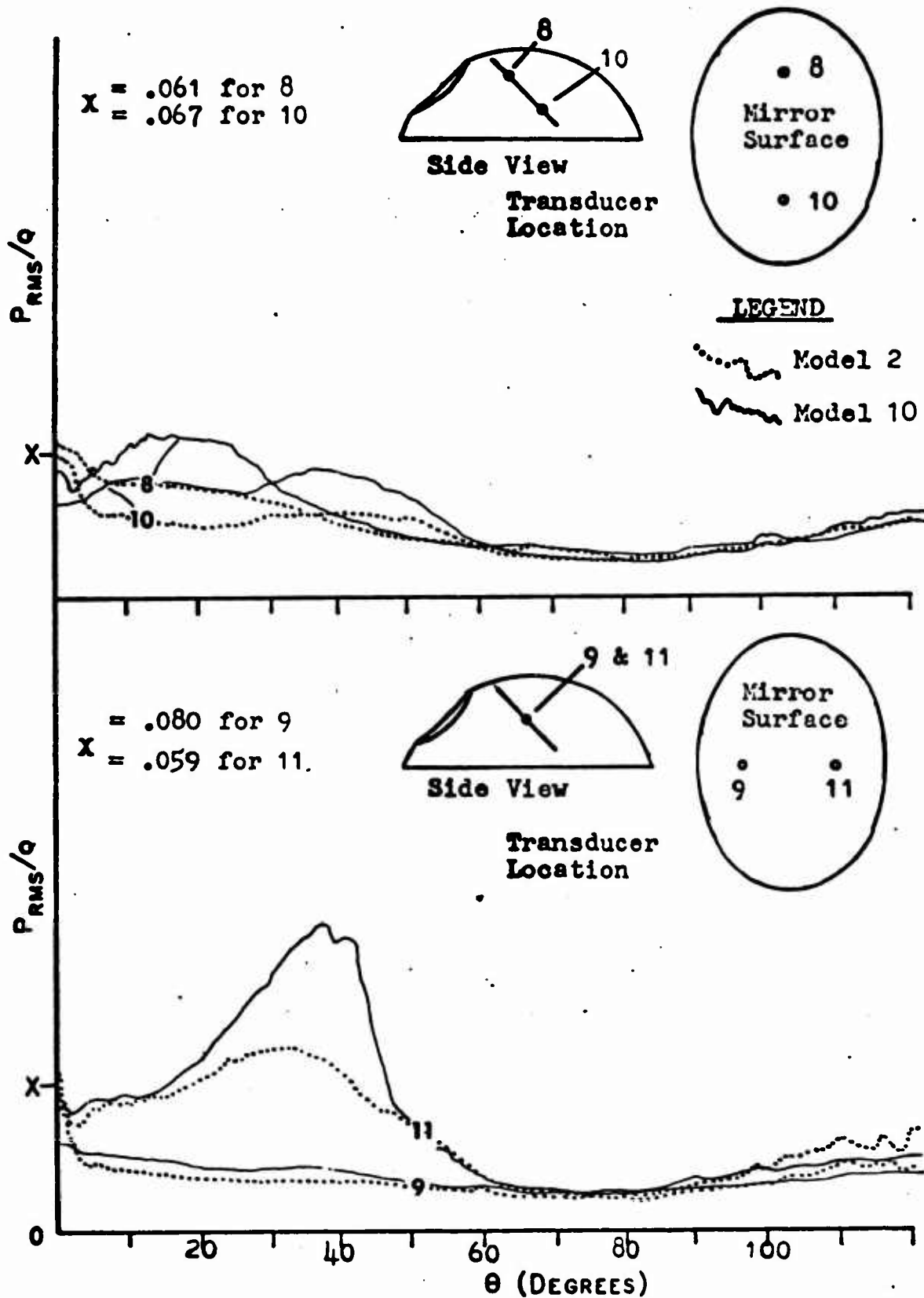


Fig. 41 PRESSURE VARIATIONS ON THE UTM SURFACE AS FUNCTION OF CAVITY ORIENTATION AND MODEL CONFIGURATION, $M = .85$

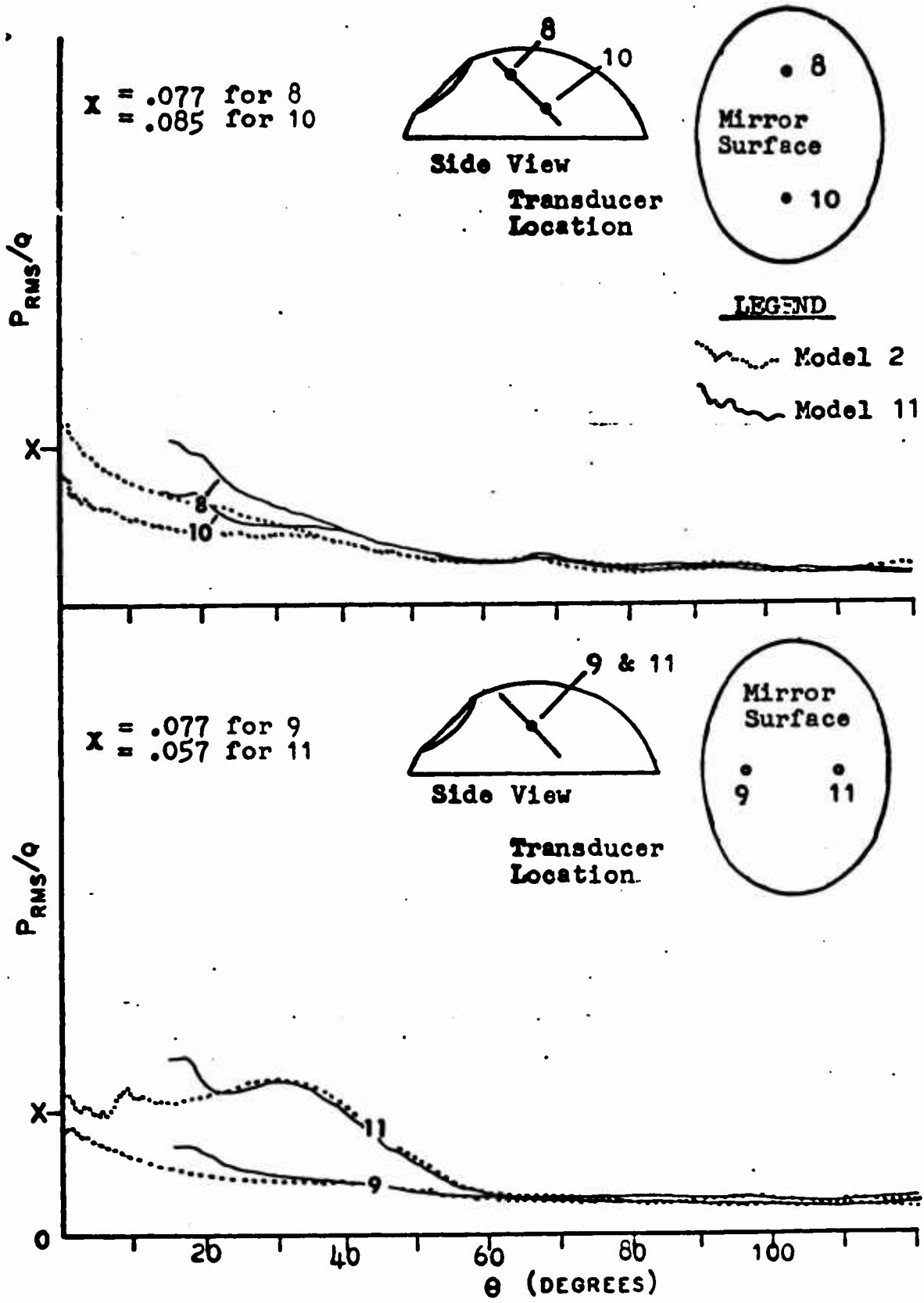


Fig. 42. PRESSURE VARIATIONS ON THE UTM SURFACE AS FUNCTION OF CAVITY ORIENTATION AND MODEL CONFIGURATION, $M = .70$

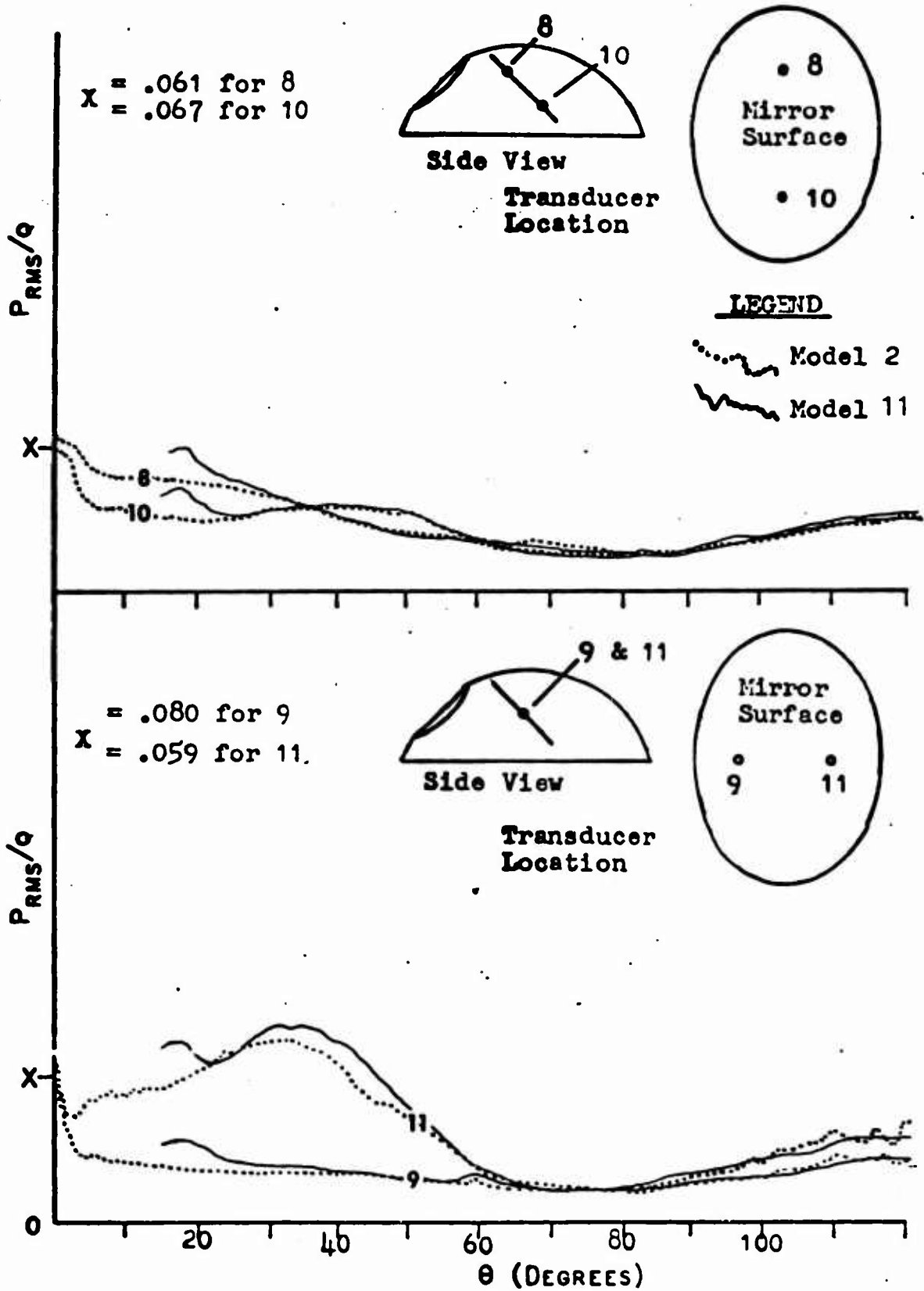


FIG. 43. PRESSURE VARIATIONS ON THE UTM SURFACE AS FUNCTION OF CAVITY ORIENTATION AND MODEL CONFIGURATION, $M = .85$

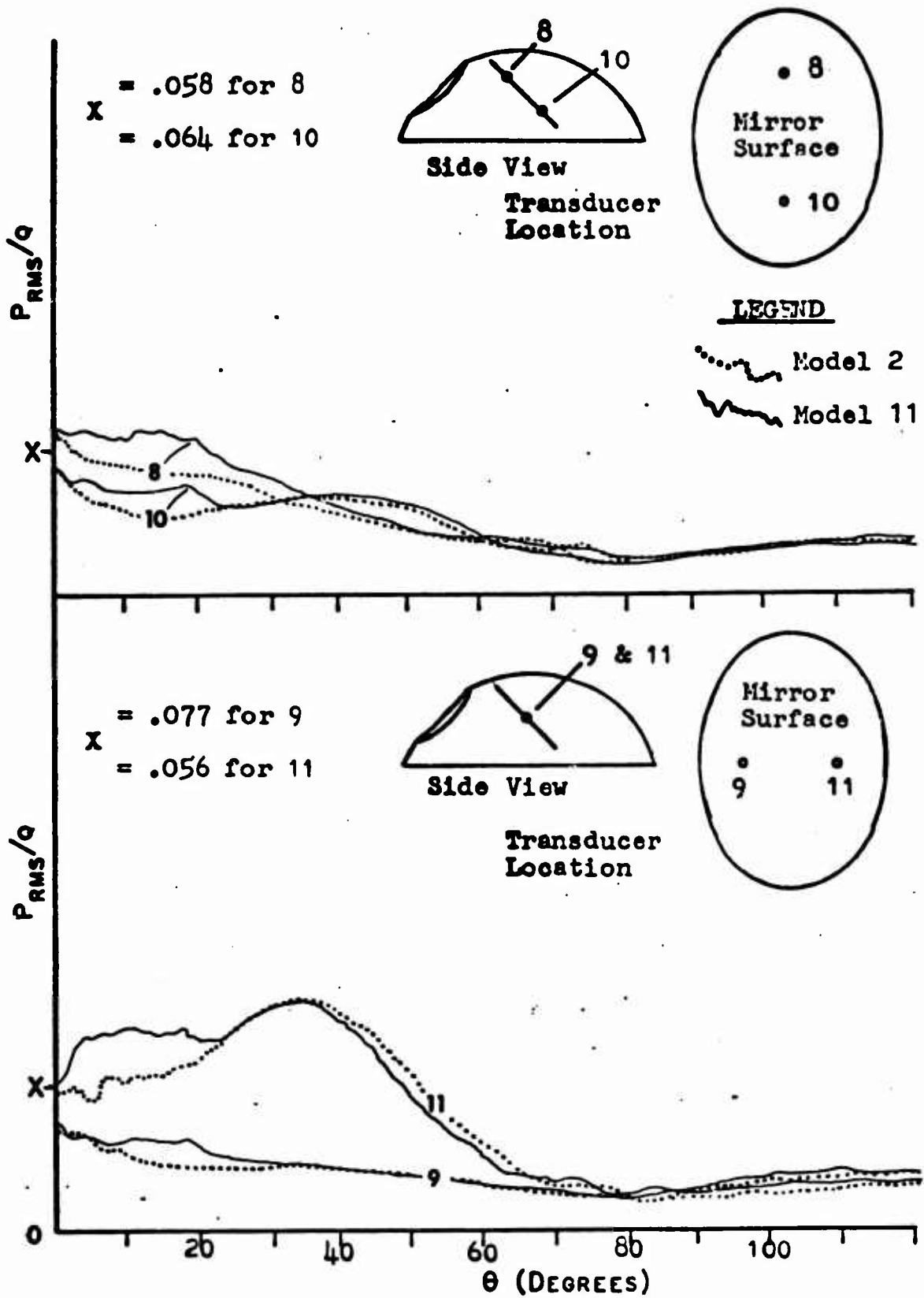


Fig. 44. PRESSURE VARIATIONS ON THE UTM SURFACE AS FUNCTION OF CAVITY ORIENTATION AND MODEL CONFIGURATION, $M = .95$

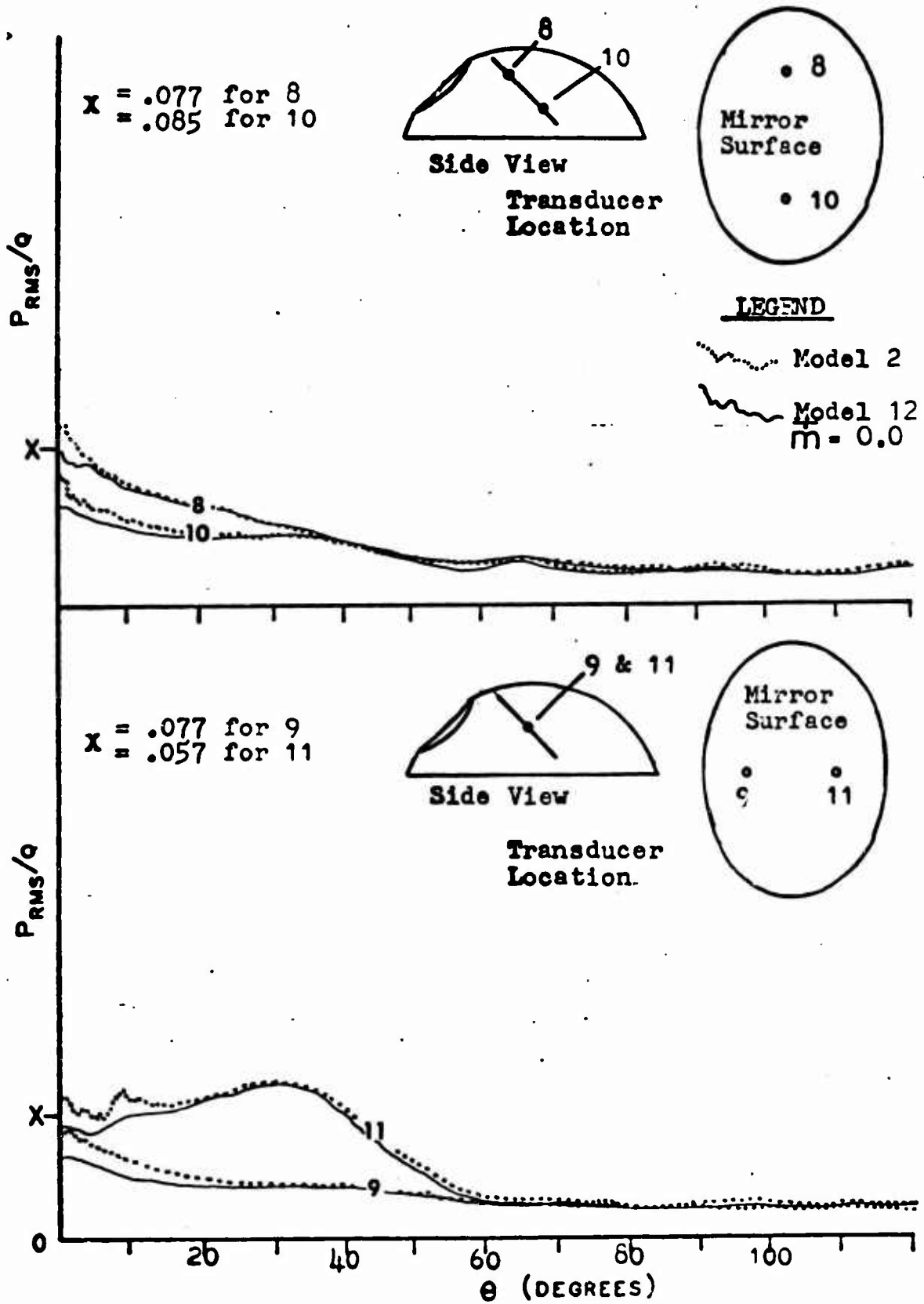


Fig. 45. PRESSURE VARIATIONS ON THE UTM SURFACE AS FUNCTION OF CAVITY ORIENTATION AND MODEL CONFIGURATION, $M = .70$

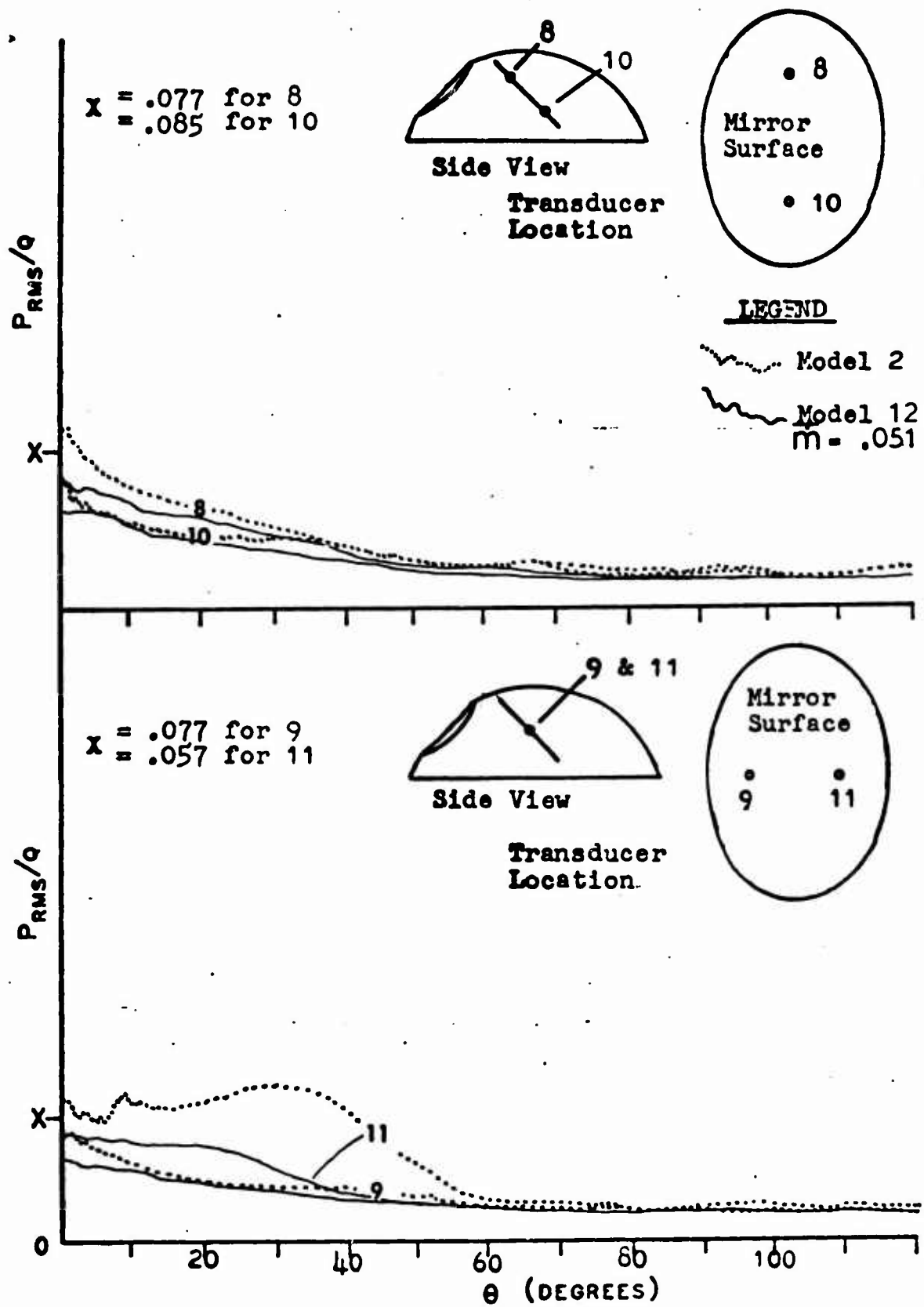


Fig. 46. PRESSURE VARIATIONS ON THE UTM SURFACE AS FUNCTION OF CAVITY ORIENTATION AND MODEL CONFIGURATION, $M = .70$

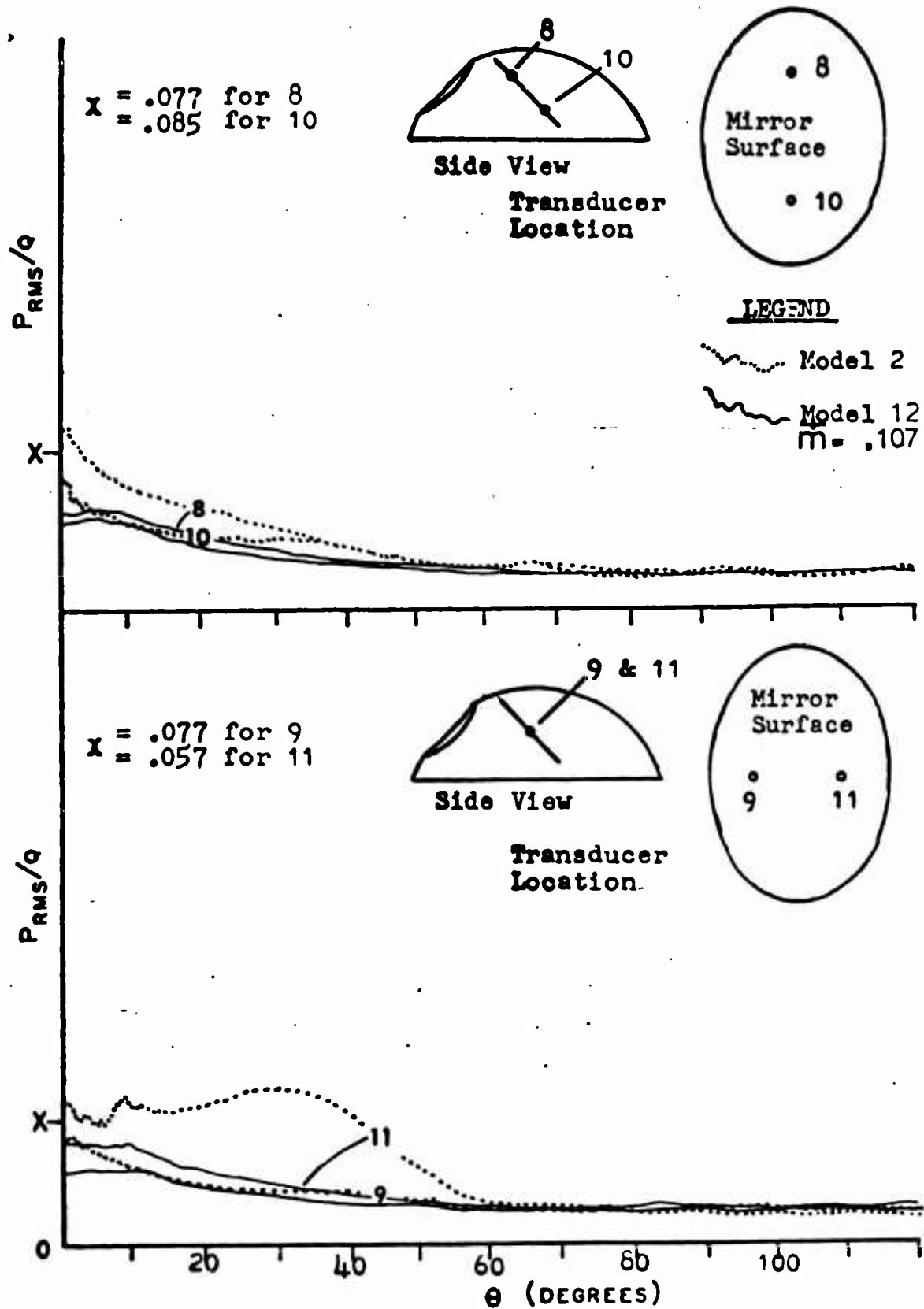


Fig. 47. PRESSURE VARIATIONS ON THE UTM SURFACE AS FUNCTION OF CAVITY ORIENTATION AND MODEL CONFIGURATION, $M = .70$

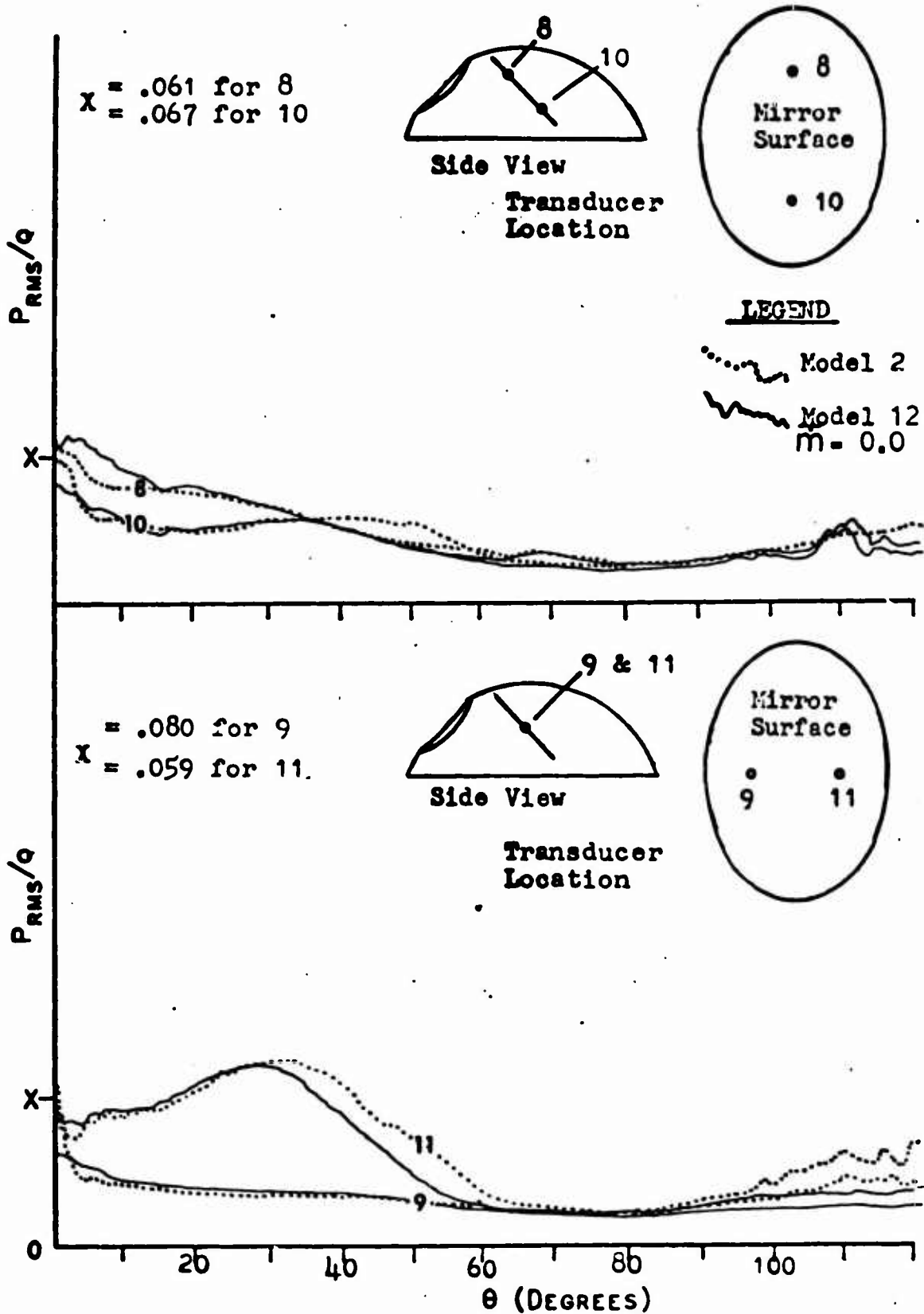


Fig. 48 PRESSURE VARIATIONS ON THE UTM SURFACE AS FUNCTION OF CAVITY ORIENTATION AND MODEL CONFIGURATION, $M = .85$

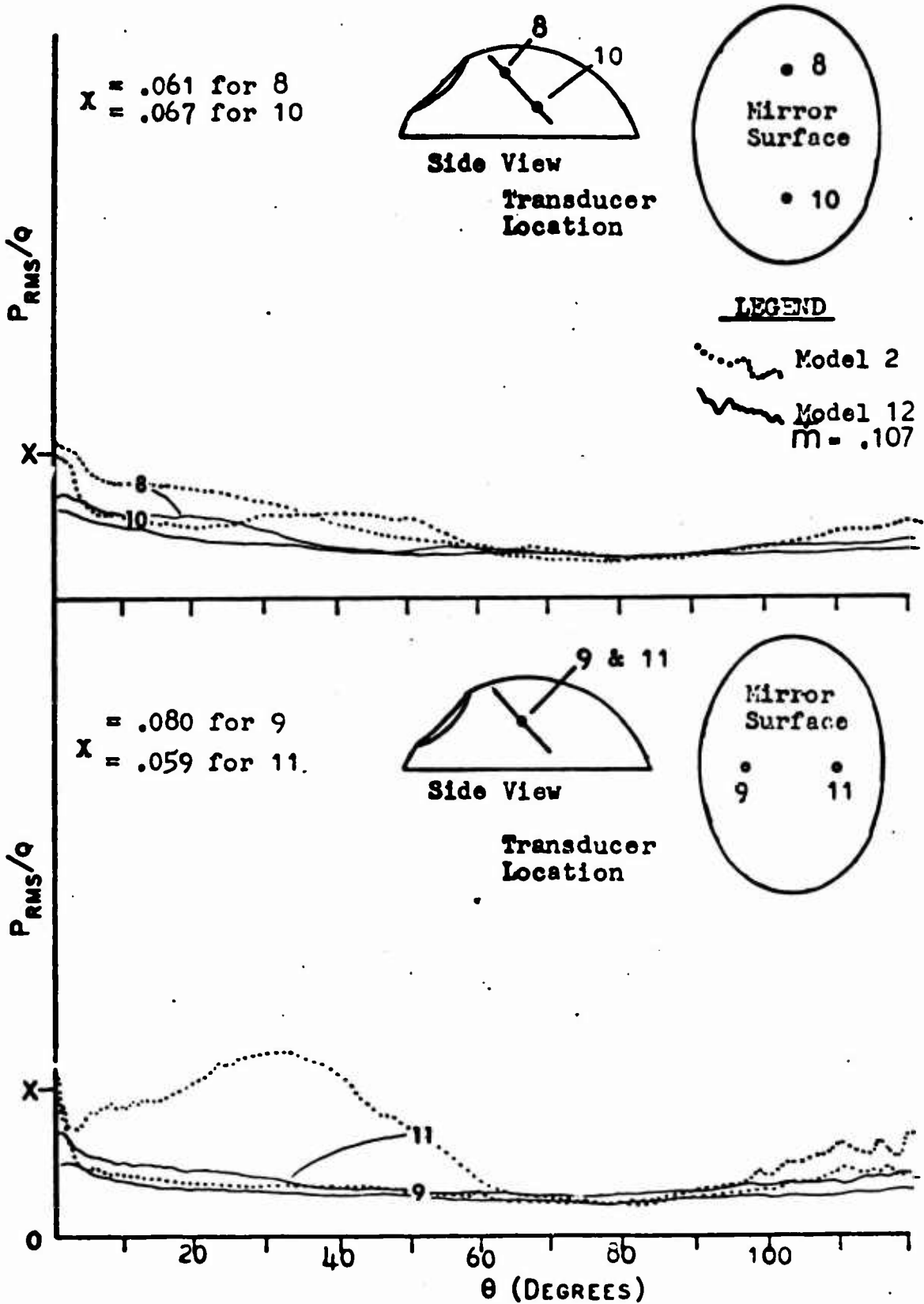


Fig. 49. PRESSURE VARIATIONS ON THE UTM SURFACE AS FUNCTION OF CAVITY ORIENTATION AND MODEL CONFIGURATION, $M = .85$

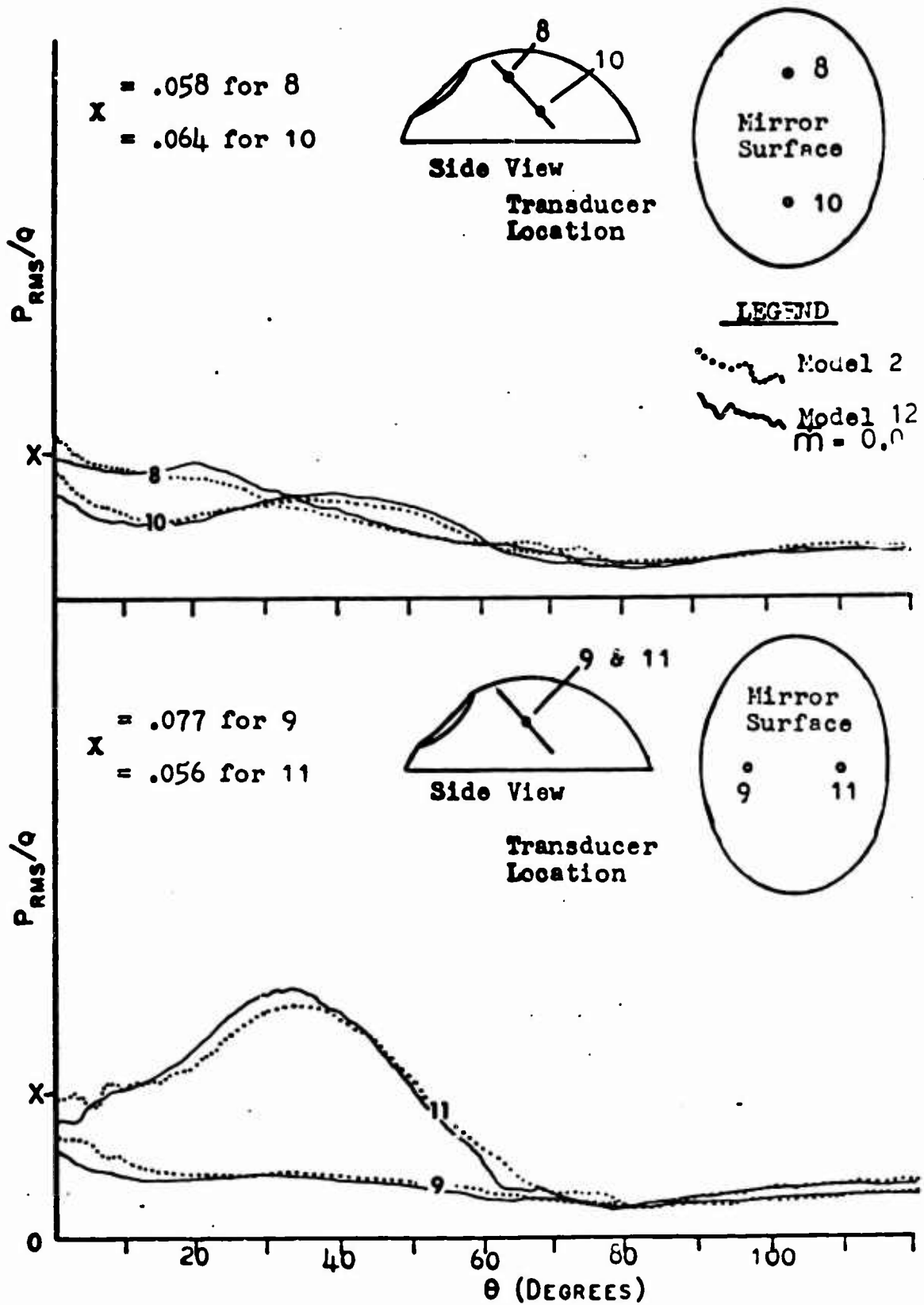


Fig. 50. PRESSURE VARIATIONS ON THE UTM SURFACE AS FUNCTION OF CAVITY ORIENTATION AND MODEL CONFIGURATION, $M = .95$

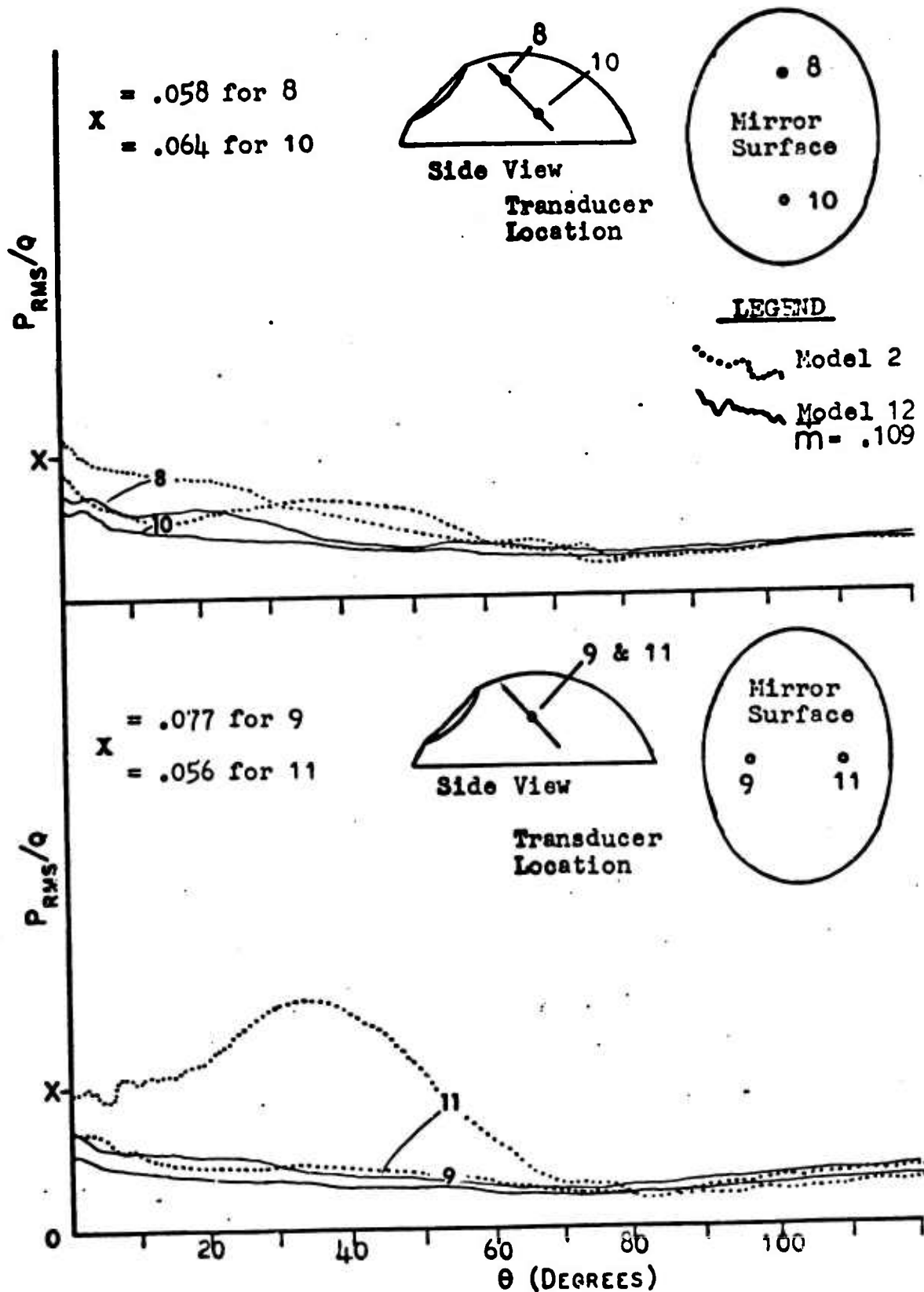


Fig. 51. PRESSURE VARIATIONS ON THE UTM SURFACE AS FUNCT, ON OF CAVITY ORIENTATION AND MODEL CONFIGURATION, $M = .95$

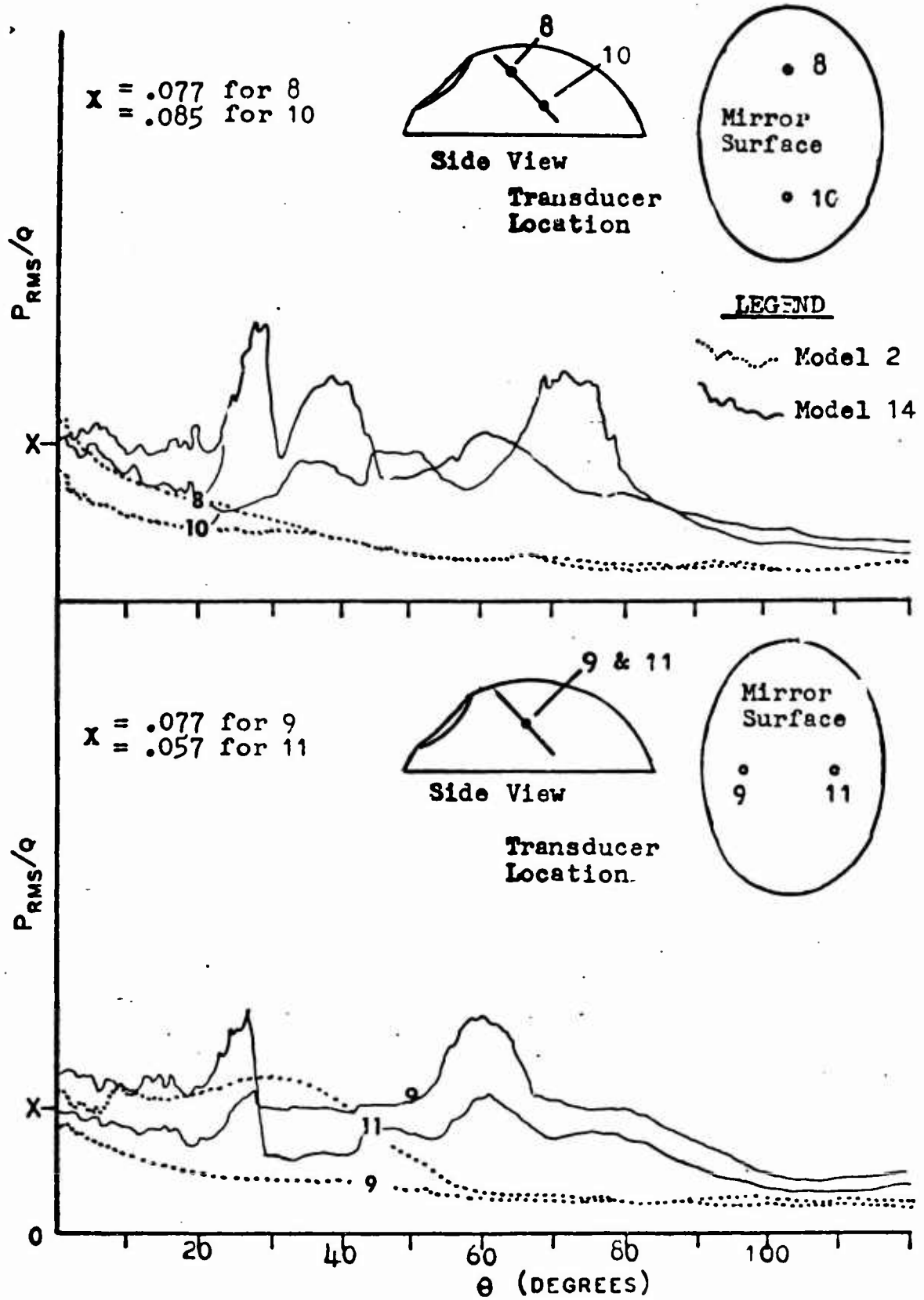


Fig. 52. PRESSURE VARIATIONS ON THE UTM SURFACE AS FUNCTION OF CAVITY ORIENTATION AND MODEL CONFIGURATION, $M = .70$

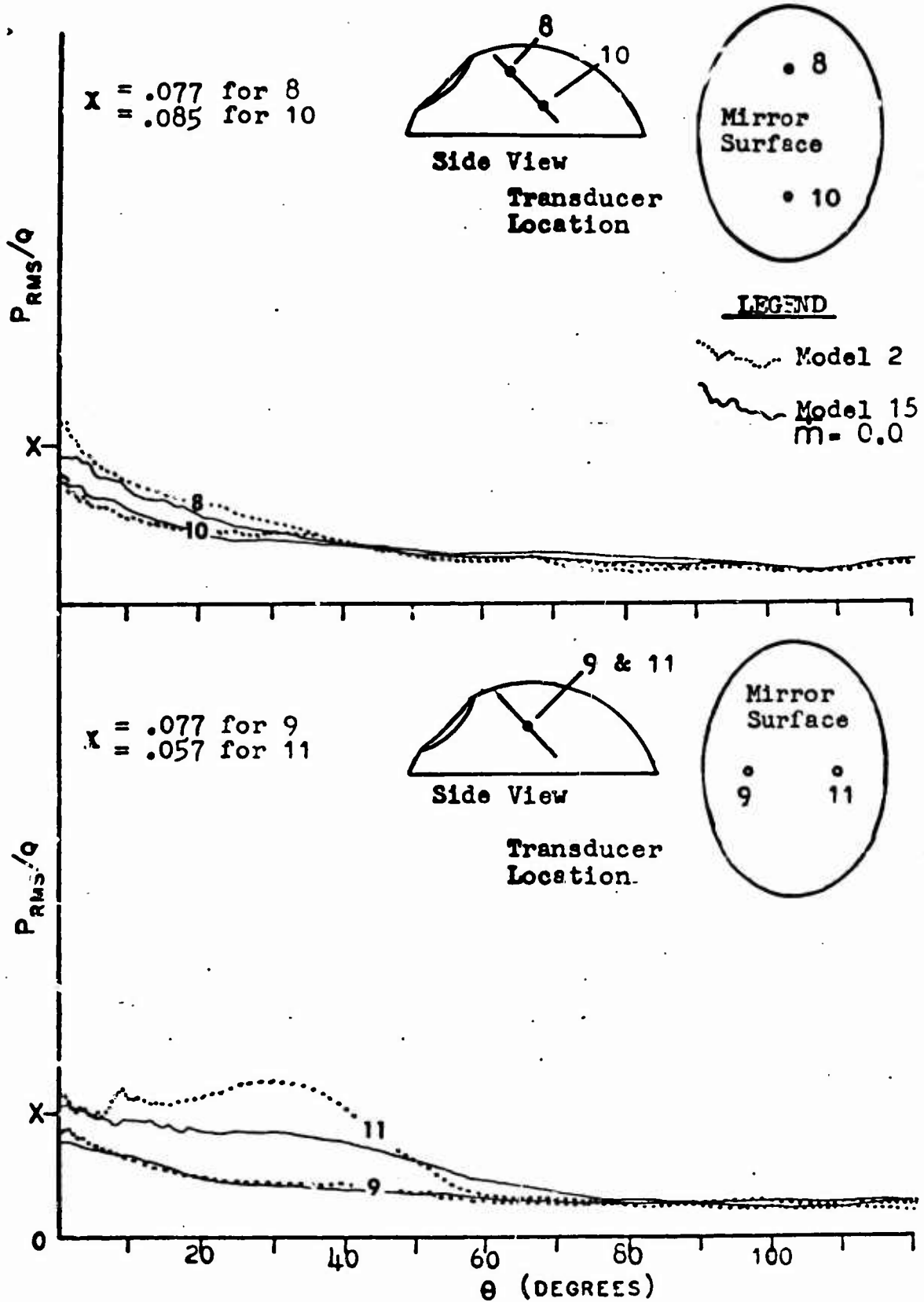


Fig. 53. PRESSURE VARIATIONS ON THE UTM SURFACE AS FUNCTION OF CAVITY ORIENTATION AND MODEL CONFIGURATION, $M = .70$

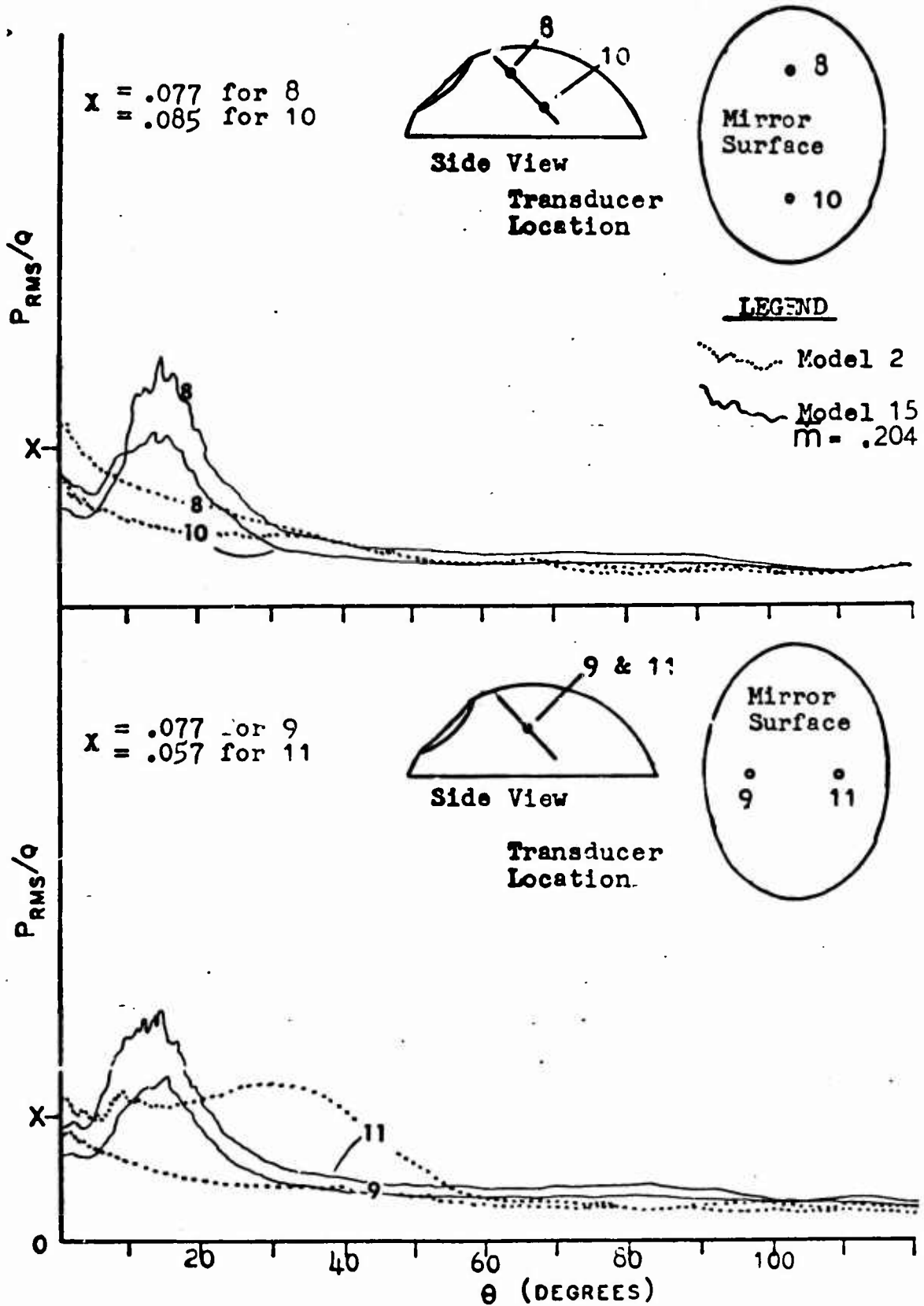


Fig. 54. PRESSURE VARIATIONS ON THE UTM SURFACE AS FUNCTION OF CAVITY ORIENTATION AND MODEL CONFIGURATION, $M = .70$

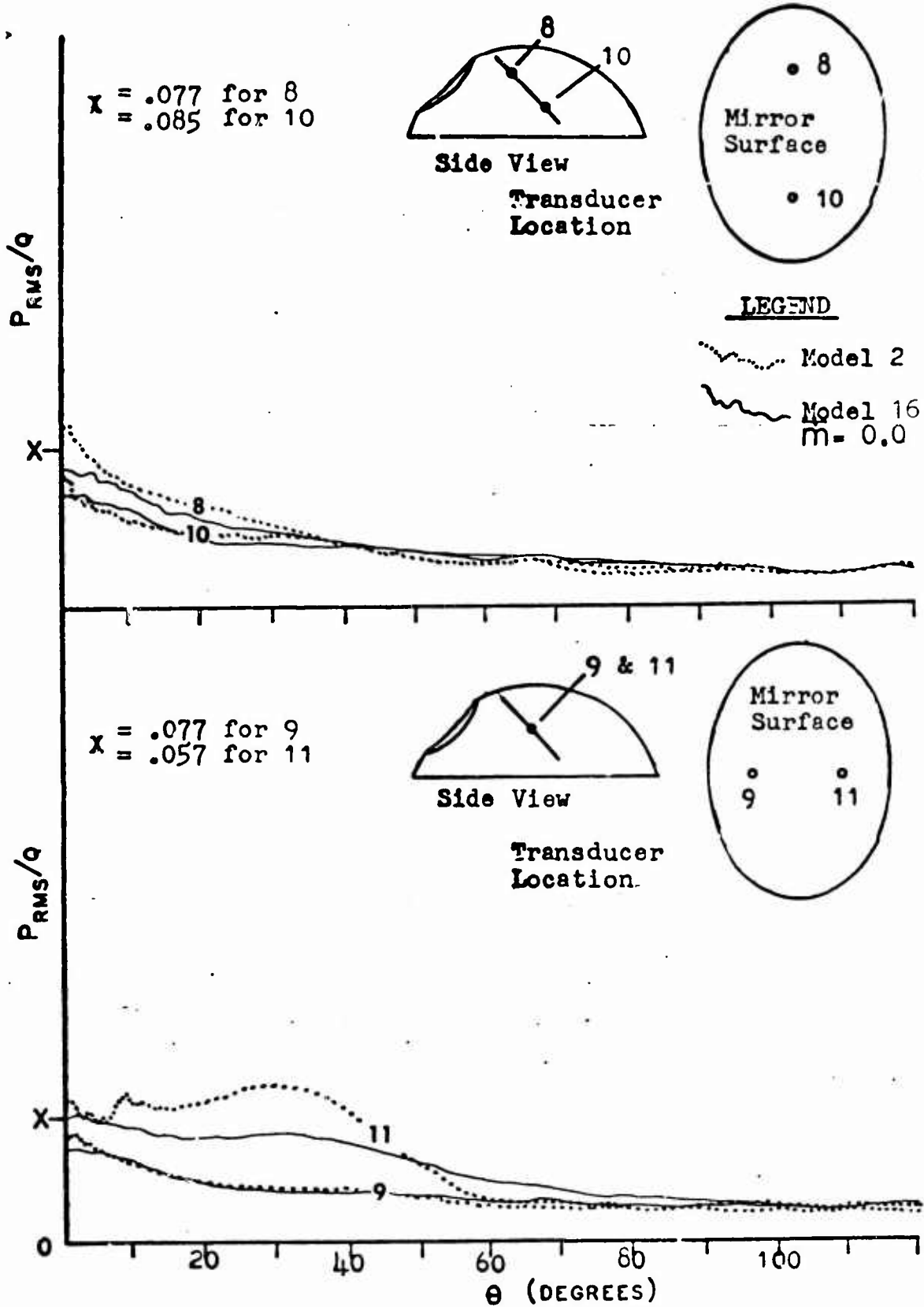


Fig. 55. PRESSURE VARIATIONS ON THE UTM SURFACE AS FUNCTION OF CAVITY ORIENTATION AND MODEL CONFIGURATION, $M=.70$

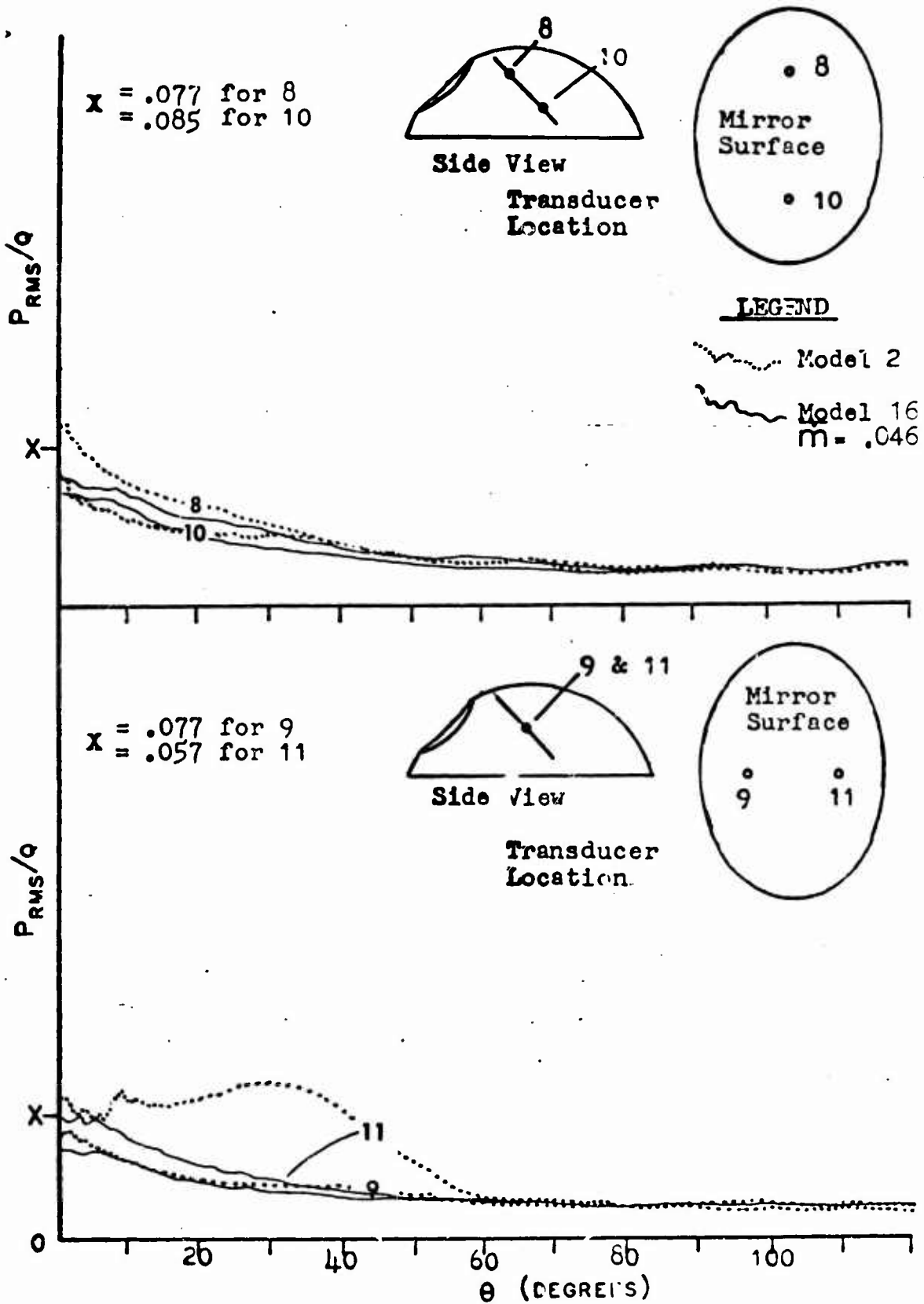


Fig. 56. PRESSURE VARIATIONS ON THE UTM SURFACE AS FUNCTION OF CAVITY ORIENTATION AND MODEL CONFIGURATION, $M = .70$

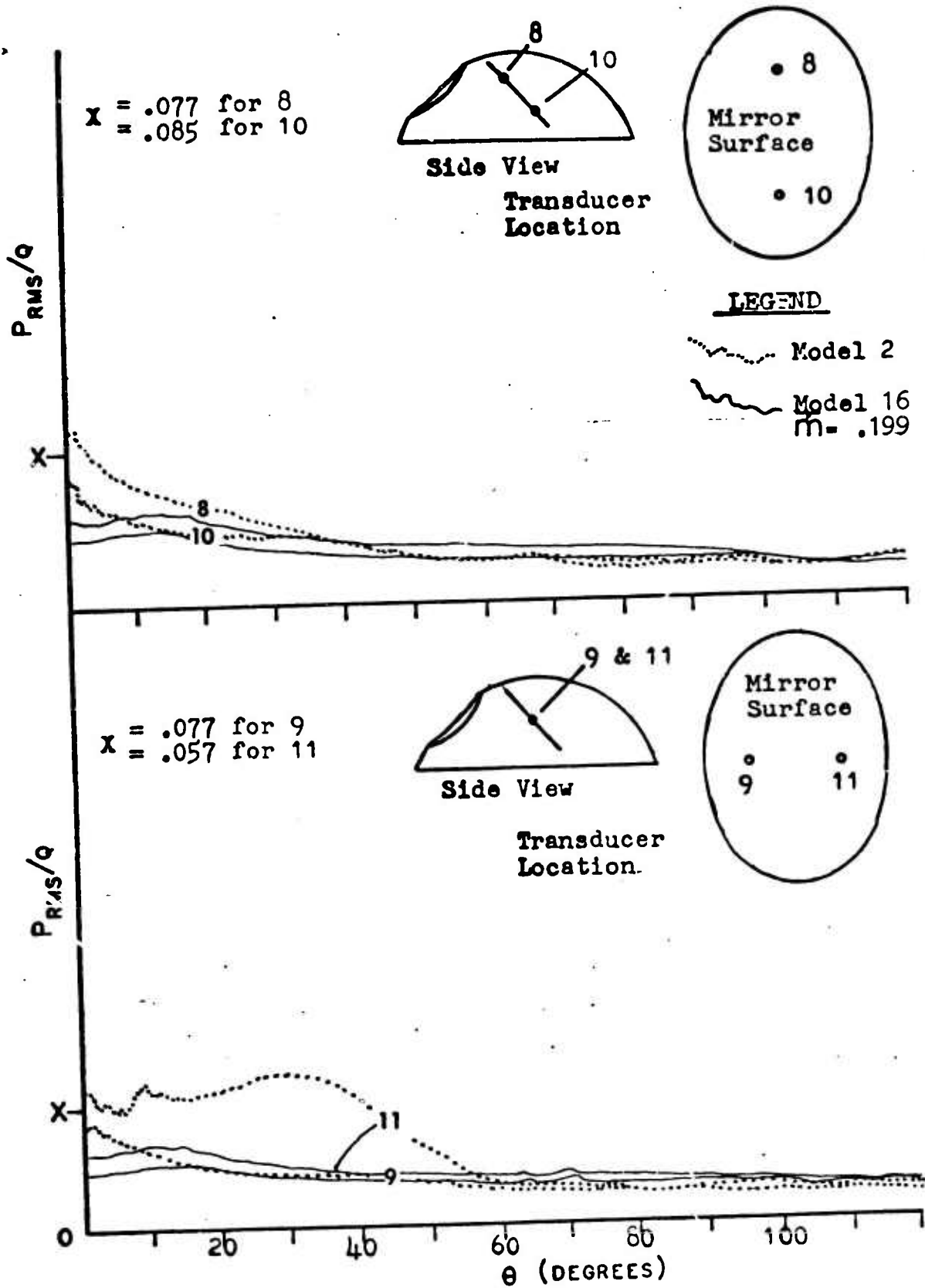


Fig. 57. PRESSURE VARIATIONS ON THE UTM SURFACE AS FUNCTION OF CAVITY ORIENTATION AND MODEL CONFIGURATION, $M = .70$

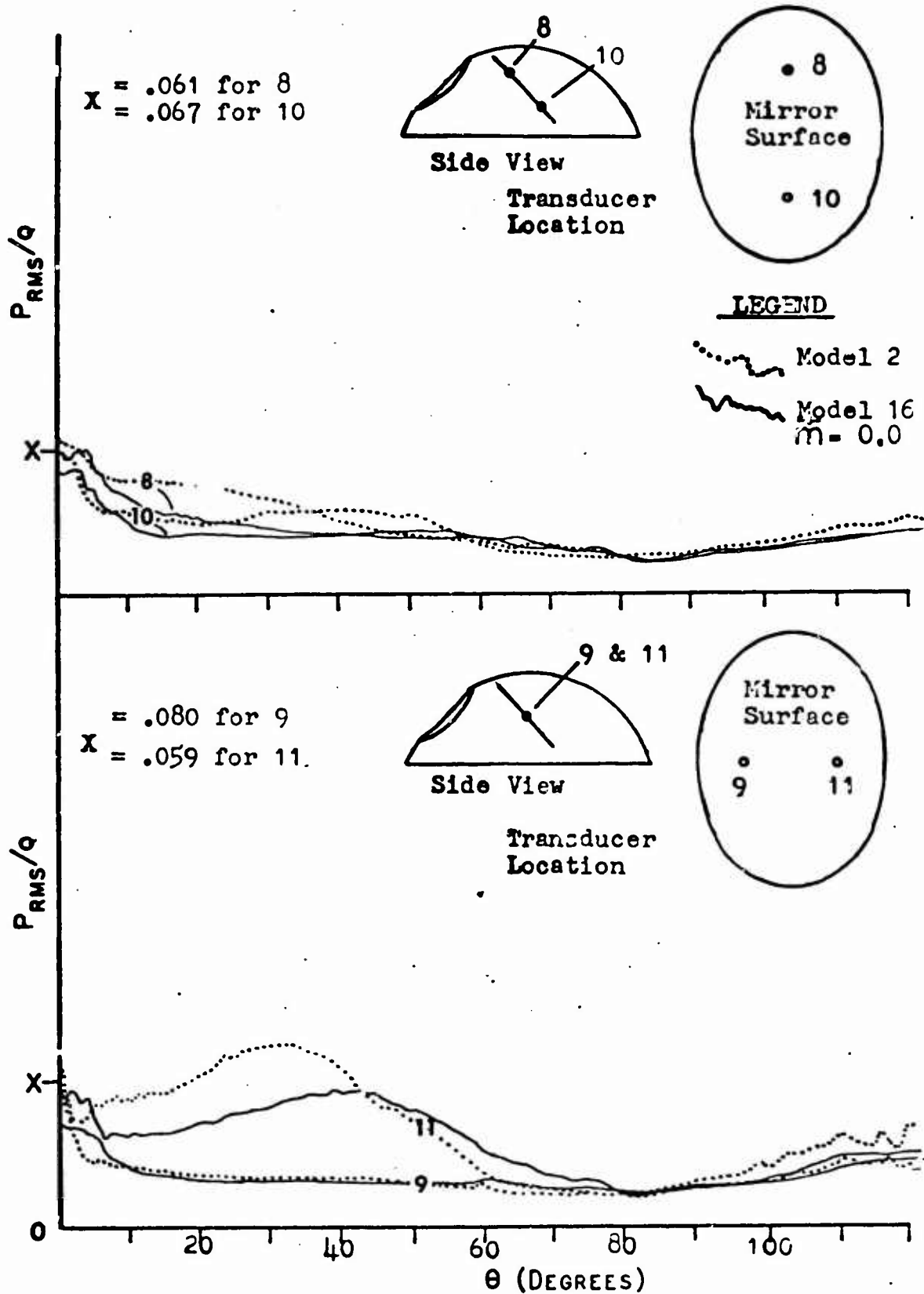


Fig. 58. PRESSURE VARIATIONS ON THE UTM SURFACE AS FUNCTION OF CAVITY ORIENTATION AND MODEL CONFIGURATION, $M = .85$

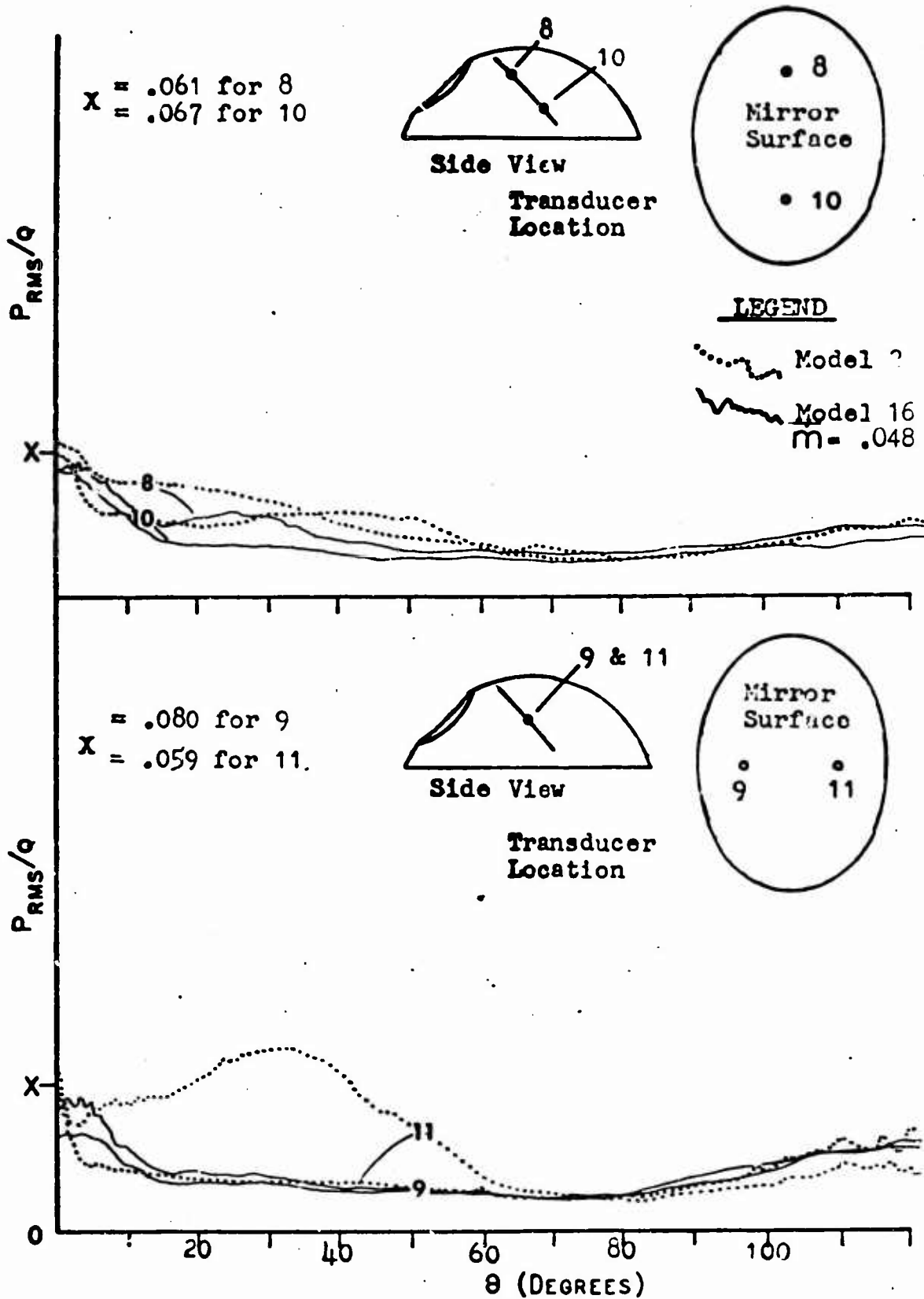


Fig. 59 PRESSURE VARIATIONS ON THE UTM SURFACE AS FUNCTION OF CAVITY ORIENTATION AND MODEL CONFIGURATION, $M = .85$

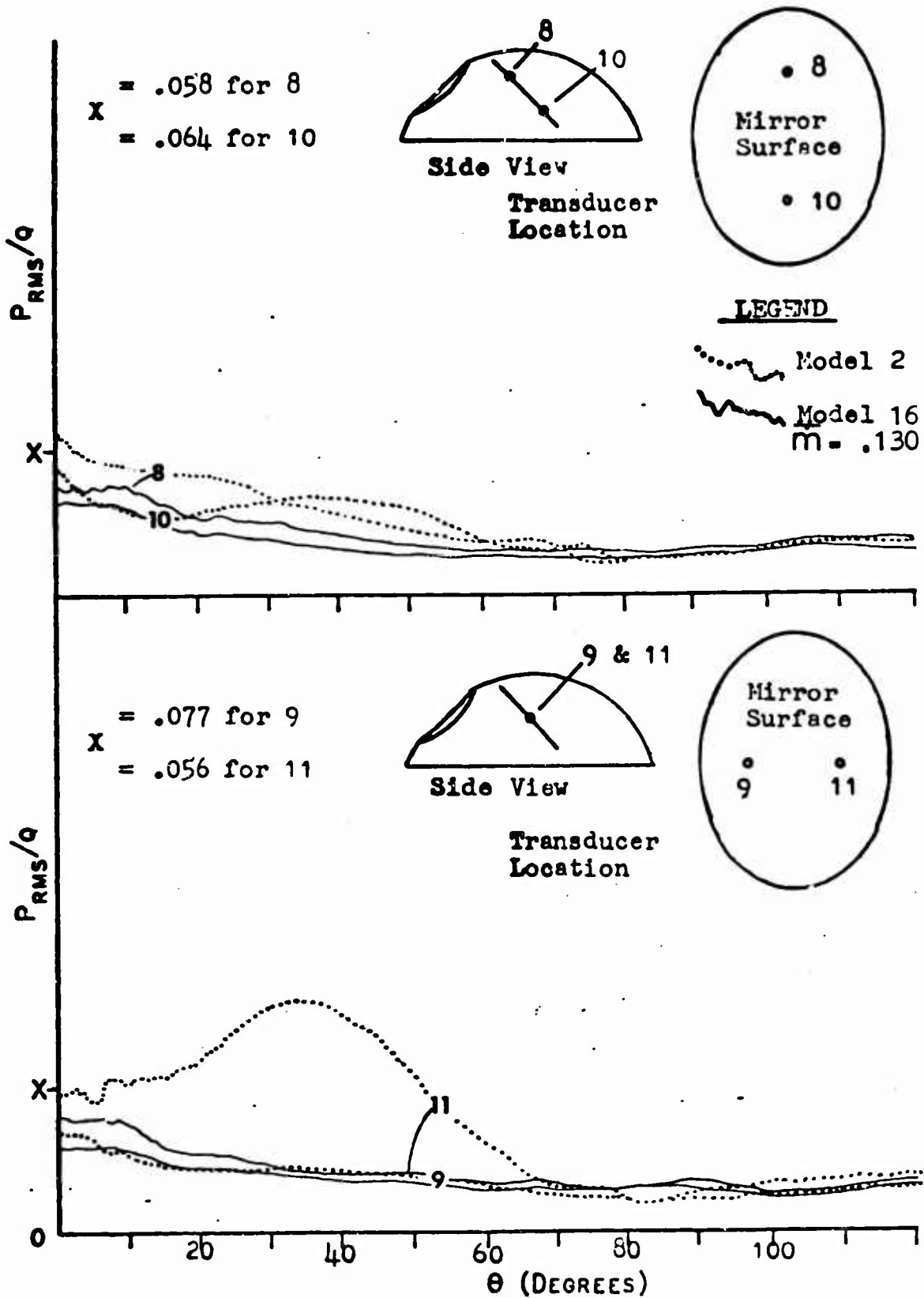


Fig. 6Q. PRESSURE VARIATIONS ON THE UTM SURFACE AS FUNCTION OF CAVITY ORIENTATION AND MODEL CONFIGURATION, $M = .95$

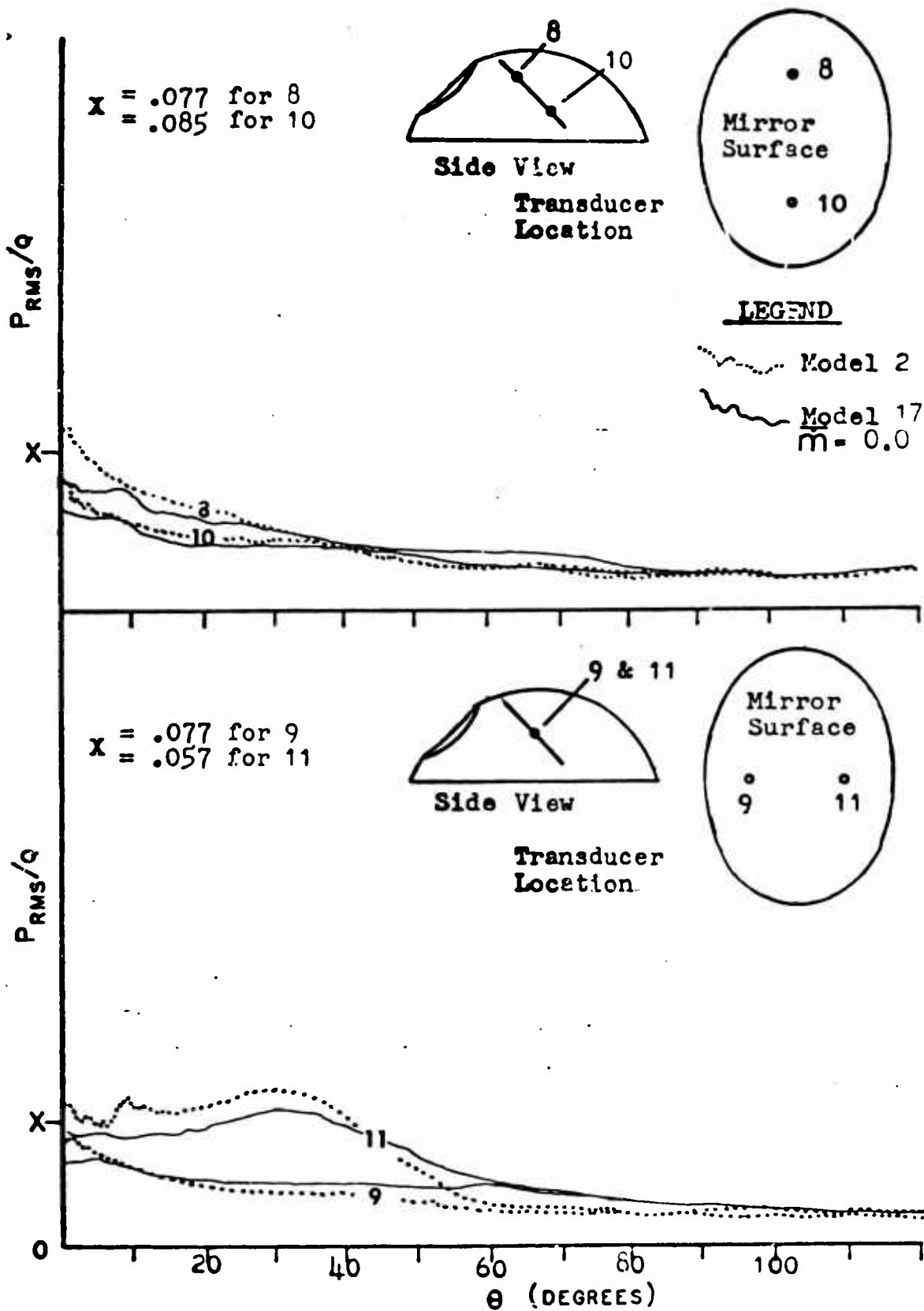


Fig. 61. PRESSURE VARIATIONS ON THE UTM SURFACE AS FUNCTION OF CAVITY ORIENTATION AND MODEL CONFIGURATION, $M = .70$

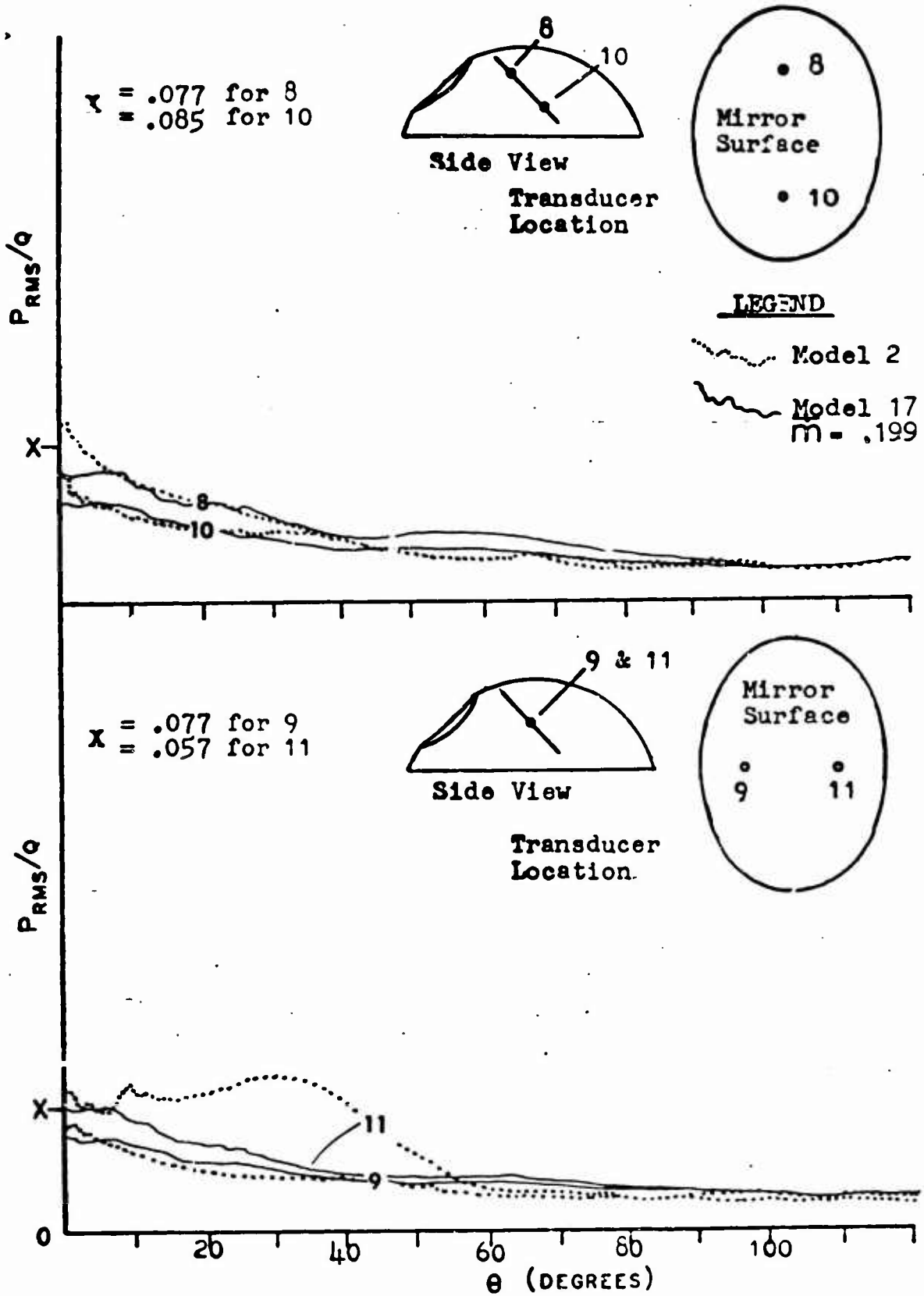


Fig. 62. PRESSURE VARIATIONS ON THE UTM SURFACE AS FUNCTION OF CAVITY ORIENTATION AND MODEL CONFIGURATION, $M = .70$

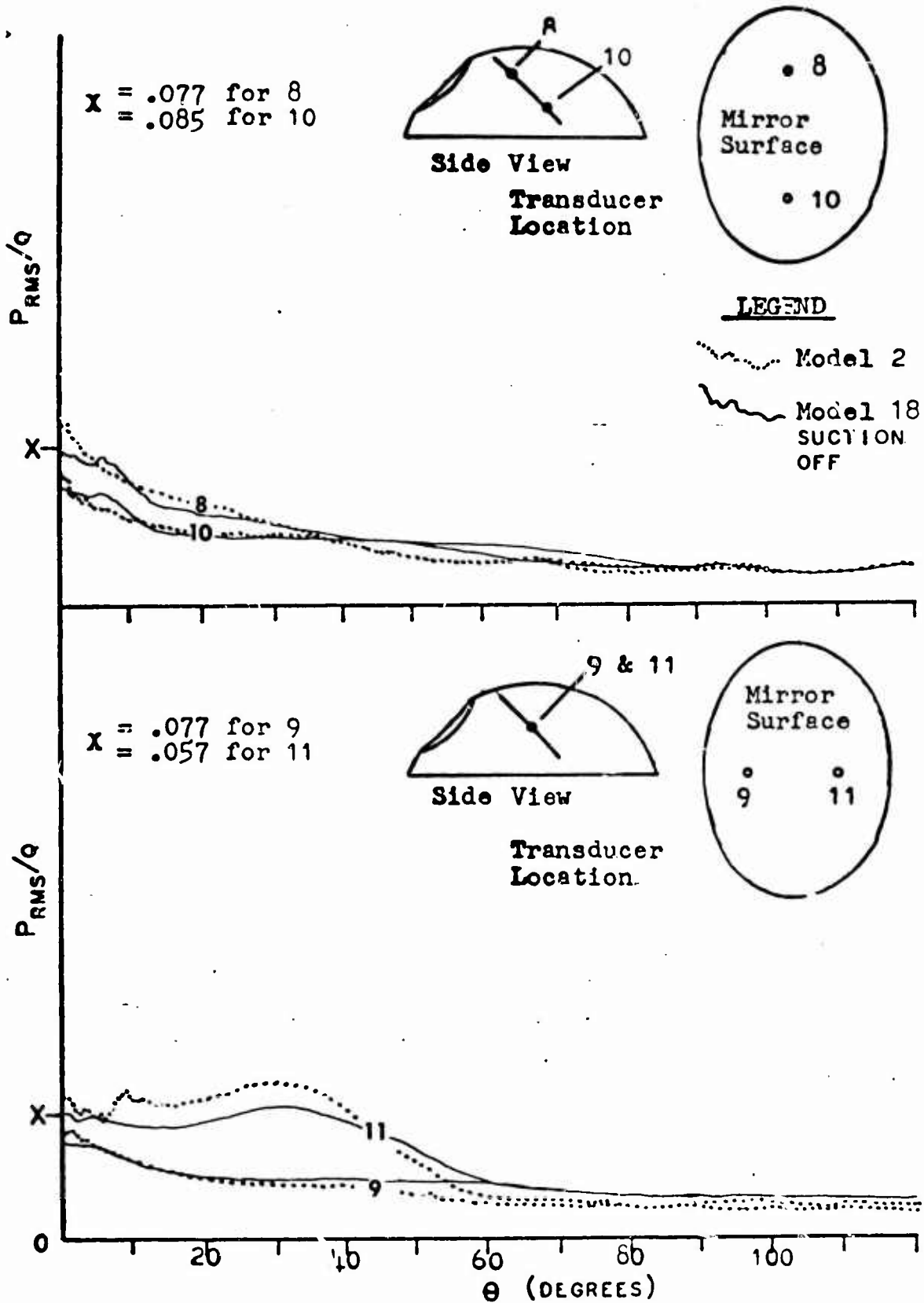


Fig. 63 PRESSURE VARIATIONS ON THE UTM SURFACE AS FUNCTION OF CAVITY ORIENTATION AND MODEL CONFIGURATION, $M_\infty = .70$

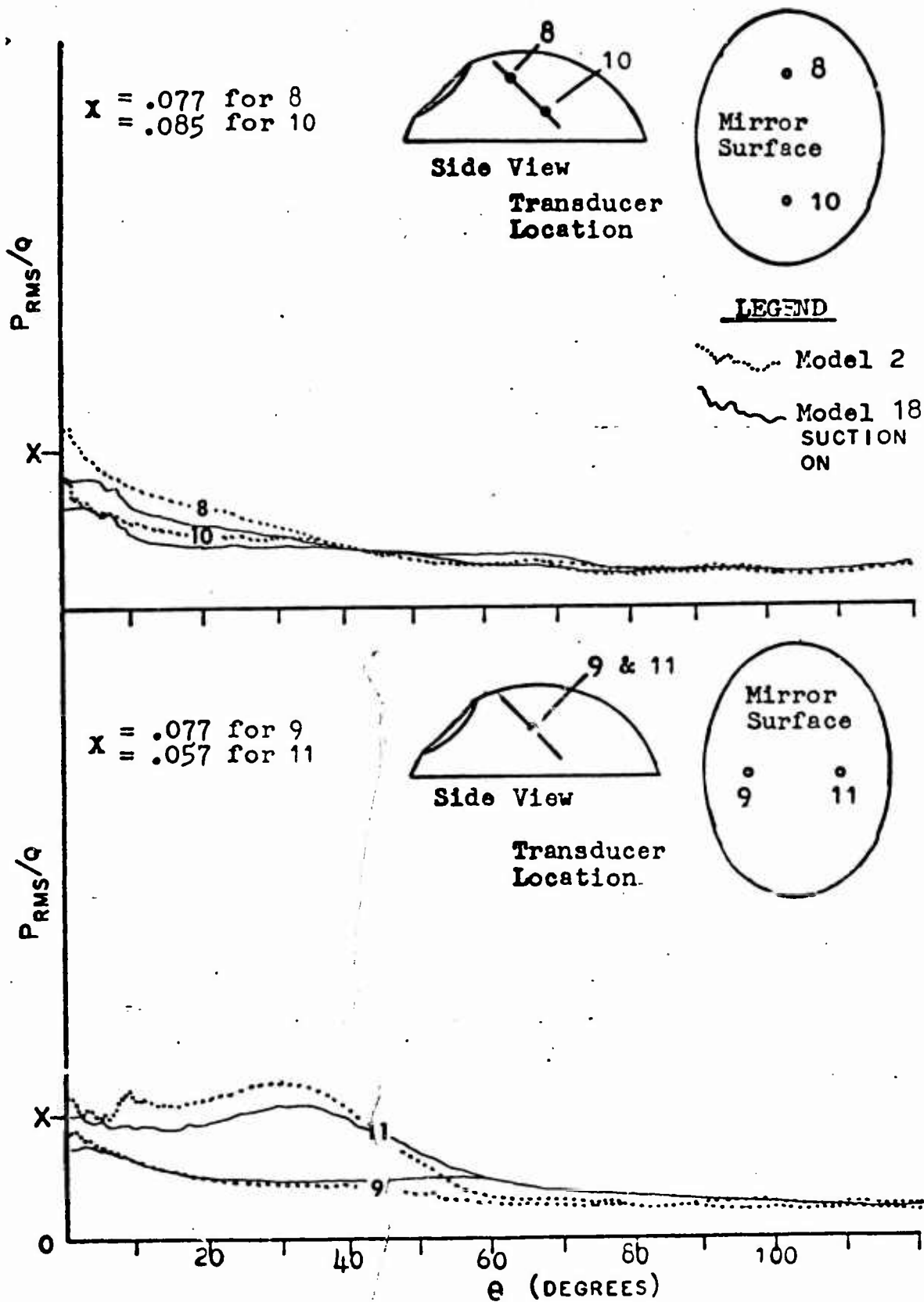


Fig. 64. PRESSURE VARIATIONS ON THE UTM SURFACE AS FUNCTION OF CAVITY ORIENTATION AND MODEL CONFIGURATION, $M = .70$

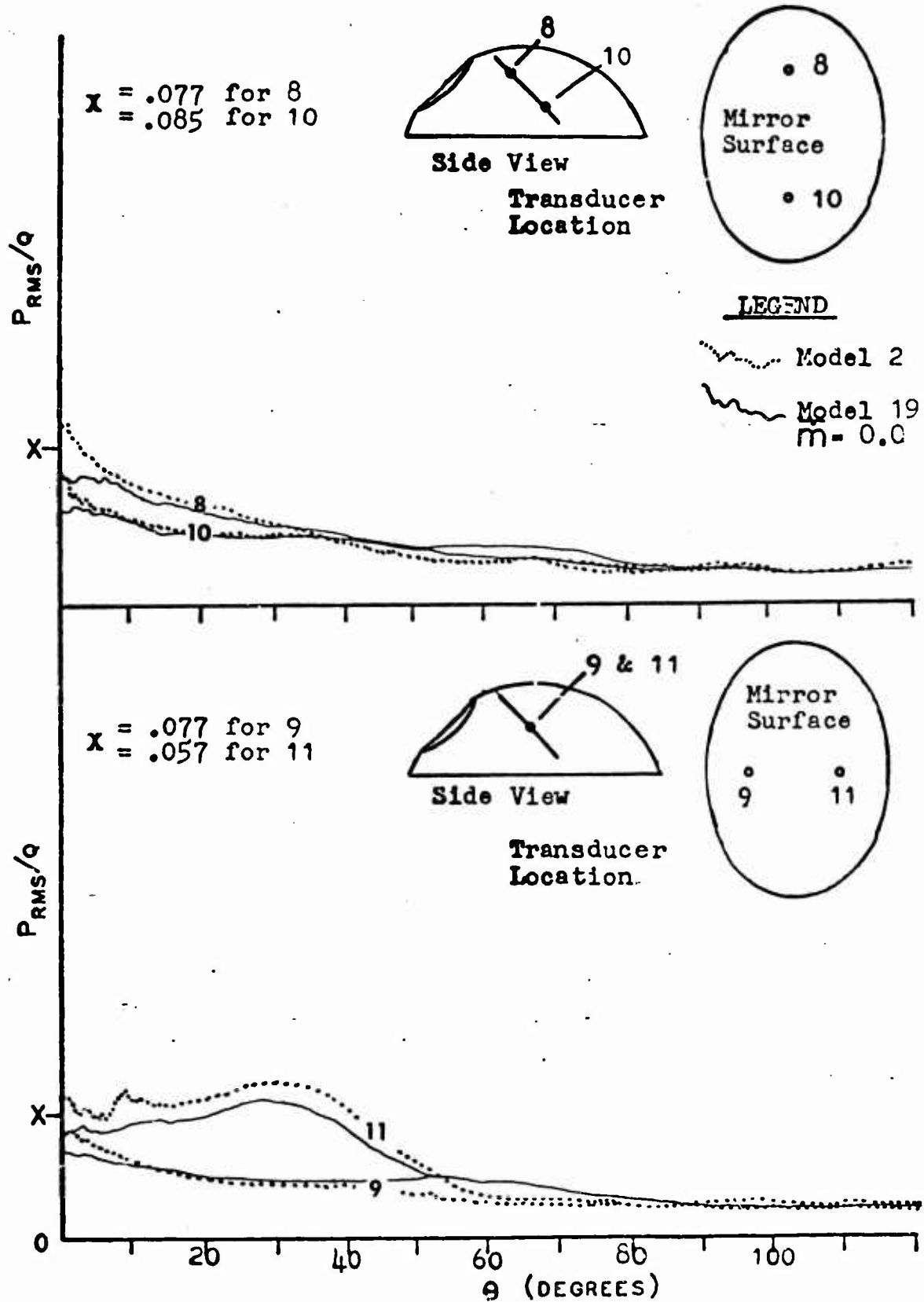


Fig. 65. PRESSURE VARIATIONS ON THE UTM SURFACE AS FUNCTION OF CAVITY ORIENTATION AND MODEL CONFIGURATION, $M = .70$

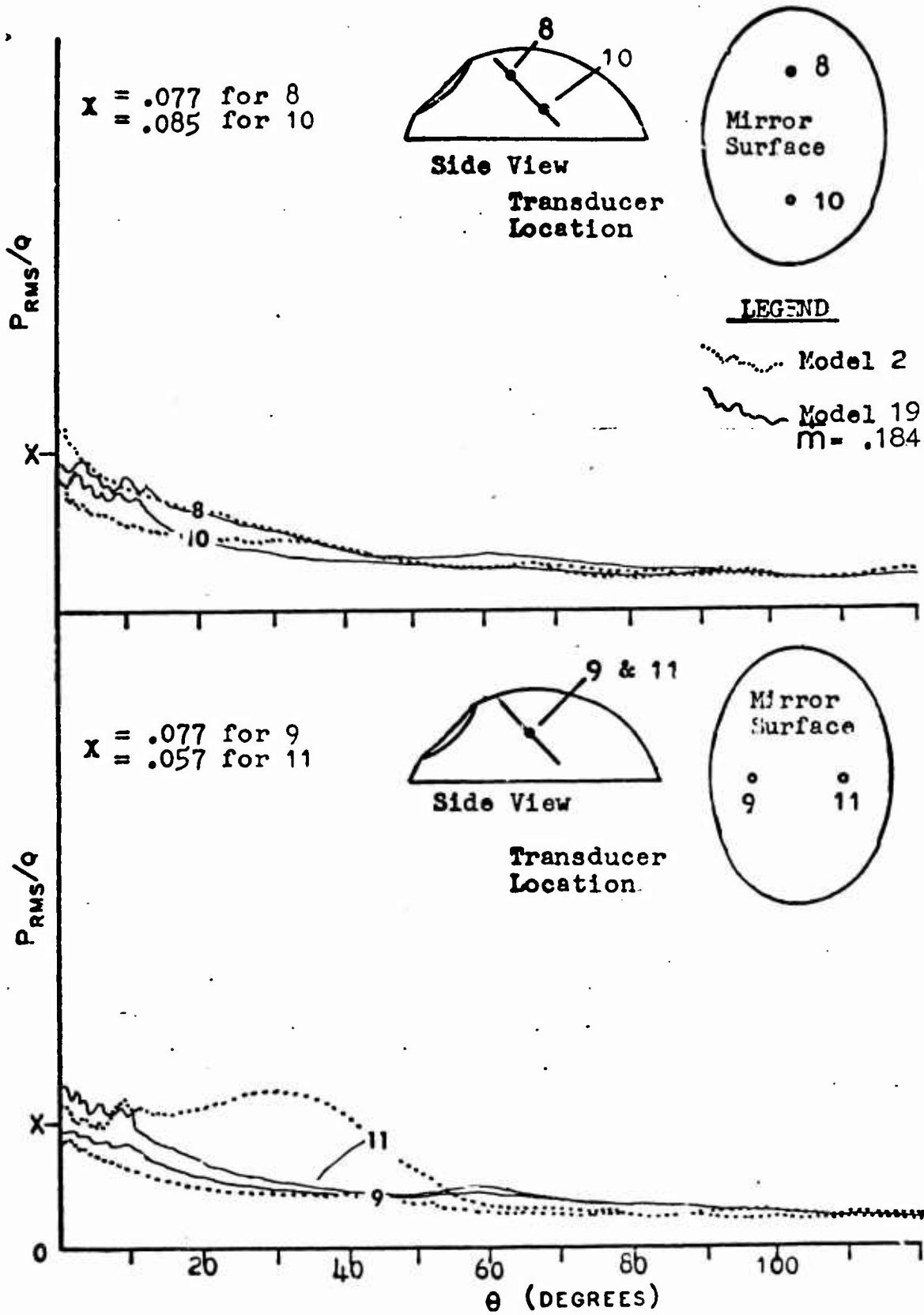


Fig. 66. PRESSURE VARIATIONS ON THE UTM SURFACE AS FUNCTION OF CAVITY ORIENTATION AND MODEL CONFIGURATION, $M = .70$

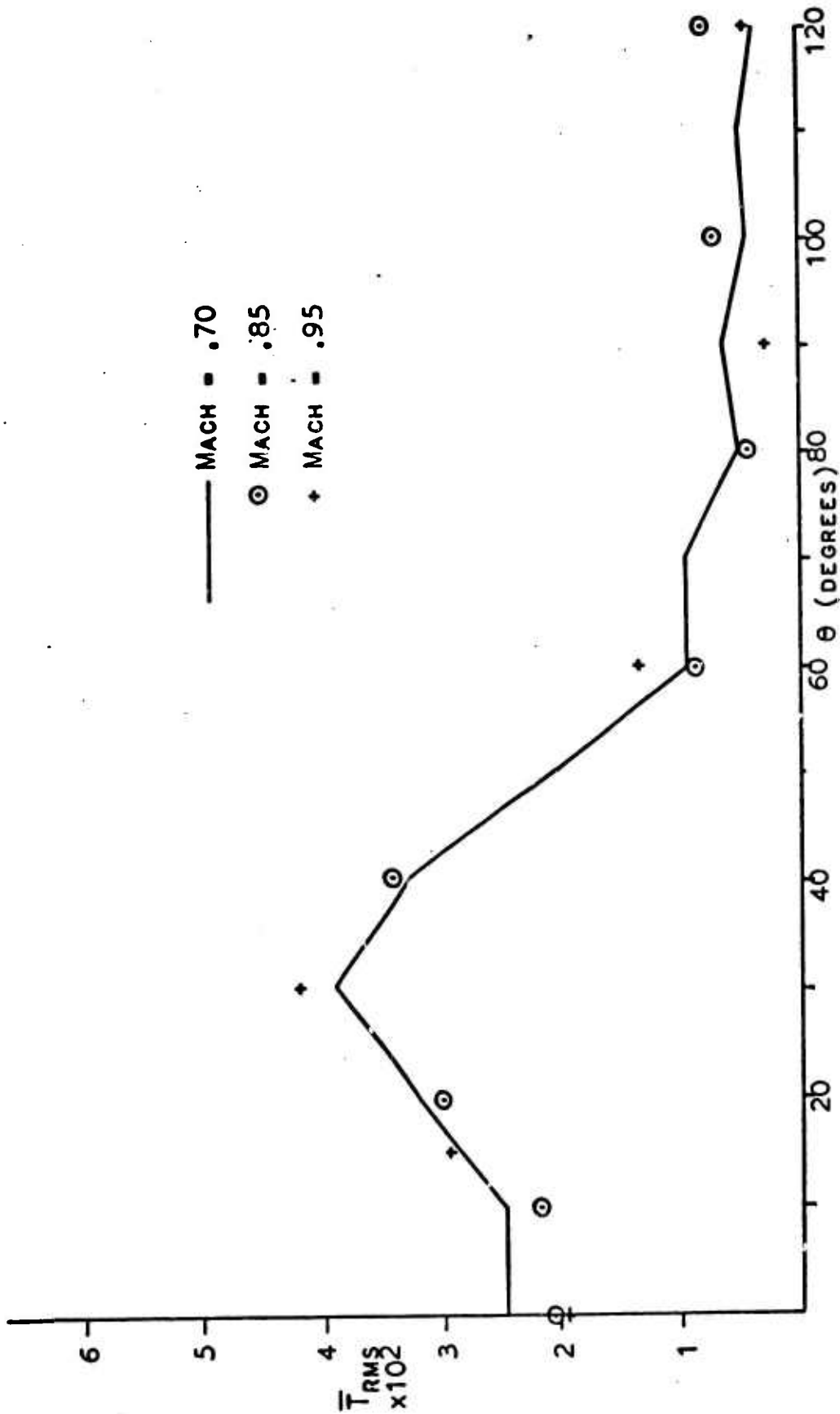


Fig. 67. Non-dimensionalized root-mean-square torque about the Modcl 2 UTM azimuth axis as a function of the orientation of the turret aperture for various values of the free stream Mach No.

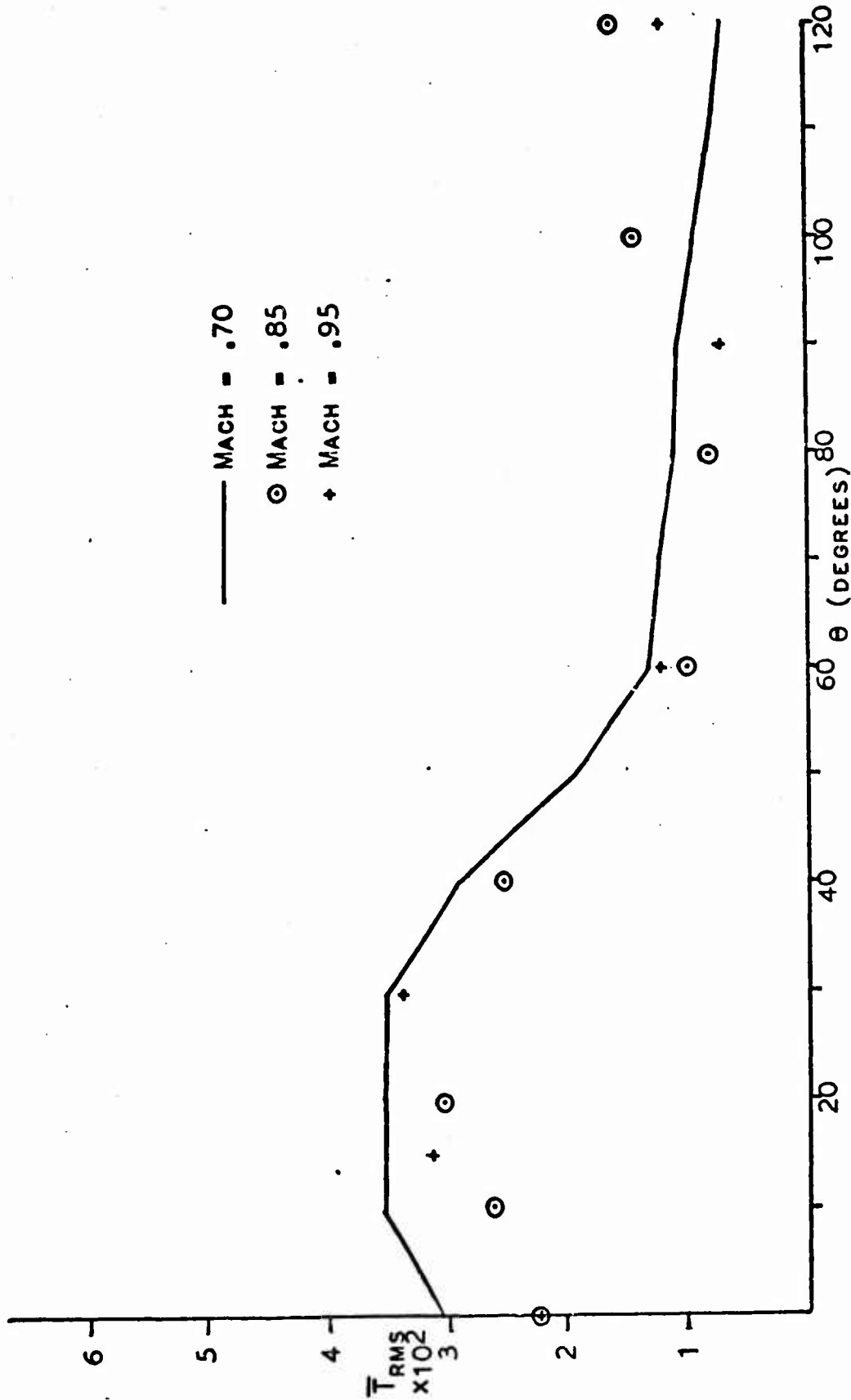


Fig. 68. Non-dimensionalized root-mean-square torque about the Model 2 UTM elevation axis as a function of the orientation of the turret aperture for various values of the free stream Mach No.

Appendix D

Turret Static Pressure Distribution

Contained in this section are Figures 69 thru 78. These depict the turret flow Mach number and C_p as functions of the local angle to U_∞ and free stream velocity for Models 1 and 2. The reader is referred to page 11 for the location of the pressure taps utilized in the experiment.

The abscissa of each graph is given as the angle of the pressure tap to U_∞ . For pressure taps 1 thru 7 the angle of the turret aperture, θ , is given by

$$\theta = \text{angle of pressure tap} - 70^\circ \quad (6)$$

and for pressure taps 9 thru 11 by

$$\theta = \text{angle of pressure tap} - 110^\circ \quad (7)$$

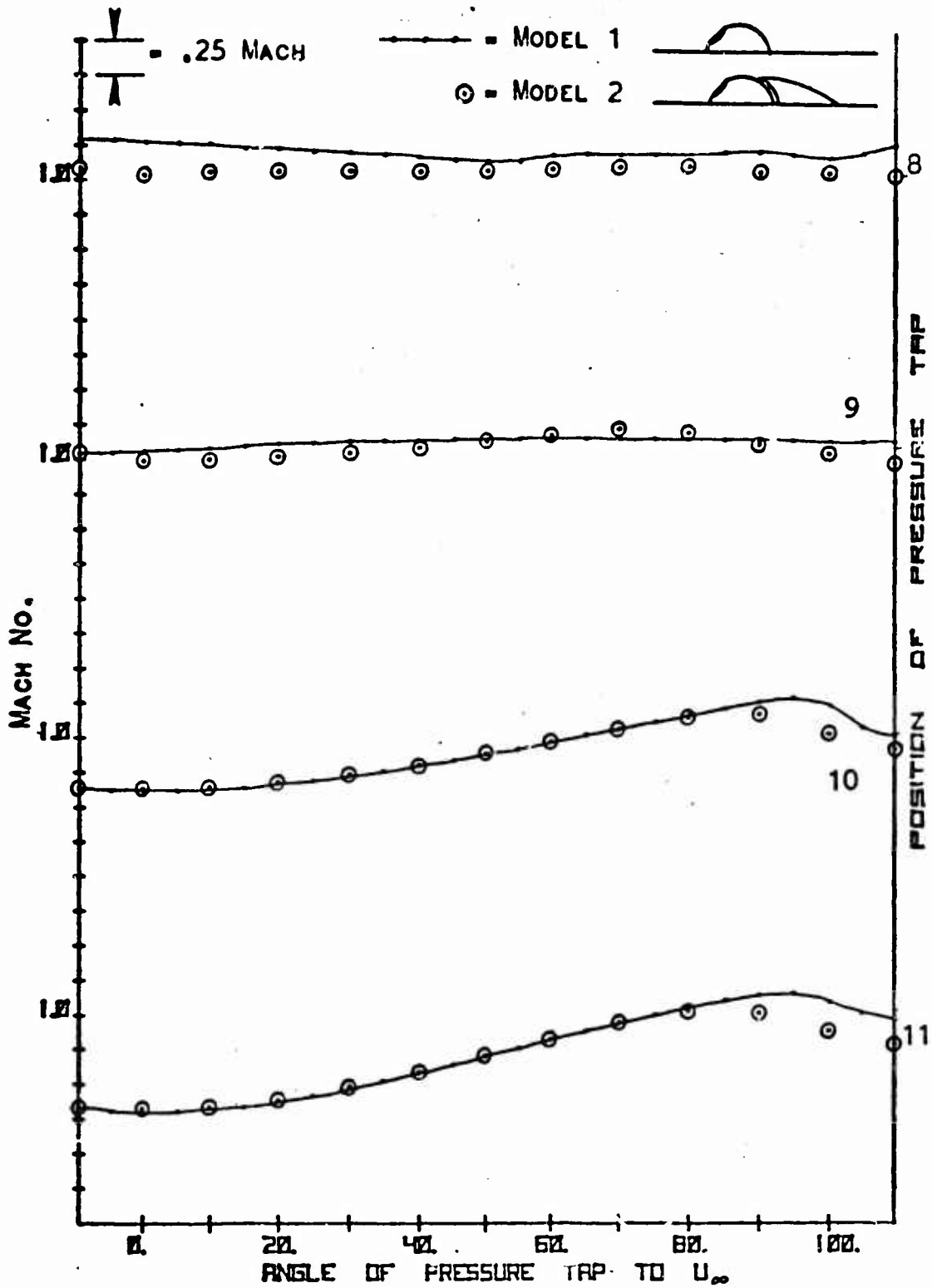


Fig. 69. Comparison of local turret flow Mach number with and without the aft fairing installed with free stream Mach = .7. See page 11 for pressure tap location.

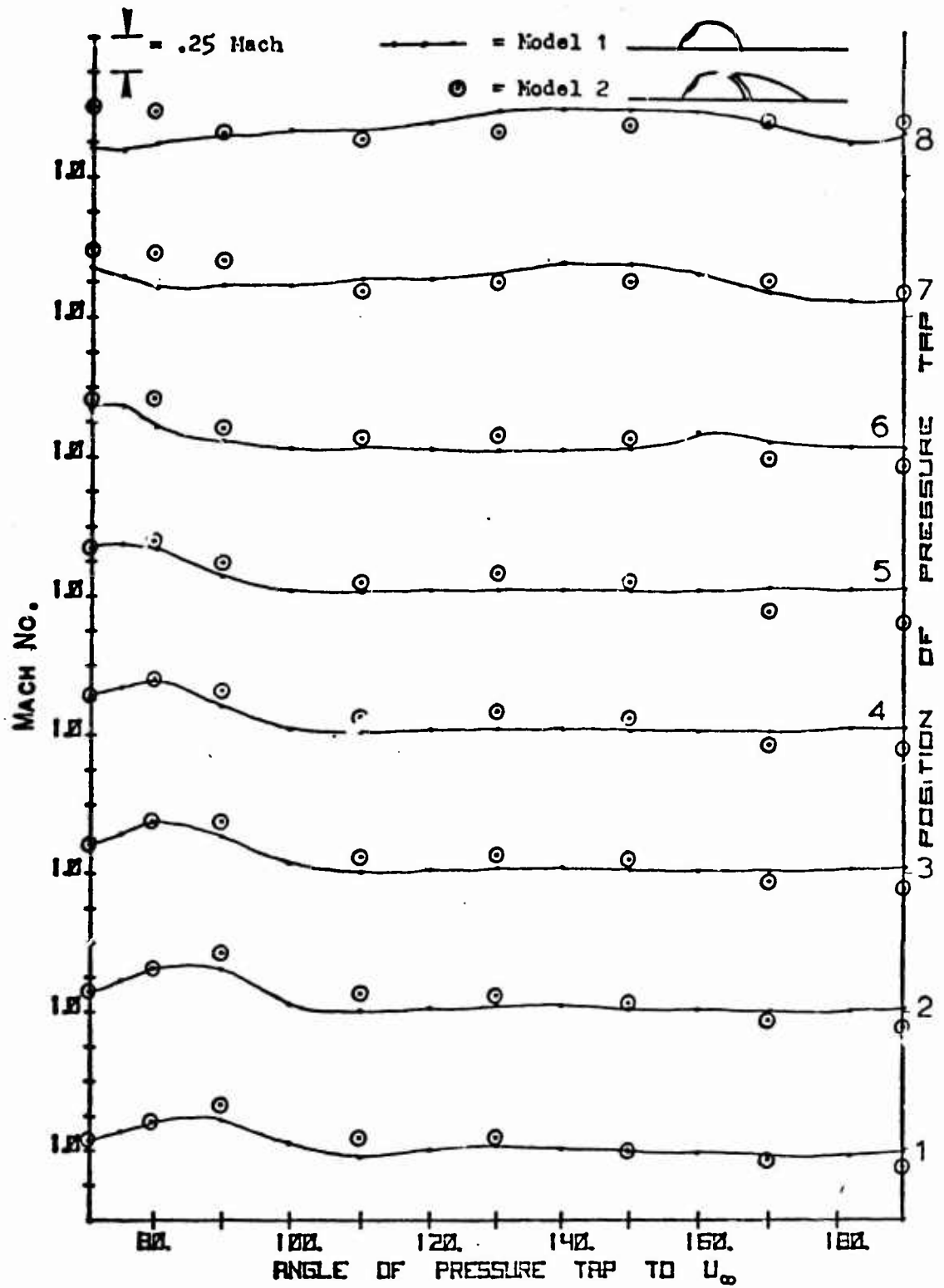


Fig. 70. Comparison of local turret flow Mach number with and without the aft fairing installed with free stream Mach = .85. See page 11 for pressure tap location.

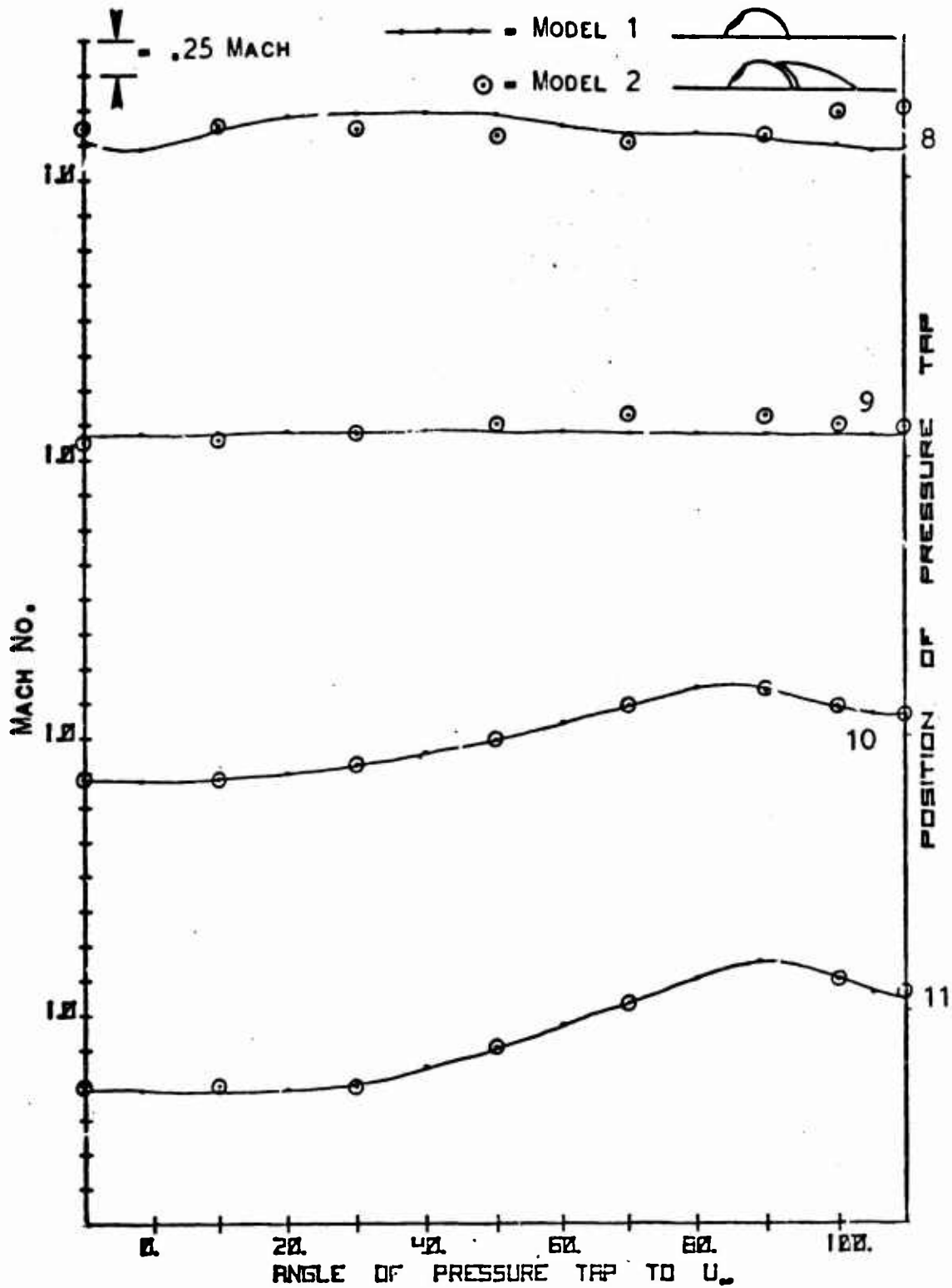


Fig. 71. Comparison of local turret flow Mach number with and without the aft fairing installed with free stream Mach = .85. See page 11 for pressure tap position.

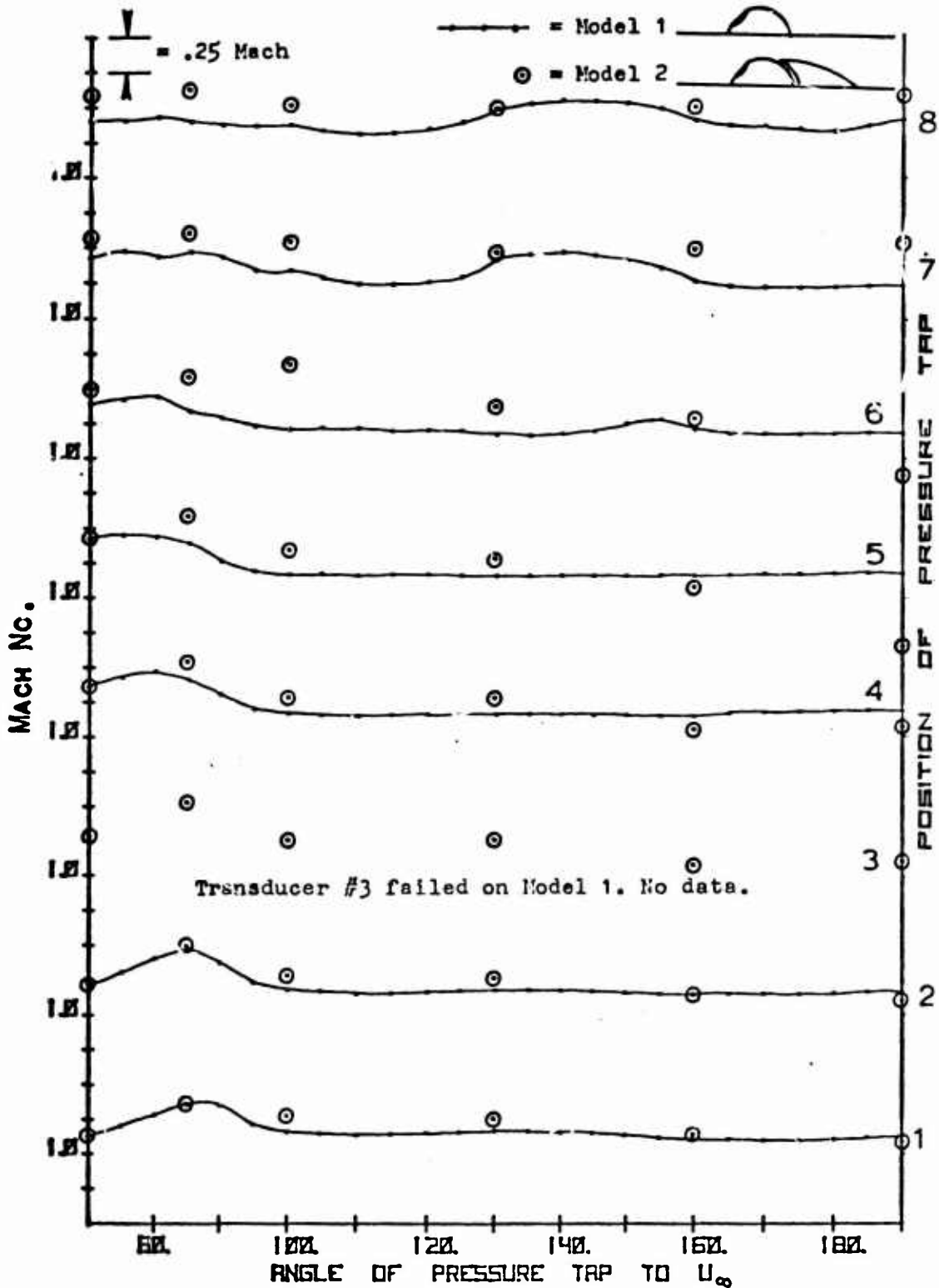


Fig. 72. Comparison of local turret flow Mach number with and without the aft fairing installed with free stream Mach = .95. See page 11 for pressure tap location.

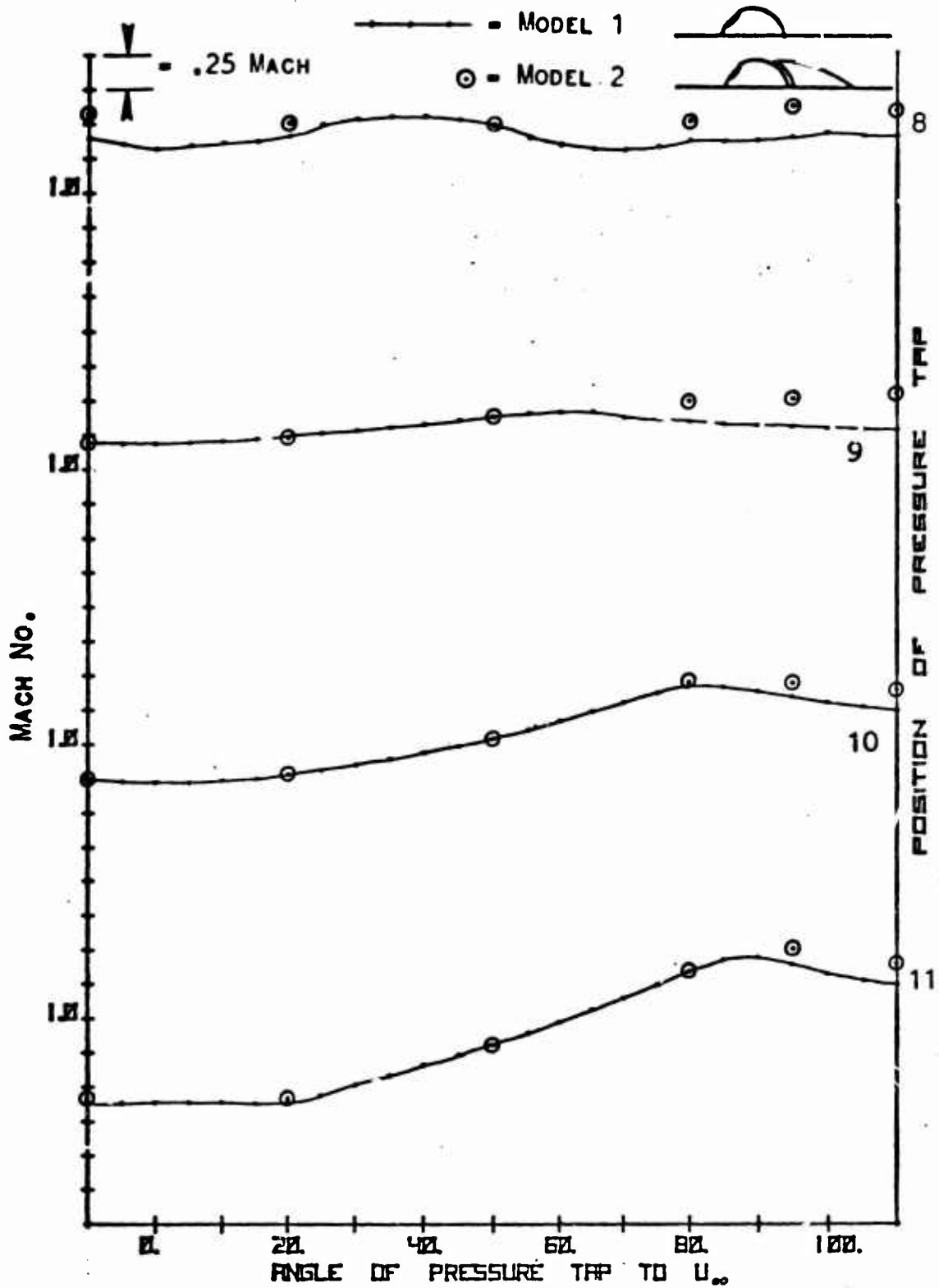


Fig. 73. Comparison of local turret flow Mach number with and without the aft fairing installed with free stream Mach = .95. See page 11 for pressure tap location.

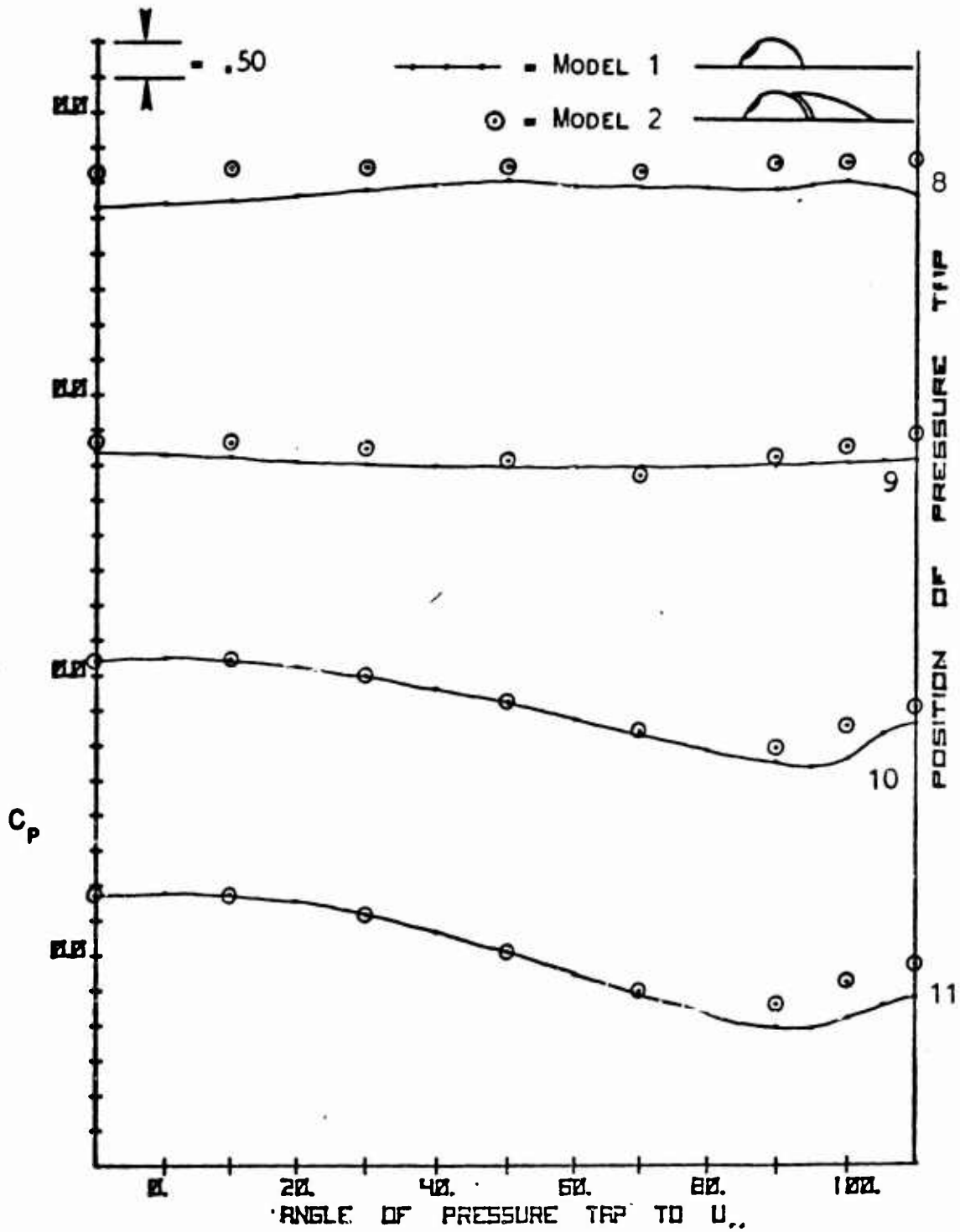


Fig. 74. Comparison of local turret flow C_p with and without the aft fairing installed^P with free stream Mach = .7. See page 11 for pressure tap location.

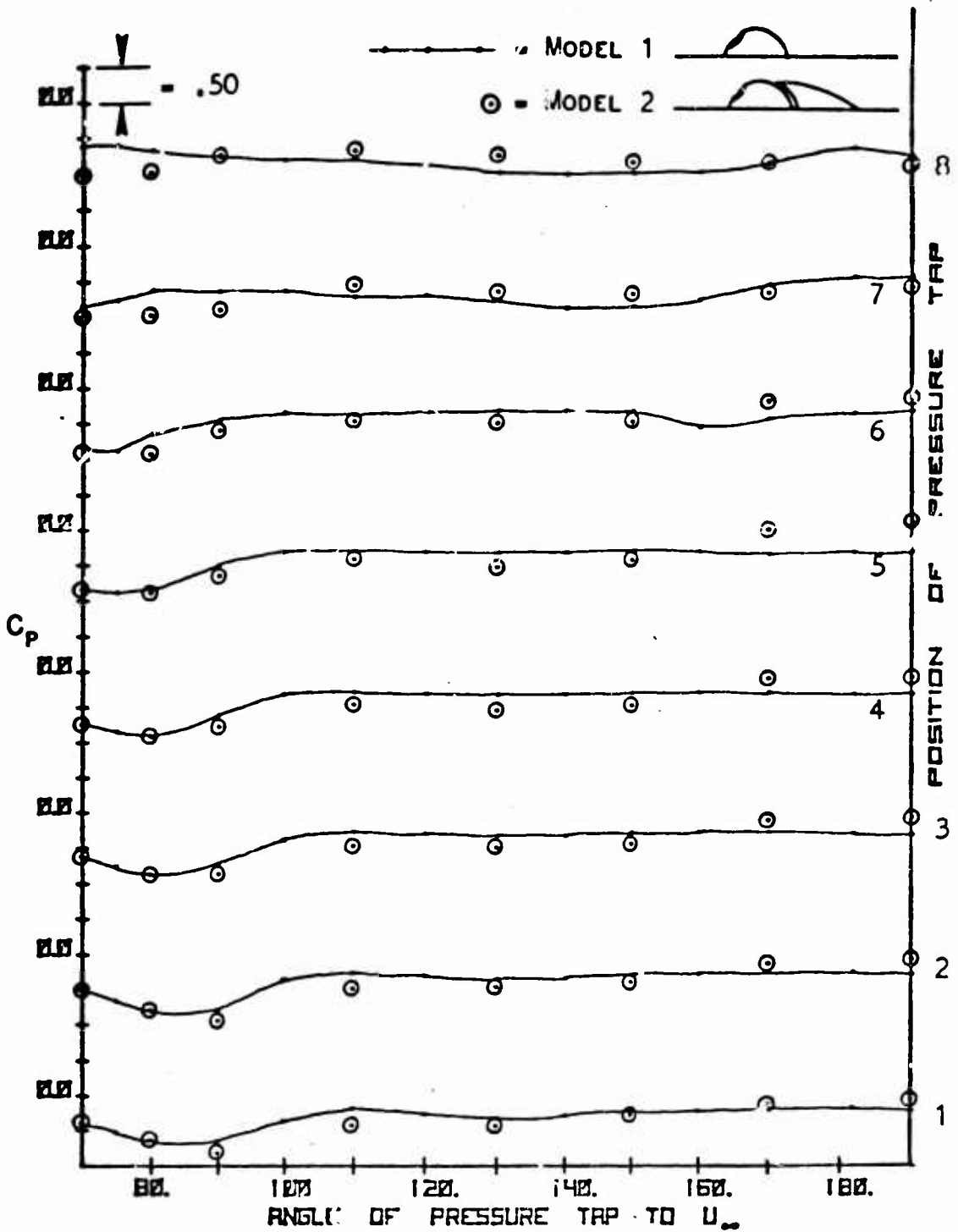


Fig. 75. Comparison of local turret flow C_p with and without the aft fairing installed^p with free stream Mach = .85. See page 11 for pressure tap location.

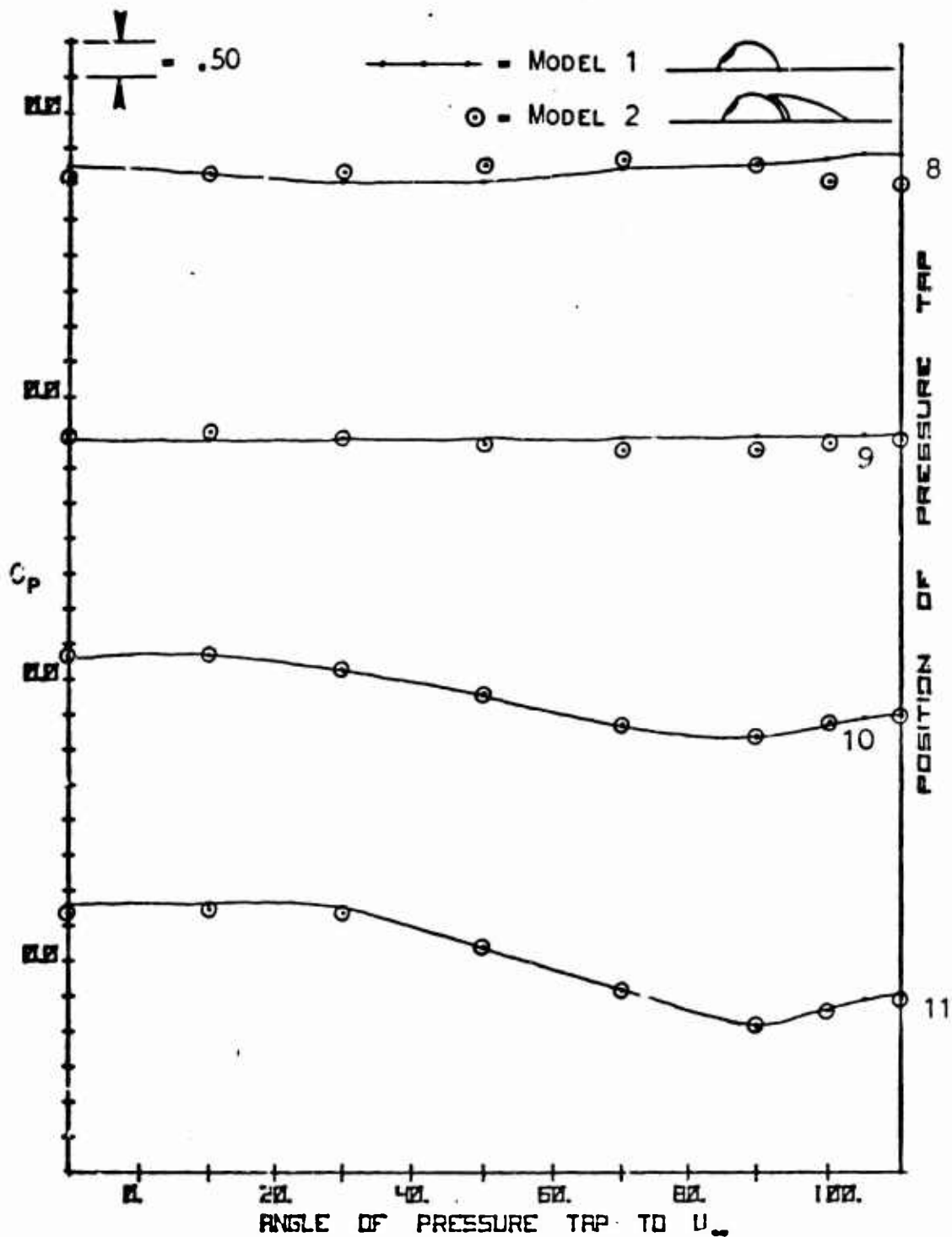


Fig. 76. Comparison of local turret flow C_p with and without the aft fairing installed^p with free stream Mach = .85. See page 11 for pressure tap location.

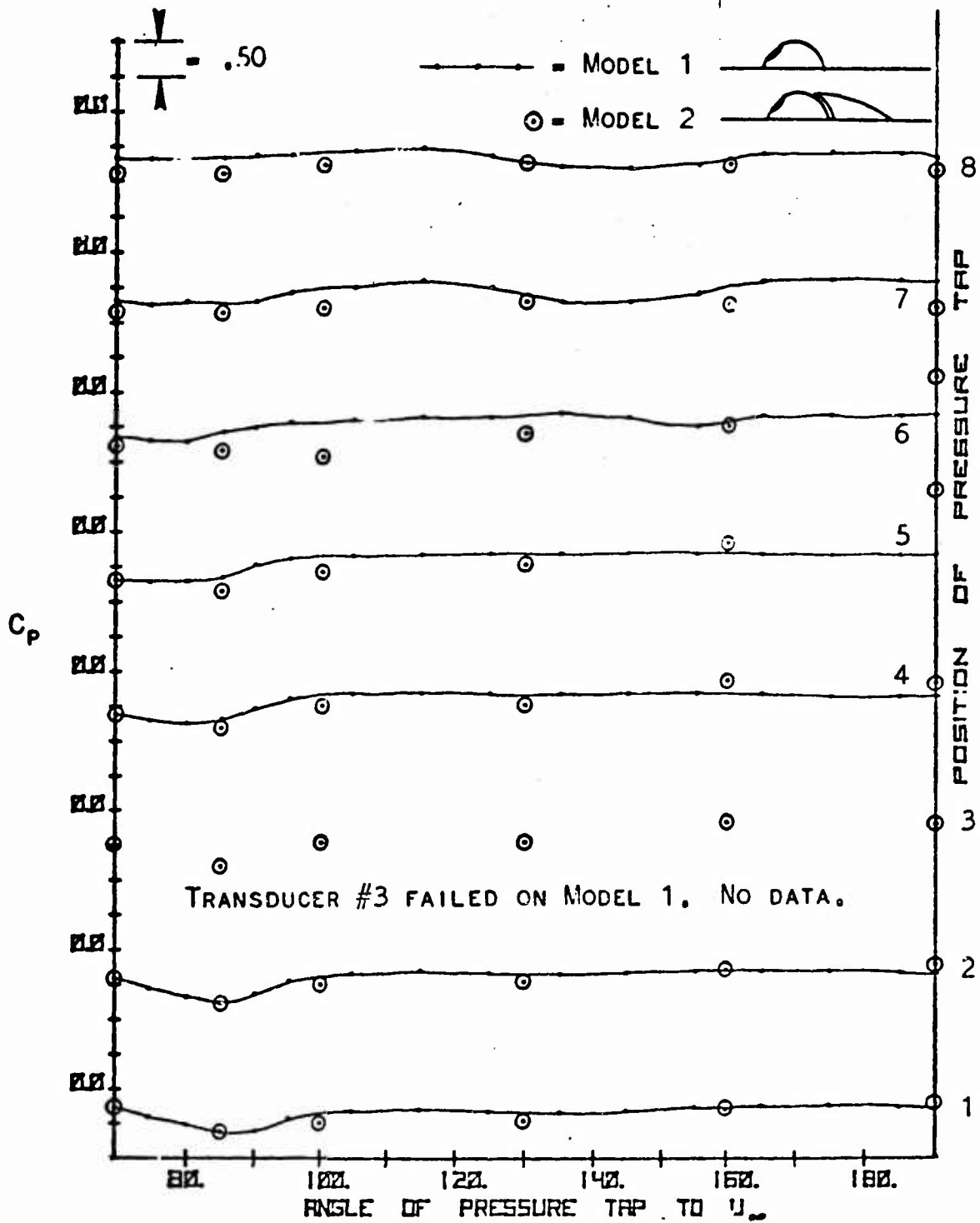


Fig. 77. Comparison of local turret flow C_p with and without the aft fairing installed^p with free stream Mach = .95. See page 11 for pressure tap location.

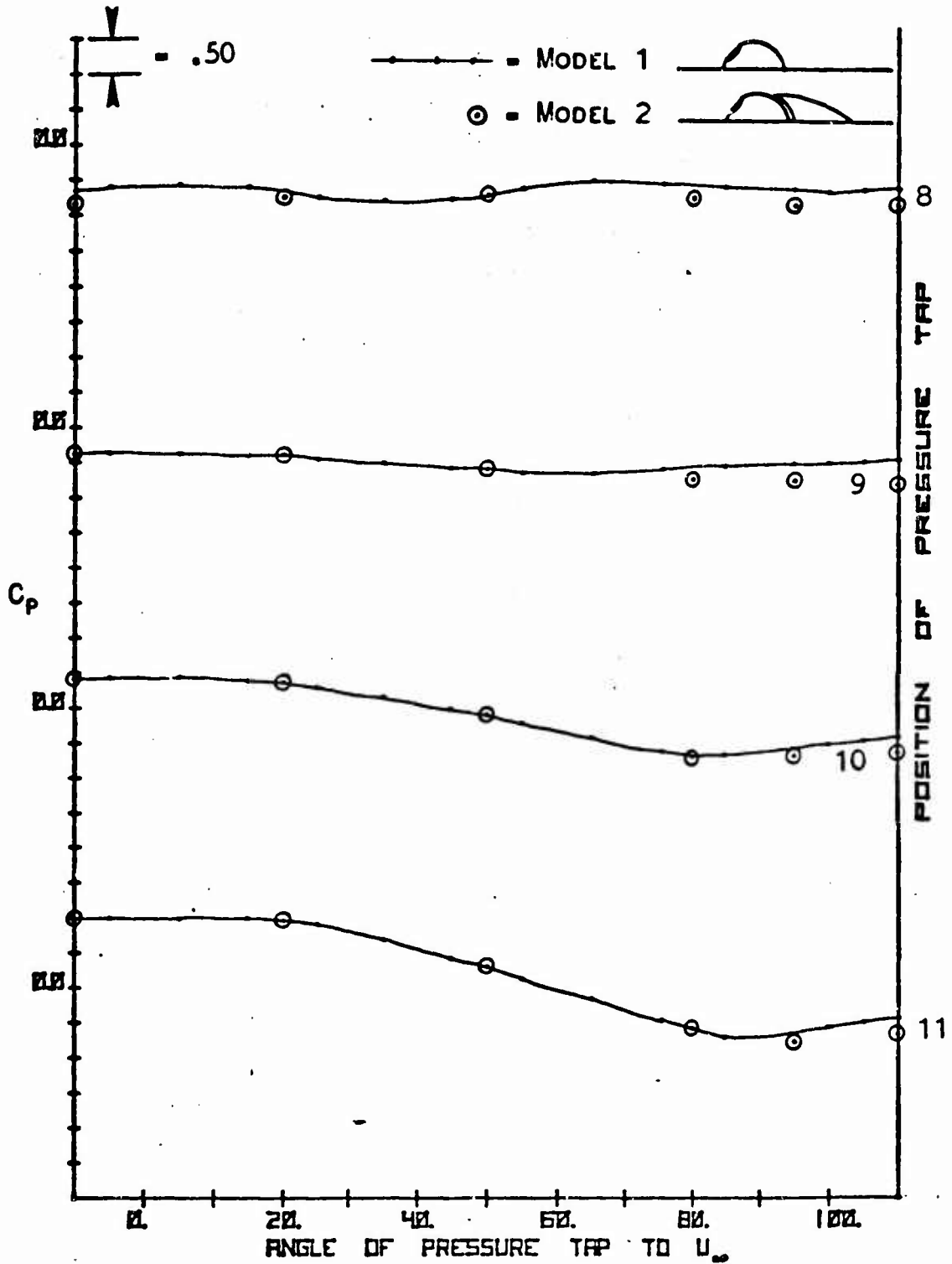


Fig. 78. Comparison of local turret flow C_p with and without the aft fairing installed^p with free stream Mach = .95. See page 11 for pressure tap location.

Appendix E

Oil Flow Visualization Drawings

This Appendix contains Figures 79 thru 82 which are drawings of oil flow patterns observed on the surface of Model 2 at various Mach numbers and θ . The position of the turret aperture is seen to have little effect on the line of flow separation.

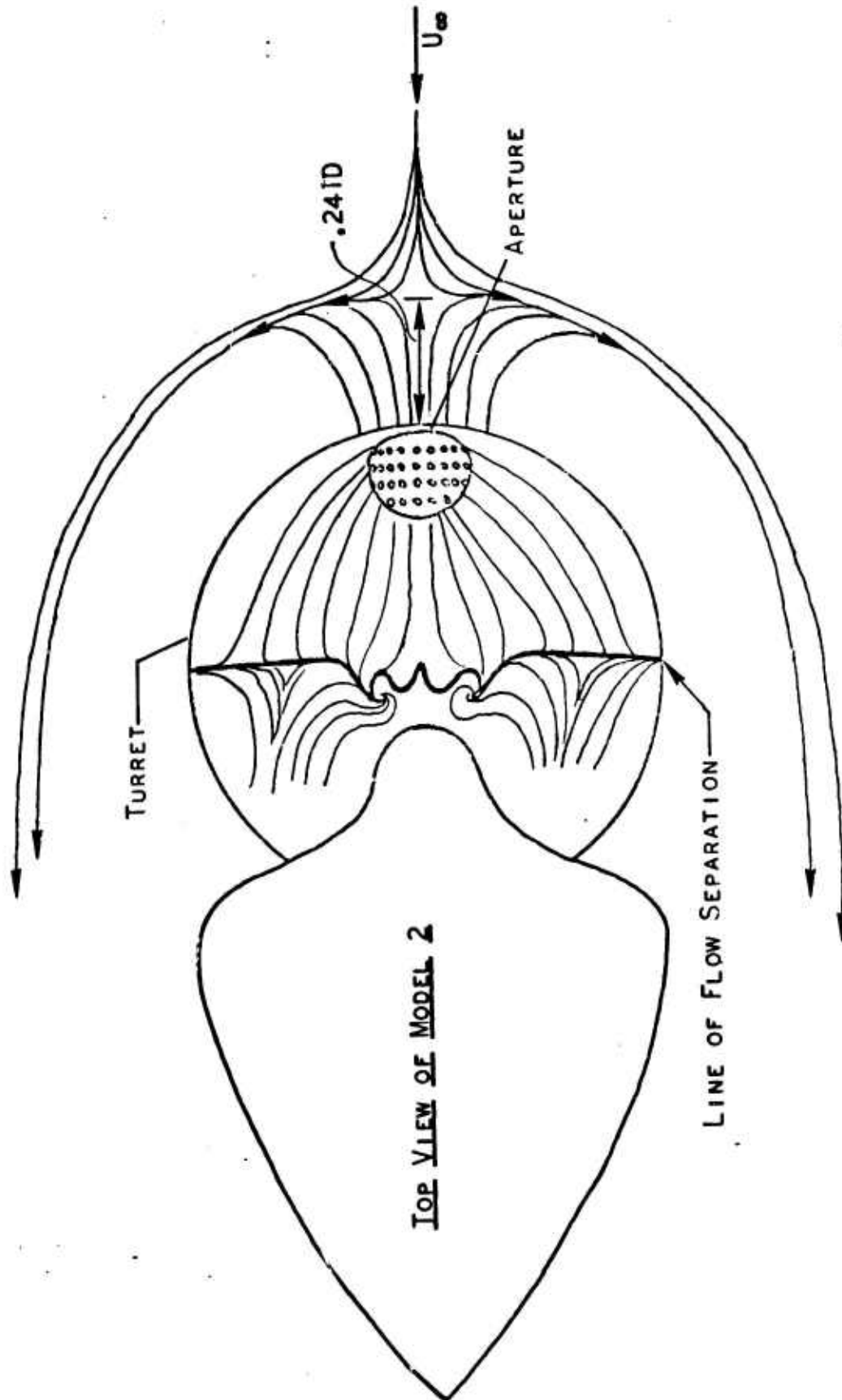


FIG. 79. OIL VISUALIZATION OF FLOW OVER MODEL 2 WITH $\theta = 0^\circ$ AND MACH = .85

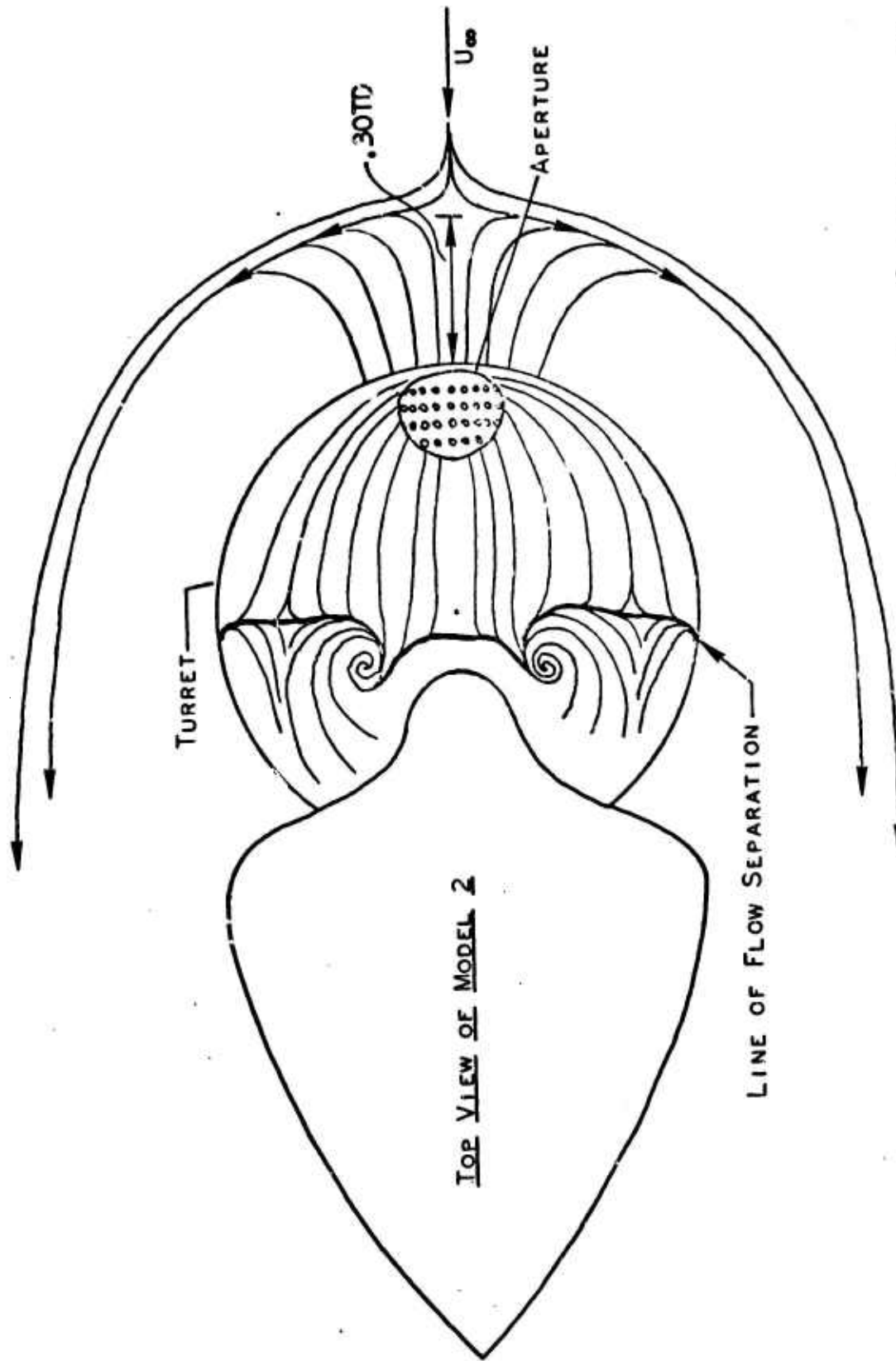


FIG. 80. OIL VISUALIZATION OF FLOW OVER MODEL 2 WITH $\theta = 0^\circ$ AND MACH = .95

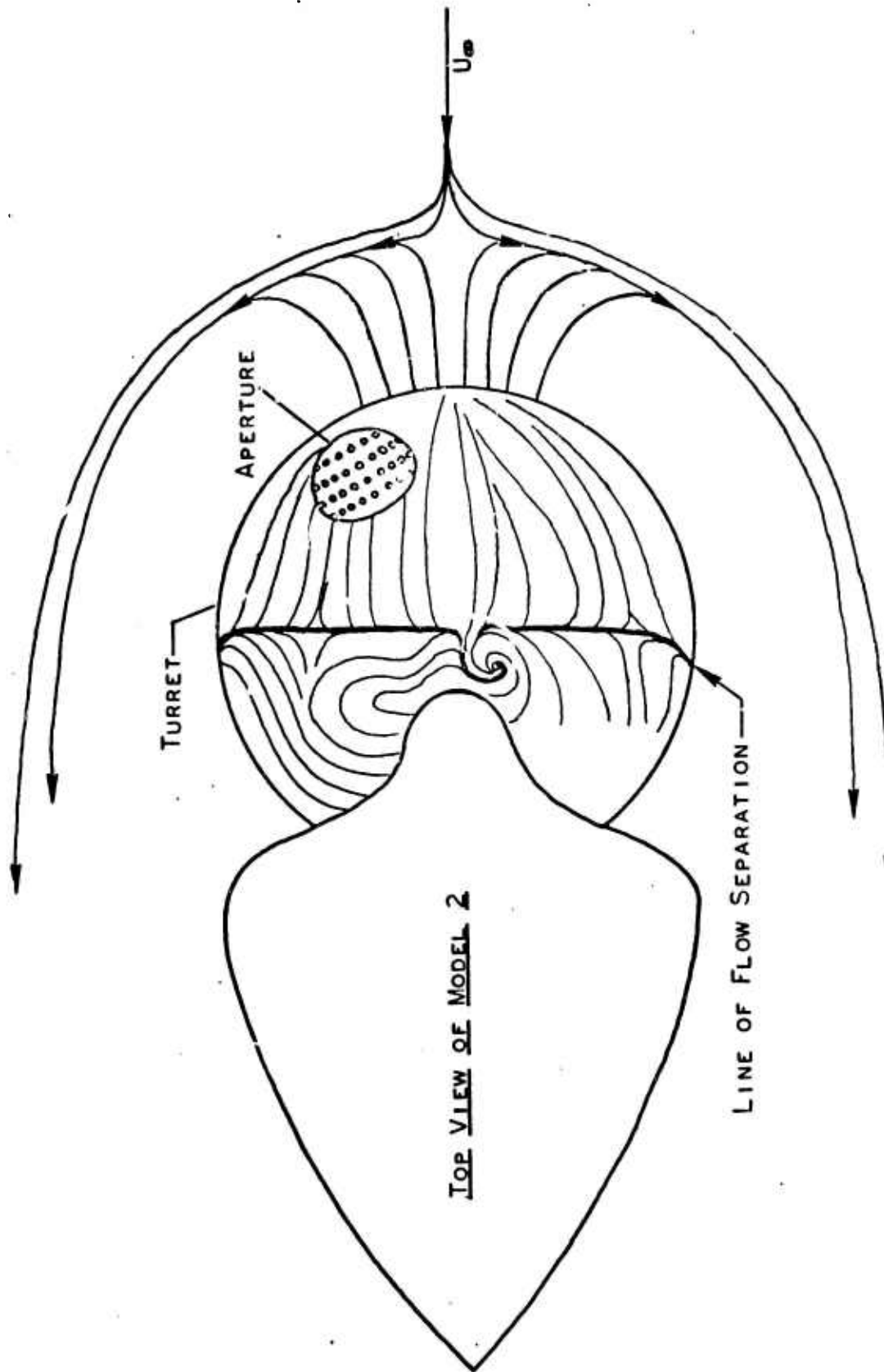


FIG. 81. OIL VISUALIZATION OF FLOW OVER MODEL 2 WITH $\theta = 30^\circ$ AND MACH = .95

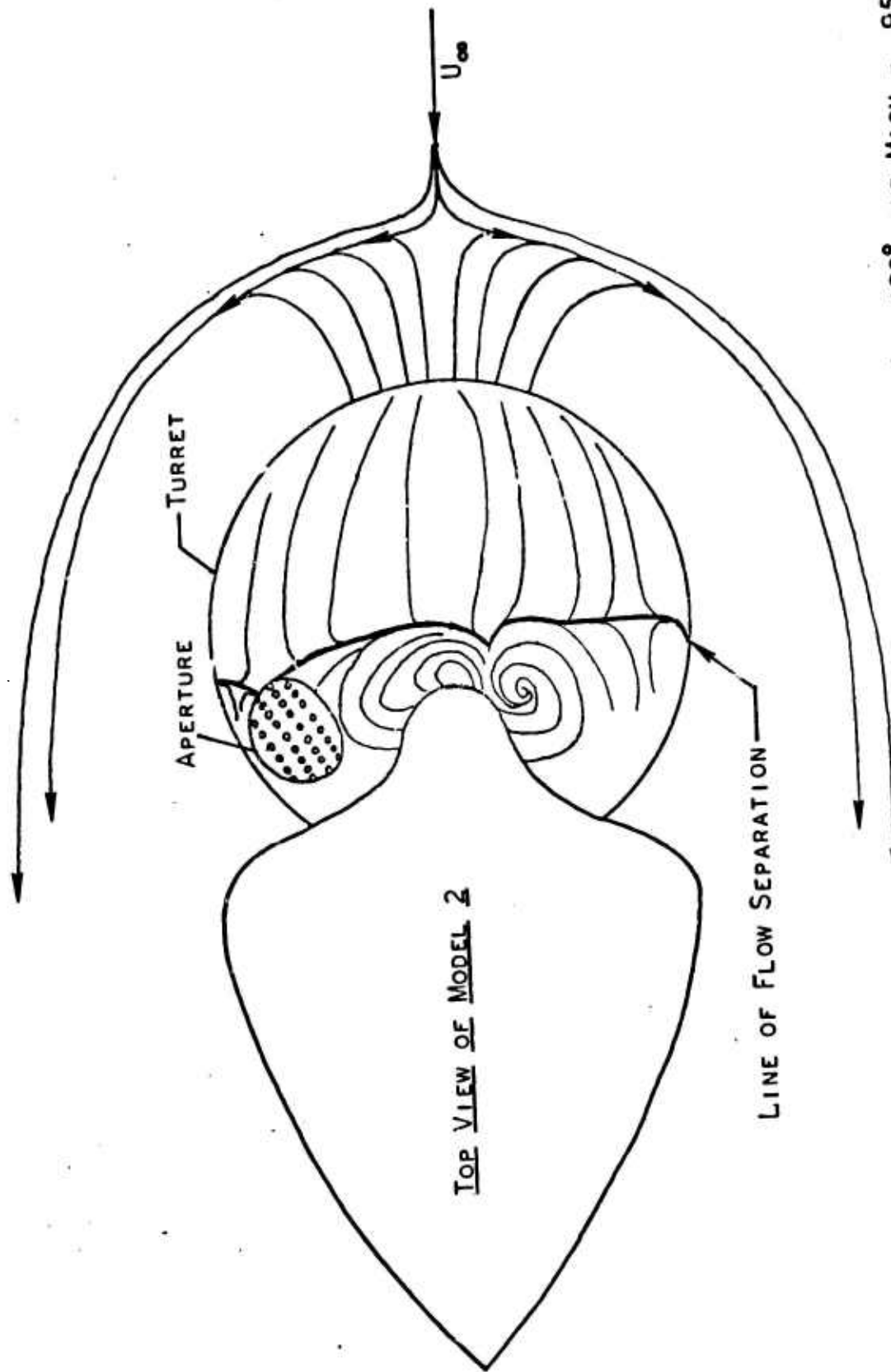


Fig. 82. OIL VISUALIZATION OF FLOW OVER MODEL 2 WITH $\theta = 120^\circ$ AND MACH = .95

Vita

Richard M. Mullane [REDACTED]

PII Redacted

[REDACTED] He attended grade schools in several states and completed high school in Albuquerque, New Mexico. Graduating from the United States Military Academy on 7 June 1967 he was awarded a Bachelor of Science in Engineering Science. After completion of navigator training in 1968 he served in tactical reconnaissance units in Southeast Asia and England. He entered the Air Force Institute of Technology in January 1974.